
**The quantum Wigner current:
A geometric approach to quantum
dynamics in phase space**

Maxime Oliva

School of Mathematics, Physics and Astrophysics

University of Hertfordshire

A thesis submitted in partial fulfillment of the requirements
for the degree of

Doctor of Philosophy

March 2019

"The meaning of life is just to be alive. It is so plain and so obvious and so simple. And yet, everybody rushes around in a great panic as if it were necessary to achieve something beyond themselves."

Alan Watts, *The Culture of Counter-culture*

Acknowledgements

I wish to thank my supervisor Dr. Ole Steuernagel. His passion, his knowledge, his instinct, his trust, and the freedom he gave me were a tremendous help for this thesis and for the work we have achieved.

I am thankful also to Dr. Alan McCall and Dr. Martin Hardcastle for the many helpful discussions, advice, and criticism.

I feel indebted to my brother Sébastien and my dad for the support they gave me when I needed it the most; and to Serena, who, always by my side, knew how to bring the best out of me.

Abstract

Phase space is the unity of position and momentum configuration space. It allows for an effective description of dynamical systems and is particularly useful when it comes to studying chaos theory and statistical mechanics.

After the advent of quantum physics early in the 20th century, E. Wigner [91], J. E. Moyal [62] and H. J. Groenewold [31] introduce a quantum theory in phase space. Despite the apparent added complexity of the mathematics involved in this new framework, the underlying classical and quantum equations show many similarities. The probability distribution in classical physics becomes the Wigner distribution, a probability distribution usually featuring negative values.

In 2013, O. Steuernagel and D. Kakofengitis, inspired by the work of H. Bauke [7] and E. Wigner [91], identified the quantum analogue of the classical phase space flow: the Wigner current \mathbf{J} [83]. This Wigner current allows the visualisation of quantum dynamics through a quantum fluid dynamics perspective in phase space.

This thesis is written by collection of five articles. They are prefaced by an introduction into the basics of quantum phase space theory and its link with both classical phase space dynamics and the standard Schrödinger approach, followed by the articles published during this PhD.

Article 1 shows the importance of the integral form of the Wigner current. We use it to derive the Ehrenfest's theorem, as well as to refute some propositions made within the community.

Article 2 shows that, using the Wigner current, an Eulerian and Lagrangian point of view do not always give the same results for the quantum case. We demonstrate that the negativities of the Wigner distribution, sign of quantumness of the system, are created by the Wigner velocity field singularities. The Wigner velocity field is the quantum analogue of the classical phase space velocity field.

In *Article 3*, we see that even though Wigner distributions of quantum systems feature spotty structures which saturate on scales a_Z [97], the construction of a superoscillating Wigner distribution allows one to generate much smaller structures, of the order of a_Z/α with α a positive constant potentially very large.

In *Article 4*, we introduce the concept of quantum shear suppression in phase space. The Wigner current features an effective quantum “viscosity”, suppressing classical dynamics fine details. This viscosity is the mechanism by which the Zurek scale is enforced dynamically onto the state in phase space.

In *Article 5*, we apply the previous ideas to Kerr-type oscillators. Its Wigner current is derived, and using it we show that its values are conserved on a ring during the time evolution of the Kerr oscillator. The shear suppression is also studied.

Contents

Introduction to phase space dynamics	1
0.1 Liouvillian mechanics	1
0.2 Quantum theory	2
0.2.1 The Schrödinger representation	2
0.2.2 The Wigner representation	2
0.2.3 Hudson’s theorem	3
0.2.4 Time evolution: Star-product and Moyal bracket	3
0.3 The Wigner current	5
0.3.1 Formal definition	5
0.3.2 Connection with the Schrödinger probability current	6
Published articles	7
1 Wigner’s representation of quantum mechanics in integral form and its applications	7
1.1 Abstract	7
1.2 Motivation and introduction	7
1.3 Wigner’s distribution and its evolution	8
1.4 Features and applications of the integral form	10
1.5 When is quantum mechanical time evolution Liouvillian?	11
1.6 Conclusion	15
2 Anharmonic quantum systems do not feature trajectories	16
2.1 Abstract	16
2.2 Introduction and motivation	16
2.3 Continuity equation, trajectories, classical phase space flow and Liouville’s theorem	18
2.3.1 Trajectories through Lagrangian decomposition	18
2.3.2 Liouvillian flow in conservative classical mechanical systems	19
2.3.3 A simple system with non-Liouvillian flow that features trajectories	20
2.4 Wigner’s quantum phase space distribution	20
2.5 Trajectories in quantum systems	21
2.6 Time evolution of the Wigner distribution	22

2.6.1	Formation of coherences and negativities of the Wigner distribution	23
2.7	Singularities in the velocity field are needed: trajectories are ill-defined	23
2.7.1	The phase space velocity w is non-linear in W	25
2.8	Short time integration of Eulerian and Lagrangian evolution equations –an analytically solvable case–	25
2.9	Misconceptions associated with phase space trajectories	27
2.9.1	There are no Wigner trajectories	27
2.9.2	The Non-Crossing Rules do not apply	27
2.9.3	Misconceptions due to incorrect decomposition of the continuity equation	28
2.9.4	Can the non-zero divergence of the current be transformed away?	29
2.9.5	There are no quantum potentials in phase space	30
2.9.6	What about positive phase space distributions?	30
2.10	Conclusions	31
3	Structures far below sub-Planck scale in quantum phase space through superoscillations	34
3.1	Abstract	34
3.2	Introduction	34
3.3	Zurek’s fundamental phase-space tiles	35
3.4	The superoscillating cross-state	36
3.5	Substructures within Zurek tiles	37
3.6	Conclusion	39
4	Dynamical shear suppression in quantum phase space	40
4.1	Abstract	40
4.2	Main text	40
4.3	Supplementary material	49
4.3.1	Fast oscillations and frequency filtering	49
4.3.2	Comparison of shear polarization Π with overlap \mathcal{P}	49
4.3.3	Identification of special states	55
4.3.4	Some properties of W and \mathbf{J}	56
4.3.5	Unit-free formulation of vorticity	56
4.3.6	Structure formation and coherences	56
4.3.7	On the term ‘viscosity’	57
4.3.8	Derivation of inequality for frequency content Ω in Eq. (4.8)	57
4.3.9	Remarks on measures δ , π and Π	58
4.3.10	Comparing polarization patterns for ‘hard’ and ‘soft’ potentials	60
4.3.11	$\Pi(t)$ and $\Omega(t)$ can evolve differently from each other	61
5	Quantum Kerr oscillators’ evolution in phase space: Wigner current, symmetries, shear suppression and special states	62
5.1	Abstract	62
5.2	Wigner distributions and Wigner current of Kerr oscillators	63

5.3	No trajectories or flow in quantum phase space	65
5.4	Pulses in Quantum phase space	67
5.5	\mathbf{J} 's viscosity and special states	69
5.6	Appendix	71
Conclusion		77
References		78

Introduction to phase space dynamics

The mathematical space we will use in this thesis is phase space. Before studying quantum phase space, we will review classical mechanics and its key features. These concepts will prove useful for the understanding of the articles following this introduction.

0.1 Liouvillian mechanics

Liouvillian mechanics describes the evolution of conservative classical systems. This theory takes place in phase space, and is particularly useful when it comes to the study of dynamical systems, as it naturally includes each state of a system as a point in phase space.

In order to describe the evolution of a classical system in phase space, one has to define the probability density $\rho(x, p, t)$. The time evolution of ρ for a 1-D system is given by Liouville's equation

$$\frac{d\rho}{dt} = \frac{\partial\rho}{\partial t} + \frac{dx}{dt} \frac{\partial\rho}{\partial x} + \frac{dp}{dt} \frac{\partial\rho}{\partial p} = \frac{\partial\rho}{\partial t} + \mathbf{v} \cdot \nabla\rho = \frac{\partial\rho}{\partial t} + \nabla \cdot \mathbf{j} = 0, \quad (1)$$

with $\mathbf{j} = \rho\mathbf{v} = \rho \begin{pmatrix} \frac{p}{m} \\ -\partial_x V \end{pmatrix}$ the classical phase space current, and \mathbf{v} its velocity field, which encodes Newton's law.

Connecting this to the Hamiltonian formalism, the time evolution of ρ can be written as

$$\frac{\partial\rho}{\partial t} = -\{\rho, H\}, \quad (2)$$

with $\{\bullet, \bullet\}$ the Poisson bracket defined by $\{f(x, p), g(x, p)\} = \frac{\partial f}{\partial x} \frac{\partial g}{\partial p} - \frac{\partial f}{\partial p} \frac{\partial g}{\partial x}$. This equation is usually referred to as the *classical Liouville equation*.

0.2 Quantum theory

Quantum theory describes atomic and subatomic systems. Despite their rigorously identical predictions, different representations of quantum theory exist.

0.2.1 The Schrödinger representation

The most famous one is undoubtedly the Schrödinger representation, in which the main mathematical tool used is the wavefunction $|\Psi\rangle$, containing all the system's information (assuming the system is a pure state). $|\Psi\rangle$'s time evolution in Schrödinger representation is described by its eponymous equation

$$i\hbar \frac{\partial |\Psi\rangle}{\partial t} = \hat{H} |\Psi\rangle, \quad (3)$$

with \hat{H} the Hamiltonian operator of the system.

The wavefunction $|\Psi\rangle$ is an object acting in a generalization of the Euclidean space: *the Hilbert space*.

Using the wavefunction $|\Psi\rangle$ of a pure state, one can define the density operator $\hat{\rho} = |\Psi\rangle \langle\Psi|$. The time evolution is then described by the von Neumann equation

$$\frac{\partial \hat{\rho}}{\partial t} = -\frac{1}{i\hbar} [\hat{\rho}, \hat{H}]. \quad (4)$$

0.2.2 The Wigner representation

This representation is the one used in this thesis. The Hilbert space wavefunction $|\Psi\rangle$ is converted to a Wigner distribution $W(x, p, t)$, a quantum phase space distribution and closest analogue of the classical probability distribution.

This framework, underrated for decades, will prove to be very useful in the following studies. It allows one to directly visualize quantum dynamics in phase space, and brings new insights on the connections between classical and quantum physics.

The Wigner distribution is defined as the Fourier transform of the non-diagonal terms $\rho(x - y, x + y, t) = \langle x - y | \hat{\rho} | x + y \rangle$ (also called coherence terms) of the density

operator [91].

For a 1-D system, the Wigner distribution W is defined by

$$W(x, p) = \frac{1}{\pi\hbar} \int_{-\infty}^{\infty} dy \langle x - y | \hat{\rho} | x + y \rangle e^{\frac{2ipy}{\hbar}}. \quad (5)$$

Despite being called a *probability distribution*, W generally features patches of negativities across phase space, which do not have any classical equivalent. For this reason, the Wigner distribution is often called a *quasi-probability distribution*. The distribution W is normalized to unity and real-valued.

With the Wigner distribution, one can directly visualize the quantum state's behavior over time. One of the main advantage of this distribution is its ability to give information of both the position and momentum of a system. Integrating over the position space leads to the quantum probability distribution in momentum space $\int dx W(x, p) = |\Phi(p)|^2 = P(p)$, while an integration over the momentum space gives the quantum probability distribution in position space $\int dp W(x, p) = |\Psi(x)|^2 = P(x)$.

Additionally, in quantum phase space, none of the operators used in the Schrödinger representation are needed. Observables are calculated using well-defined functions of x and p .

0.2.3 Hudson's theorem

Hudson's theorem is an important theorem regarding the emergence of negativities in quantum phase space [41].

This theorem states that *for a continuous non-relativistic quantum system, the Wigner distribution of a pure state is strictly positive if and only if the state is gaussian.*

This means that a Wigner distribution which is not gaussian features negative patches in phase space.

0.2.4 Time evolution: Star-product and Moyal bracket

Star-product and commutators

In quantum phase space dynamics, the Hilbert operators of the Schrödinger representation are mapped into phase space as real functions of x and p . One can define a phase space analogue of the operator product in Hilbert space: *the star-product* [62, 31].

The star-product maps the non-commutativity of Hilbert space operators onto their equivalent functions in the Wigner representation.

The star-product of two real-valued functions $f(x, p)$ and $g(x, p)$ is defined by

$$f(x, p) \star g(x, p) = f(x, p) e^{\frac{i\hbar}{2}(\overleftarrow{\partial}_x \overrightarrow{\partial}_p - \overleftarrow{\partial}_p \overrightarrow{\partial}_x)} g(x, p) \quad (6)$$

$$= f(x, p) \sum_{l=0}^{\infty} \left(\frac{i\hbar}{2}\right)^l \left(\overleftarrow{\partial}_x \overrightarrow{\partial}_p - \overleftarrow{\partial}_p \overrightarrow{\partial}_x\right)^l g(x, p). \quad (7)$$

$\overleftarrow{\partial}_i$ is the derivative with respect to $i = \{x, p\}$ acting on the left side function f , and $\overrightarrow{\partial}_i$ the derivative acting on the right side function g .

Both the standard Hilbert commutator and its phase space analogue share similar properties: they are non-commutative, they can be used to time-evolve an initial state, and they lead to the same expectation values.

Using the star-product, one can define the quantum phase space commutator

$$[f, g]_{\star} = f \star g - g \star f. \quad (8)$$

Moyal bracket and quantum Liouville equation

We can now study the time evolution of the Wigner distribution, using the *Moyal bracket* [62].

The Moyal bracket $\{\{\bullet, \bullet\}\}$ of two functions $\alpha(x, p)$ and $\beta(x, p)$ is defined using the quantum phase space commutator

$$\{\{\alpha, \beta\}\} = \frac{1}{i\hbar} [\alpha, \beta]_{\star} = \frac{1}{i\hbar} (\alpha \star \beta - \beta \star \alpha). \quad (9)$$

Applied to Eq. (4), it gives us the quantum version of the Liouville equation called the *quantum Liouville equation*:

$$\frac{\partial W(x, p, t)}{\partial t} = - \{\{W(x, p, t), H(x, p)\}\} \quad (10)$$

$$= -\frac{1}{i\hbar} (W(x, p, t) \star H(x, p) - H(x, p) \star W(x, p, t)) \quad (11)$$

$$= -\frac{2}{\hbar} W(x, p, t) \sin\left(\frac{\hbar}{2}(\overleftarrow{\partial}_x \overrightarrow{\partial}_p - \overleftarrow{\partial}_p \overrightarrow{\partial}_x)\right) H(x, p). \quad (12)$$

In the Taylor expansion of the sine function in Eq. (12), the Moyal bracket is such that the first order term of the equation corresponds to the classical Poisson bracket introduced earlier, see Eq. (2). The other terms are quantum corrections.

0.3 The Wigner current

The Wigner current allows us to use a fluid dynamics perspective in quantum phase space. It can feature stagnation points, like in classical fluid mechanics, and reveals hidden topological order in quantum dynamics [83]. It can also be “viscous”, as described in Article 4.

0.3.1 Formal definition

The Wigner current \mathbf{J} is the quantum equivalent of the classical phase space current \mathbf{j} [see Eq. (1)].

In the quantum mechanical case, that is for a Hamiltonian $H(x, p) = T(p) + V(x)$, with T the kinetic term and V the potential term, the current \mathbf{J} is defined by splitting the Hamiltonian in the quantum Liouville equation:

$$\frac{\partial W}{\partial t} = -\{\{W, H\}\} = -\{\{W, T\}\} - \{\{W, V\}\}. \quad (13)$$

The time evolution of the Wigner distribution can then be written as the divergence of the Wigner current \mathbf{J} ,

$$\frac{\partial W}{\partial t} = -\nabla \cdot \mathbf{J} = -\partial_x J_x - \partial_p J_p, \quad (14)$$

with $\partial_x J_x = \{\{W, T\}\}$ and $\partial_p J_p = \{\{W, V\}\}$.

The components of \mathbf{J} are

$$\mathbf{J} = \begin{pmatrix} J_x \\ J_p \end{pmatrix} = \begin{pmatrix} \frac{p}{M} W \\ -\sum_{l=0}^{\infty} \frac{(-1)^l (\frac{\hbar}{2})^{2l}}{(2l+1)!} \partial_x^{2l+1} V \partial_p^{2l} W \end{pmatrix}. \quad (15)$$

As we can see, despite the simplicity of the J_x component, the J_p component is a series of derivatives acting on both $V(x)$ and $W(x, p, t)$. This form is similar to the one originally introduced by Wigner in his paper [91]. Taking the zeroth order of \mathbf{J} gives the classical phase space current defined in Eq. (1).

But using the very definition of the Wigner function [see Eq. (5)], one can write the evolution equation as:

$$\partial_t W = -\frac{1}{\pi\hbar} \int dy \langle x-y | \frac{1}{i\hbar} [\hat{\rho}, \hat{H}] | x+y \rangle e^{2ipy}. \quad (16)$$

It follows that one can write \mathbf{J} as an integral [44]:

$$\mathbf{J} = \left(\begin{array}{c} \frac{p}{m\pi\hbar} \int_{-\infty}^{\infty} dy \langle x-y | \hat{\rho} | x+y \rangle e^{\frac{2ipy}{\hbar}} \\ \frac{-1}{\pi\hbar} \int_{-\infty}^{\infty} dy \left(\frac{V(x+y)-V(x-y)}{2y} \right) \langle x-y | \hat{\rho} | x+y \rangle e^{\frac{2ipy}{\hbar}} \end{array} \right) \quad (17)$$

Note that this integral form is more general than Eq. (15) and does not require an analytical potential.

0.3.2 Connection with the Schrödinger probability current

As W is directly linked to the position (respectively momentum) quantum probability in Hilbert space via integration over the momentum (respectively position) space, such integration of \mathbf{J} 's time evolution equation also gives the time evolution of the quantum probability current of the Schrödinger representation,

$$\int_{-\infty}^{\infty} (\partial_t W + \partial_x J_x + \partial_p J_p) dp = \partial_t P(x, t) + \partial_x \hat{j}_\Psi(x, t) = 0, \quad (18)$$

with $\hat{j}_\Psi(x, t)$ the quantum probability current defined by

$$\hat{j}_\Psi(x, t) = \frac{\hbar}{2im} (\Psi^*(x, t) \partial_x \Psi(x, t) - \Psi(x, t) \partial_x \Psi^*(x, t)). \quad (19)$$

Similarly, the quantum probability current in momentum is obtained by integrating the continuity equation over the position space.

Article 1

Wigner's representation of quantum mechanics in integral form and its applications

by

D. Kakofengitis, M. Oliva, O. Steuernagel [44]

1.1 Abstract

We consider quantum phase-space dynamics using Wigner's representation of quantum mechanics. We stress the usefulness of the integral form for the description of Wigner's phase-space current \mathbf{J} as an alternative to the popular Moyal bracket. The integral form brings out the symmetries between momentum and position representations of quantum mechanics, is numerically stable, and allows us to perform some calculations using elementary integrals instead of Groenewold star products. Our central result is an explicit, elementary proof which shows that only systems up to quadratic in their potential fulfil Liouville's theorem of volume preservation in quantum mechanics. Contrary to a recent suggestion, our proof shows that the non-Liouvillian character of quantum phase-space dynamics cannot be transformed away.

1.2 Motivation and introduction

Wigner's representation of quantum mechanics in phase-space [91] is equivalent to Heisenberg's, Schrödinger's and Feynman's [95]. The description of the time evolu-

tion of Wigner’s phase-space distribution function W uses Moyal brackets [62], the quantum analogue of classical Poisson brackets. The similarity of the Moyal form with classical physics explains its popularity.

Moyal’s bracket is defined as an infinite series of derivatives, which can make it cumbersome to use and also numerically unstable. It has limited applications because it assumes that the potential can be Taylor expanded. The integral form of quantum phase-space dynamics [91, 5] is an alternative to Moyal’s form, it also applies to piecewise or singular potentials and displays symmetries between momentum and position representation not obvious when using Moyal’s formulation only.

We recently showed that in anharmonic quantum systems the violation of Liouville’s volume preservation can be so large that quantum phase-space volumes locally change at singular rates [68]. These singularities are of central importance; they are responsible for the generation of quantum coherences.

Here, we investigate a recent suggestion by Daligault [20], who provided a recipe that might enable us to “transform away” the violation of Liouville’s theorem in anharmonic quantum-mechanical systems.

We illustrate the power of the integral form of Wigner’s representation, which allows us to give an elementary proof that Daligault’s suggestion amounts to a specific modification that makes the dynamics classical and is incompatible with his stated aim of finding a Liouvillian system that reproduces quantum dynamics.

Our proof shows that the singularities, reported in Ref. [68], cannot be removed to make quantum phase-space dynamics divergence-free.

1.3 Wigner’s distribution and its evolution

In Wigner’s representation of quantum mechanics [91, 38] Wigner’s phase-space distribution is the “*closest quantum analogue of the classical phase-space distribution*” [97]. It is defined as

$$W(x, p, t) = \frac{1}{\pi\hbar} \int dy \varrho(x - y, x + y, t) e^{\frac{2i}{\hbar}py}, \quad (1.1)$$

$$= \frac{1}{\pi\hbar} \int ds \tilde{\varrho}(p - s, p + s, t) e^{-\frac{2i}{\hbar}xs}; \quad (1.2)$$

here, $\hbar = h/(2\pi)$ is Planck’s constant, integrals run from $-\infty$ to $+\infty$: $\int = \int_{-\infty}^{\infty}$, and ϱ and $\tilde{\varrho}$ are the density operator in position and momentum representation, respectively.

Wigner’s distribution W is set apart from other quantum phase-space distribu-

tions [38] by the fact that only W simultaneously yields the correct projections in position and momentum ($\varrho(x, x, t) = \int dp W$ and $\tilde{\varrho}(p, p, t) = \int dx W$) as well as state overlaps $|\langle \psi_1 | \psi_2 \rangle|^2 = 2\pi\hbar \int \int dx dp W_1 W_2$, while maintaining its form (1.1) when evolved in time. Additionally, the Wigner distribution's averages and uncertainties evolve *momentarily* classically [76, 6].

In this work we consider one-dimensional conservative systems in a pure state with quantum-*mechanical* Hamiltonians

$$\hat{\mathcal{H}}(\hat{x}, \hat{p}) = \frac{\hat{p}^2}{2M} + \hat{V}(\hat{x}) . \quad (1.3)$$

The Wigner function's time evolution arises, in analogy to Eq. (1.1), from a Wigner-transform [which can be implemented as a fast Fourier transform (FFT)] of the von Neumann equation $i\hbar \frac{\partial \hat{\varrho}}{\partial t} = [\hat{\mathcal{H}}, \hat{\varrho}]$ as [91, 38]

$$\begin{aligned} \partial_t W = & -\frac{p}{M} \frac{1}{\pi\hbar} \int dy \partial_x \varrho(x-y, x+y, t) e^{\frac{2i}{\hbar}py} \\ & + \frac{i}{\pi\hbar^2} \int dy [V(x+y) - V(x-y)] \times \varrho(x-y, x+y, t) e^{\frac{2i}{\hbar}py} , \end{aligned} \quad (1.4)$$

also known as the quantum Liouville equation.

Throughout, we write partial derivatives as $\frac{\partial^n}{\partial x^n} = \partial_x^n$.

If the potential V can be globally Taylor expanded, the integrals (1.4) yields the Moyal bracket $\{\{\cdot, \cdot\}\}$ [62]

$$\frac{\partial W}{\partial t} = \{\{\mathcal{H}, W\}\} = \frac{1}{i\hbar} (\mathcal{H} \star W - W \star \mathcal{H}) \quad (1.5)$$

$$= \frac{2}{\hbar} \mathcal{H} \sin\left(\frac{\hbar}{2} \left(\overleftarrow{\partial}_x \overrightarrow{\partial}_p - \overleftarrow{\partial}_p \overrightarrow{\partial}_x\right)\right) W . \quad (1.6)$$

Here we use Groenewold star products (\star) [31], defined as $f \star g = f e^{\frac{i\hbar}{2} (\overleftarrow{\partial}_x \overrightarrow{\partial}_p - \overleftarrow{\partial}_p \overrightarrow{\partial}_x)} g$; the arrows indicate whether derivatives are executed on f or g .

Equations (1.4) or (1.6) can be written as the continuity equation [91]

$$\partial_t W + \nabla \cdot \mathbf{J} = \partial_t W + \partial_x J_x + \partial_p J_p = 0 . \quad (1.7)$$

Comparing Eqs. (1.7) and (1.4), we identify the Wigner current $\mathbf{J} = \begin{pmatrix} J_x \\ J_p \end{pmatrix}$, with

position component

$$J_x = \frac{p}{M\pi\hbar} \int dy \varrho(x-y, x+y, t) e^{\frac{2i}{\hbar}py} = \frac{p}{M} W, \quad (1.8)$$

and momentum component

$$J_p = -\frac{1}{\pi\hbar} \int dy \left[\frac{V(x+y) - V(x-y)}{2y} \right] \times \varrho(x-y, x+y, t) e^{\frac{2i}{\hbar}py}. \quad (1.9)$$

If the potential can be Taylor expanded, the explicit form of the components of Wigner current \mathbf{J} in Eq. (1.6) is [91, 81, 23, 83]

$$\mathbf{J} = \mathbf{j} + \begin{pmatrix} 0 \\ -\sum_{l=1}^{\infty} \frac{(i\hbar/2)^{2l}}{(2l+1)!} \partial_p^{2l} W \partial_x^{2l+1} V(x) \end{pmatrix}. \quad (1.10)$$

Here, with $\mathbf{v} = \begin{pmatrix} p/M \\ -\partial_x V \end{pmatrix}$, $\mathbf{j} = W\mathbf{v}$ is the classical and $\mathbf{J} - \mathbf{j}$ are quantum terms.

1.4 Features and applications of the integral form

The integral form (1.4) is more general than the Moyal expression since it does not rely on V being analytic.

A numerical implementation of the integral form can use fast Fourier transforms. In the case of potentials featuring high order Taylor terms, high order numerical derivatives can render Eq. (1.10) poorly convergent [83].

In Ref. [83] we showed (note typographical errors in Eqs. (4) and (5) of [83]) that the p projection of J_x yields the quantum probability current j in position space,

$$\begin{aligned} \int dp J_x &= \frac{\hbar}{2iM} \int dy \varrho(x-y, x+y, t) \partial_y \delta(y) \\ &= \sum_k P_k \frac{\hbar}{2iM} (\Psi_k^* \partial_x \Psi_k - \Psi_k \partial_x \Psi_k^*) = j(x, t), \end{aligned} \quad (1.11)$$

where we used Dirac's δ and wrote the density matrix as $\varrho(x, x', t) = \sum_k P_k \Psi_k(x, t) \Psi_k^*(x', t)$, a statistical mixture of pure states. Additionally,

$$\int dx J_x = \frac{p}{M} \int ds \tilde{\varrho}(p-s, p+s, t) \delta(s) = \frac{p}{M} \tilde{\varrho}(p, p, t). \quad (1.12)$$

Analogously to Eq. (1.11), the quantum probability current \tilde{j} in momentum space [83],

is

$$\begin{aligned}
\int dx J_p &= -\frac{1}{\pi\hbar} \iint dy dx \left[\frac{V(x+y) - V(x-y)}{2y} \right] \times \varrho(x-y, x+y, t) e^{\frac{2i}{\hbar}py} \\
&= \frac{1}{i\sqrt{2\pi\hbar^3}} \int_{-\infty}^p dp' \int dp'' \left[\tilde{V}^*(p'' - p') \tilde{\varrho}(p'', p') - \tilde{V}(p'' - p') \tilde{\varrho}(p', p'') \right] = \tilde{j}(p, t),
\end{aligned} \tag{1.13}$$

(where $\tilde{V}(p) = \frac{1}{\sqrt{2\pi\hbar}} \int dx V(x) e^{-\frac{i}{\hbar}px}$), while

$$\begin{aligned}
\int dp J_p &= - \int dy \left[\frac{V(x+y) - V(x-y)}{2y} \right] \times \varrho(x-y, x+y, t) \delta(y) \\
&= -\varrho(x, x, t) \frac{dV}{dx}.
\end{aligned} \tag{1.14}$$

We would like to emphasize that the quantum terms of Eq. (1.10) do not contribute in Eq. (1.14).

Averaging over Eqs. (1.12) and (1.14), reproduces Ehrenfest's theorem [95]

$$\iint dx dp J_x = \frac{\langle \hat{p} \rangle}{M} = \frac{d\langle \hat{x} \rangle}{dt} \tag{1.15}$$

and

$$\iint dx dp J_p = - \left\langle \frac{d\hat{V}}{dx} \right\rangle = \frac{d\langle \hat{p} \rangle}{dt}. \tag{1.16}$$

Where applicable, the Moyal bracket formalism [95] yields the same results. Note the various subtleties associated with the interpretation of Ehrenfest's theorem [6, 76].

1.5 When is quantum mechanical time evolution Liouvillian?

To investigate whether quantum phase-space dynamics is Liouvillian we determine the divergence of its quantum phase-space velocity field \mathbf{w} [23, 89, 20]. \mathbf{w} is the

quantum analogue of the classical velocity field \mathbf{v} (Eq. (1.10)):

$$\mathbf{w} = \frac{\mathbf{J}}{W} = \mathbf{v} + \frac{1}{W} \left(\begin{array}{c} 0 \\ -\sum_{l=1}^{\infty} \frac{(i\hbar/2)^{2l}}{(2l+1)!} \partial_p^{2l} W \partial_x^{2l+1} V \end{array} \right). \quad (1.17)$$

To rephrase the continuity equation (1.7) in terms of \mathbf{w} , we switch to the Lagrangian decomposition [23, 89, 20]

$$\frac{dW}{dt} = \partial_t W + \mathbf{w} \cdot \nabla W = -W \nabla \cdot \mathbf{w}. \quad (1.18)$$

Note that \mathbf{w} is singular at zeros of W since, generally, zeros of W do not coincide with zeros of its derivatives. This implies, among other things, that the concept of trajectories in quantum phase-space cannot be applied to the dynamics of anharmonic systems [68].

Problems associated with the singularities have been observed multiple times [77, 89], they badly affect numerical quantum phase-space studies [89].

It would therefore be intriguing to be able to transform such problems away, as suggested by Daligault [20]. He speculated that it might be possible to add an auxiliary field $\delta\mathbf{J}$ to \mathbf{J} in Eq. (1.7) which would not modify the dynamics since it is assumed to be divergence-free. Yet, this auxiliary field might yield a modification to the velocity field such that their sum fulfills Liouville's theorem: $\nabla \cdot (\mathbf{w} + \delta\mathbf{w}) = 0$. If possible, we could deploy the machinery of classical phase-space transport equations to solve quantum problems.

We now prove that we cannot get rid of the non-Liouvillian character of quantum phase-space dynamics in anharmonic systems in the way Daligault suggested.

To do this, we need to establish when \mathbf{J} obeys Liouville's theorem, i.e., when the divergence of \mathbf{J} 's velocity field vanishes everywhere in phase-space. With $\mathbf{w} = \mathbf{J}/W$ we have

$$\nabla \cdot \mathbf{w} = \partial_x \left(\frac{J_x}{W} \right) + \partial_p \left(\frac{J_p}{W} \right) = \partial_x \left(\frac{p}{M} \right) + \partial_p \left(\frac{J_p}{W} \right) = \partial_p \left(\frac{J_p}{W} \right) = 0. \quad (1.19)$$

Integrating gives us $\int_{-\infty}^p dp' \partial_{p'} \frac{J_p(x,p',t)}{W} = \frac{J_p}{W} = C(x)$ which implies $\int dp J_p = C(x) \int dp W = C(x) \varrho(x, x, t)$. With $-\frac{dV}{dx} \varrho(x, x, t) = C(x) \varrho(x, x, t)$, from (1.14), it follows that $\nabla \cdot \mathbf{w} = 0$ implies

$$J_p + \delta J_p = -W \frac{\partial}{\partial x} [V(x) + \delta V(x)]. \quad (1.20)$$

We have shown that the application of Daligault's recipe filters through in a very

specific form: the dynamics becomes classical and the shift only affects the potential (since the goal is to not affect the time evolution of W). Strictly speaking, in Eq. (1.20), we should write $\delta V(x, W(x, p, t))$ to remind ourselves of Daligault’s assumption that δJ_p depends on W . But to yield Liouvillian dynamics δV must not depend on p ; hence $\delta V(x, W(x, p, t)) = \delta V(x)$.

For systems in which the potential can be globally Taylor expanded, Eq. (1.20) shows us that quantum terms must not be present in Eq. (1.10). To fulfill Liouvillian behavior for all times the potential V might be of “harmonic” form: $V = V_{\text{harmonic}} = \frac{K}{2}x^2 + ax + b$ with arbitrary real K , a , and b and, therefore, $\delta V = 0$.

Alternatively, the auxiliary field has the trivial form $\delta \mathbf{J} = \mathbf{j} - \mathbf{J}$ which subtracts all the quantum parts in Eq. (1.10), so that the potential assumes the form $V + \delta V = V_{\text{harmonic}}$. This is neither what Daligault intended nor is it helpful, in fact, it is not even permissible since such a field would not fulfill the condition $\nabla \cdot \delta \mathbf{J} = 0$.

One might wonder whether there is some other option, perhaps the anharmonic quantum terms $\mathbf{J} - \mathbf{j}$ in Eq. (1.10) are present but the initial state W_0 has some special form that cancels all anharmonic terms yet does not force the trivial form $V + \delta V = V_{\text{harmonic}}$ on us.

This cannot be though: if $J_p + \delta J_p$ fulfills Eq. (1.20), the dynamics is classical and anharmonic, shearing the phase-space distribution. Since a Wigner distribution can be expanded in the coherent-state basis, we assume, without loss of generality, that the initial state W_0 is a coherent state. Classically shearing a phase-space distribution bends it out of shape while keeping it positive, this violates the constraint that a positive Wigner distribution has Gaussian form [41]: anharmonic positivity-preserving classical dynamics is incompatible with quantum phase-space dynamics.

Generalizing Daligault’s recipe slightly: might modifications to the J_x component help? We doubt it, if the system is Hamiltonian; even if not quantum *mechanical* but, say, of the classical Kerr-oscillator type, one would, according to Eq. (1.18), still end up with Liouvillian dynamics: $\frac{d}{dt}W = 0$. W cannot change sign, Daligault’s recipe could never give us quantum dynamics, i.e., negativity formation in phase-space [68].

In their monograph on the Wigner representation, Zachos *et al.* [95] argue that anharmonic quantum systems cannot fulfill Liouville’s theorem since the difference between the Moyal and Poisson brackets is nonzero for anharmonic quantum systems. In light of Daligault’s speculation that a mapping to *another* system might exist, that reproduces the same dynamics and fulfills Liouville’s theorem, we feel the above proof with the explicit use of \mathbf{J} is needed to settle the matter.

Figure 1.1 shows that the divergence $\nabla \cdot \mathbf{w}$ becomes singular when $W = 0$. This

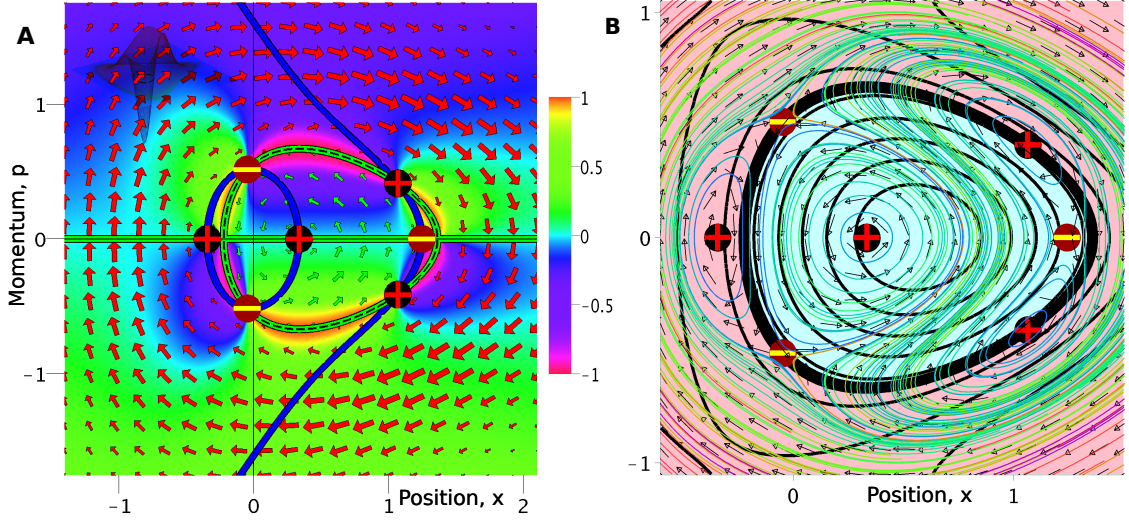


Figure 1.1: **A**, Singularities of $\nabla \cdot \mathbf{w}$ coincide with zeros of W . \mathbf{J} depicted by arrows (red for clockwise and green for inverted flow [83]), together with the zeros of the J_x and J_p components (green and blue lines, respectively), is superimposed on top of a color plot of $\frac{2}{\pi} \arctan(\nabla \cdot \mathbf{w})$. The inset shows the corresponding Wigner distribution for the first excited state of an anharmonic Morse oscillator [19] with potential $V(x) = 3[1 - \exp(-x/\sqrt{6})]^2$. The red crosses and yellow bars mark the locations of the flow's stagnation points, with Poincaré-Hopf indices [83] $\omega = +1$ and -1 . Parameters: $\hbar = 1$ and $M = 1$. The black dashed line marks the zero contour of the Wigner distributions (compare inset); here the divergence $\nabla \cdot \mathbf{w}$ is singular [68].

B, Integrated Fieldlines of \mathbf{J} cross Wigner Distribution Contours. Thin colored lines display fieldlines of \mathbf{J} , displayed together with normalized current $\mathbf{J}/\|\mathbf{J}\|$ (black arrows), and its stagnation points, for the same state as depicted in **A**. W 's zero contour, around the negative (light cyan-colored) patch at the center, is highlighted by a thick black line. Many fieldlines, for this first excited state, cut across the Wigner distribution's contours and enter and leave the negative area.

follows from Eq. (1.17). It indicates qualitatively that, since quantum states almost always have zero-lines [41], there will almost always be regions of singularities of $\nabla \cdot \mathbf{w}$. In this sense, the attempt to transform away non-Liouvillian behavior of quantum dynamics appears futile. Instead, such divergences explain certain numerical problems [68] and emphasize how very different quantum and classical phase-space dynamics are: whereas classical dynamics constitute one extreme ($\nabla \cdot \mathbf{w} = 0$ always), quantum dynamics (for anharmonic systems) constitute another ($|\nabla \cdot \mathbf{w}| = \infty$, almost always, somewhere in phase-space).

Since Eq. (1.7) features singular divergence of the velocity field one should perhaps stress quantum dynamics from the continuity equation point of view rather than referring to quantum Liouville equations.

1.6 Conclusion

We showed that the integral form of Wigner's representation of quantum mechanics should be consulted as an alternative to Moyal's formulation. It is more general than Moyal's form. If high order derivatives are present in Moyal's form, the integral form tends to converge better in numerical calculations, which can be implemented as FFTs. It can make mathematical manipulations more transparent than Moyal's form, and it displays symmetries between position and momentum configuration space more clearly.

Article 2

Anharmonical quantum systems do not feature trajectories

by

M. Oliva, D. Kakofengitis, O. Steuernagel [68]

2.1 Abstract

Phase space dynamics in classical mechanics is described by transport along trajectories. Anharmonic quantum mechanical systems do not allow for a trajectory-based description of their phase space dynamics. This invalidates some approaches to quantum phase space studies. We first demonstrate the absence of trajectories in general terms. We then give an explicit proof for all quantum phase space distributions with negative values: we show that the generation of coherences in anharmonic quantum mechanical systems is responsible for the occurrence of singularities in their phase space velocity fields, and vice versa. This explains numerical problems repeatedly reported in the literature, and provides deeper insight into the nature of quantum phase space dynamics.

2.2 Introduction and motivation

The phase space dynamics of classical conservative mechanical systems is described by the transport equations of Hamiltonian flow, along trajectories. For quantum mechanical systems this is only true for harmonic potentials, anharmonic quantum

mechanical systems do not transport quantum phase space distributions along trajectories.

This important fact is not appreciated by all: a number of incorrect schemes to model quantum dynamics using phase space trajectories have been devised [55, 15, 56, 36, 52, 77, 63, 53, 72, 21, 73, 20, 89, 94, 12, 79], leading to confusion [92, 54, 81, 93, 51, 49, 22, 80]. The schemes' failures have, in some quarters, given phase space representations of quantum mechanics an undeservedly poor standing [1].

Here we revisit the basic features of quantum dynamics in phase space [78, 95, 39] in order to identify concepts of classical dynamics that cannot be applied to quantum systems (recent reviews on quantum-classical methods can be found in [60, 32, 47]). Our analysis deepens our understanding of the behaviour of quantum dynamics in phase space. We show how the generation of quantum coherences renders quantum dynamics in phase space very different from classical dynamics.

In Section 2.3 we explain how phase space trajectories arise from solutions of first order differential equations as integral curves describing the transport of a density distribution.

In Section 2.4, we emphasize that quantum phase space-based studies [78, 39, 95] of quantum dynamics are no more involved than methods using von Neumann's equation to propagate the density matrix.

Section 2.5 emphasizes that a priori it is not clear whether quantum dynamics can be described using trajectories.

In Section 2.6 we show that anharmonic systems are described by evolution equations which are higher order differential equations, these generally do not permit a trajectory description but create quantum coherences; we additionally emphasize that harmonic systems cannot generate quantum coherences.

We explicitly prove in Section 2.7 that quantum phase space distributions with negative values (such as Wigner's distribution) cannot feature trajectories because the quantum analog of Hamilton's phase space velocity field becomes singular. We show why such singularities are *needed* to create quantum coherences.

The singularities affect numerical performance badly, see reference [61], in Section 2.8 we explain why, using a simple toy system.

Several misconceptions and incorrect conclusions drawn from ill-fated applications of the trajectory concept are reported in the literature. Some are examined in Section 2.9 in order to explain how they fail and to further illuminate differences between classical and quantum dynamics; before we conclude.

2.3 Continuity equation, trajectories, classical phase space flow and Liouville's theorem

The transport of a density $\rho(\mathbf{r}, t)$, where the initial density $\rho(\mathbf{r}, 0)$ and its current \mathbf{j} encode the boundary conditions, is governed by a continuity equation

$$\partial_t \rho(\mathbf{r}, t) + \nabla \cdot \mathbf{j}(\mathbf{r}, t) = 0 . \quad (2.1)$$

Here we write $\frac{\partial}{\partial t} = \partial_t$, $\mathbf{r} = \begin{pmatrix} \mathbf{x} \\ \mathbf{p} \end{pmatrix}$ parametrizes locations in phase space and $\nabla = \begin{pmatrix} \partial_{\mathbf{x}} \\ \partial_{\mathbf{p}} \end{pmatrix}$; we denote vectors in bold face, and ' \cdot ' stands for scalar product.

A time-dependent solution for ρ of the Eulerian type (integrated over a time-differential dt while keeping the position \mathbf{r} fixed), is of the form

$$\rho(\mathbf{r}, t + dt) = \rho(\mathbf{r}, t) - dt \nabla \cdot \mathbf{j} . \quad (2.2)$$

From a fluid dynamics perspective, the Eulerian approach tends to be in *conservation form* and its solutions therefore well behaved numerically.

2.3.1 Trajectories through Lagrangian decomposition

If the current factorizes as

$$\mathbf{j}(\mathbf{r}, t) = \rho(\mathbf{r}, t) \mathbf{v}(\mathbf{r}, t), \quad (2.3)$$

where \mathbf{v} is the velocity field, the continuity equation (2.1) can be rewritten in Lagrangian decomposition [23, 89, 20]

$$\frac{d}{dt} \rho = \partial_t \rho + \mathbf{v} \cdot \nabla \rho = -\rho \nabla \cdot \mathbf{v} . \quad (2.4)$$

If equation (2.4) is of first order in the derivatives, linear in ρ , and all quantities are mathematically well behaved, its solution allows for a trajectory-based description, in Lagrangian (or co-moving) transport form [20, 89]

$$\rho(\mathbf{r}_t, t) = e^{-\int_0^t d\tau \nabla \cdot \mathbf{v}(\mathbf{r}_\tau, \tau)} \rho(\mathbf{r}_0, 0) , \quad (2.5)$$

where *trajectories* are functions \mathbf{r}_t , parameterized by time t , arising through integra-

tion of \mathbf{v} starting from \mathbf{r}_0

$$\mathbf{r}_t(\mathbf{r}_0) = \mathbf{r}_0 + \int_0^t d\tau \mathbf{v}(\mathbf{r}_\tau, \tau). \quad (2.6)$$

Trajectories are integral curves describing the transport of a density distribution.

From a fluid dynamics perspective, the Lagrangian approach tends not to be in conservation form and its solutions therefore poorly behaved numerically.

From a mathematical perspective, solution (2.5) is found using the method of characteristics (also known as Lagrange-Charpit method) which requires the governing equation (2.4) to be of first order in its derivatives of ρ . For example, diffusion equations are of second order and do not admit trajectory-based solutions.

2.3.2 Liouvillian flow in conservative classical mechanical systems

The natural setting for the dynamics of a mechanical particle is its phase space [64]. In this work we discuss a particle with mass M moving in one dimension x only. The associated two-dimensional phase space is parameterized by vectors $\mathbf{r} = \begin{pmatrix} x \\ p \end{pmatrix}$, subject to a conservative hamiltonian $H = p^2/(2M) + V(x)$. In this case, the particle's phase space velocity

$$\mathbf{v}(\mathbf{r}) = \frac{d}{dt} \mathbf{r}_t = \begin{pmatrix} p/M \\ -\partial_x V(x) \end{pmatrix}, \quad (2.7)$$

encapsulates Newton's laws, and features volume preserving or 'Liouvillian' dynamics: $\nabla \cdot \mathbf{v} = 0$. As a function of \mathbf{r} only, \mathbf{v} is independent of time t and state $\rho(\mathbf{r}, t)$.

The Liouvillian nature of classical Hamiltonian current implies with $\nabla \cdot \mathbf{j} = \mathbf{v} \cdot \nabla \rho$, that the total derivative (2.4) is zero: the value of ρ , while the dynamics sweeps it along its trajectories, stays constant $\rho(\mathbf{r}_t(\mathbf{r}_0), t) = \rho(\mathbf{r}_0, 0)$. In this case, solution (2.5), viewed as the function $\rho(\mathbf{r}, t)$, through relabelling $\mathbf{r} = \mathbf{r}_t$, simplifies to the pull-back form

$$\rho(\mathbf{r}, t) = \rho \left(\mathbf{r} - \int_0^t d\tau \mathbf{v}(\mathbf{r}_\tau), 0 \right). \quad (2.8)$$

2.3.3 A simple system with non-Liouvillian flow that features trajectories

A free particle slowed down by friction $\dot{p} = -\gamma p$ is a classical system violating Liouville's theorem. With $p_t = p_0 e^{-\gamma t}$ and $x_t = x_0 + (1 - e^{-\gamma t})p_0/(m\gamma)$, Kramer's evolution equation $\partial_t \rho = [-p/m\partial_x + \gamma p\partial_p + \gamma]\rho$, where the diffusive Brownian motion term has been neglected, yields the trajectories-based solution of transport form (2.5)

$$\rho(x, p, t) = \exp[\gamma t] \rho_0\left(x - \frac{p}{\gamma m}(e^{\gamma t} - 1), p e^{\gamma t}\right). \quad (2.9)$$

The coefficient function $\exp[\gamma t]$ keeps this distribution normalized while the dynamics shrinks volumes uniformly across phase space: $\nabla \cdot \mathbf{v} = \nabla \cdot (p/m, -\gamma p) = -\gamma$.

2.4 Wigner's quantum phase space distribution

Attempts to understand and numerically approximate quantum dynamics of anharmonic systems has frequently relied on the concept of phase space trajectories in a way unsuitable for this task [55, 15, 56, 36, 52, 77, 63, 53, 72, 21, 73, 20, 89, 94, 12, 79]. This seems to be the reason for the fatigue expressed by fellow researchers who perceive the 'Wigner method' (and other phase space methods) as unsuitable for finding ways of reducing computational complexities [1].

We have not found a rigorous explanation for the supposed unsuitability of Wigner's representation of quantum mechanics. In the general case it is not justifiable since *"All calculation methods scale in proportion to the volume of phase space that the molecular encounter occupies. Therefore, phase space is a common denominator by which different methods of calculation can be compared and the feasibility of the calculation estimated."* [48]

Recent work shows that the propagation of the Wigner distribution is suitable for the study of quantum dynamics of anharmonic systems [13] and that its study provides new valuable insight [47].

A quantum state's density matrix $\varrho(x, x', t) = \langle x|\hat{\varrho}(t)|x'\rangle$, can equivalently be described by Wigner's phase space-based quantum distribution $W(x, p, t)$ [91, 38, 95, 17], both are based in spaces of equal dimension:

$$W_\varrho(x, p, t) \equiv \frac{1}{\pi\hbar} \int_{-\infty}^{\infty} dy e^{-\frac{2i}{\hbar}py} \langle x+y|\hat{\varrho}(t)|x-y\rangle. \quad (2.10)$$

W can numerically be generated quickly through fast Fourier transforms of ϱ .

W is real-valued (unlike ϱ), non-local (through y), and normalized

$$\int_{-\infty}^{\infty} \int_{-\infty}^{\infty} dx dp W(x, p, t) = 1.$$

Generally, the Wigner distribution has negative patches [41], like many other quantum phase space distributions [38], this will be important for part of our discussion, in Section 2.7.

Specifically, Wigner’s distribution is set apart from other quantum phase space distributions [38] by the fact that only Wigner’s simultaneously yields the correct projections in Schrödinger’s position $\varrho(x, x, t) = \int_{-\infty}^{\infty} dp W(x, p, t)$ and momentum representation $\tilde{\varrho}(p, p, t) = \int_{-\infty}^{\infty} dx W(x, p, t)$, while maintaining its form (2.10) when evolved in time and giving the overlap between states in the simple form $|\langle \psi_a | \psi_b \rangle|^2 = 2\pi\hbar \int_{-\infty}^{\infty} dx \int_{-\infty}^{\infty} dp W_a W_b$. Finally, the Wigner distribution’s averages and uncertainties evolve momentarily classically [76, 6]. W is considered the “*closest quantum analogue of the classical phase-space distribution*” [97].

For specificity we choose Wigner’s distribution for our discussions of quantum phase space behaviour. Most of our results apply to other quantum phase space distributions as well; the proof in section 2.7 explicitly applies only to those [38] that have negative patches in phase space.

2.5 Trajectories in quantum systems

Note that by trajectories we mean integral curves that obey the equations of motion, we neither discuss paths (which do not have to follow equations of motion) nor center-of-mass trajectories as discussed by Heisenberg [34].

A priori it is not clear that one must not use trajectories for quantum phase space descriptions of anharmonic systems.

Heisenberg’s uncertainty principle is at times interpreted to mean that quantum mechanics does not allow for a trajectory-based description. This interpretation is incorrect:

Phase space trajectories are a fruitful mathematical device for the description of quantum dynamics of a system if the potential is of the quadratic form (2.14). This statement applies to non-dissipative systems, even driven ones. For such systems the trajectory-description (2.8) (for W rather than ρ) applies. Using trajectories, which in this case follow the classical law (2.7), is in fact simpler and, in this sense, even superior to the use of standard Schrödinger wave function propagators, see Takabayasi in Ref. [85] p. 352.

Bohm's representation of quantum theory uses configuration space trajectories [58, 37] and these have experimental relevance [46].

The concept of paths has been fruitful in path-integral formalisms applied to configuration or phase space.

Semiclassical methods employ classical trajectories along which quantum objects are carried [35, 88, 8].

When trajectory techniques can be implemented for quantum dynamical phase space studies they permit us to launch large numbers of trajectories while allowing us to efficiently parallelize computer code [61, 89].

In what follows, we will, however, see that in anharmonic quantum systems the divergence of the velocity field in phase space is non-zero. One might still hope to describe the propagation of W in phase space by Eq. (2.5) [or Eq. (2.19)]. But it turns out that the divergence of the quantum mechanical velocity field in phase space is singular, see Section 2.7 and Fig. 2.2 (c). This cannot be avoided [44], and therefore we can explicitly prove, by contradiction, that trajectories do not exist globally for systems whose phase space distributions can develop areas with negative values, see Section 2.7.

2.6 Time evolution of the Wigner distribution

The time evolution of $W(x, p, t) = W(\mathbf{r}, t)$ is given by the Eulerian continuity equation [91]

$$\partial_t W(\mathbf{r}, t) = -\nabla \cdot \mathbf{J}(\mathbf{r}, t) . \quad (2.11)$$

Generally, the Wigner current \mathbf{J} has an integral representation [91, 38, 5, 44], but for potentials $V(x)$ that can be Taylor-expanded, giving rise to finite forces only, \mathbf{J} is of the Moyal form [91, 62]

$$\mathbf{J} = \begin{pmatrix} J_x \\ J_p \end{pmatrix} = \mathbf{j} + \begin{pmatrix} 0 \\ -\sum_{l=1}^{\infty} \frac{(i\hbar/2)^{2l}}{(2l+1)!} \partial_p^{2l} W \partial_x^{2l+1} V \end{pmatrix} . \quad (2.12)$$

Here, with $\mathbf{j} = W\mathbf{v}$, $\mathbf{J} - \mathbf{j}$ are the 'quantum correction' terms.

Fieldlines of Wigner current are well defined and their depiction has helped to reveal the topological charge conservation of \mathbf{J} 's stagnation points [83, 43].

In analogy to the classical Euler solution (2.2), the integration of the continuity

equation (2.11) yields

$$W(\mathbf{r}, t + dt) = W(\mathbf{r}, t) - dt \nabla \cdot \mathbf{J}, \quad (2.13)$$

which is in conservation form.

2.6.1 Formation of coherences and negativities of the Wigner distribution

The primary difference between classical and quantum states is the ability of a quantum particle to form non-local coherences (to be present in both holes of a double slit [25, 35]). Precisely these nonlocal coherences in configuration space are revealed by the Wigner distribution's negative patches [25] in phase space, and vice versa [57, 97, 30]. Coherences or negative patches can only be generated in anharmonic systems. Harmonic systems (and their isomorphic partners [82]) are of the quadratic form

$$\hat{H}_{quadratic}(\hat{x}, \hat{p}) = \frac{\hat{p}^2}{2M} + \frac{K}{2}\hat{x}^2 + a\hat{x} + b \quad (2.14)$$

(here K , a and b are any real constants). They can feature negative patches of the Wigner distribution only if these are inserted into the initial condition, $W_0(\mathbf{r})$, but they cannot *generate* them, see Eq. (2.19) below.

2.7 Singularities in the velocity field are needed: trajectories are ill-defined

We now prove that the Lagrangian transport form is ill-defined in the quantum case. Following references [23, 89, 20] we rewrite continuity equation (2.11) for W in Lagrangian decomposition (2.4)

$$\frac{dW}{dt} = \partial_t W + \mathbf{w} \cdot \nabla W = -W \nabla \cdot \mathbf{w} . \quad (2.15)$$

Here, the quantum phase space velocity field \mathbf{w} [23, 89, 20], corresponding to the hamiltonian velocity field \mathbf{v} , is

$$\mathbf{w} = \frac{\mathbf{J}}{W} = \mathbf{v} + \frac{1}{W} \left(- \sum_{l=1}^{\infty} \frac{(i\hbar/2)^{2l}}{(2l+1)!} \partial_p^{2l} W \partial_x^{2l+1} V \right). \quad (2.16)$$

\mathbf{w} is singular at zeros of W since, generally, zeros of W do not coincide with zeros of its derivatives [43].

For time-differentials dt , the formal solution of Eq. (2.15), written in pull-back form, like Eq. (2.8), has the transport form [20, 89]

$$W(\mathbf{r}, t + dt) = e^{-dt \nabla \cdot \mathbf{w}} W(\mathbf{r} - dt \mathbf{w}, t), \quad (2.17)$$

where the transport shift can be expressed via a translation using the convective operator $\mathbf{w} \cdot \nabla$

$$W(\mathbf{r} - dt \mathbf{w}, t) = e^{-dt \mathbf{w} \cdot \nabla} [W(\mathbf{r}, t)]. \quad (2.18)$$

We emphasize that the Lagrangian decomposition, although technically correct, splits up the well behaved expressions in the continuity equation (2.11) and in this way creates singularities in the evolution equation (2.15) and the exponents of its solution (2.17) and (2.18).

Following references [20, 89] we formally extend the integration in time for the transport form (2.17). To this end we temporarily assume that globally $W > 0$ in order to remove singularities in \mathbf{w} in Eq. (2.16) and that, additionally, W and V are of such a form that $|\nabla \cdot \mathbf{w}| < \infty$. We formally arrive at the integrated transport form [20, 89]

$$W(\mathbf{r}_t, t) = e^{-\int_0^t d\tau \nabla \cdot \mathbf{w}(\mathbf{r}_\tau, \tau)} W(\mathbf{r}_0, 0). \quad (2.19)$$

Trahan and Wyatt deduced [89] “*two important non-crossing rules that follow directly from Eq. [(2.19)]: (i) a trajectory cannot cross a surface on which the density is zero; (ii) the sign of the density riding along the trajectory cannot change.*”

Hudson’s theorem [41], however, shows that for anharmonic systems the Wigner distribution can at best be positive everywhere in phase space for one point in time only. Time evolution in an anharmonic potential immediately introduces zero-lines of W somewhere in phase space. At W ’s zeros the Picard-Lindelöf theorem is violat-

ed, integrals (2.6), (2.17), (2.18) and (2.19) do not exist globally. Therefore, the Lagrangian transport solution and trajectories \mathbf{r}_t do not exist across phase space.

In other words, Eq. (2.19) proves that bounded magnitude of $\nabla \cdot \mathbf{w}$ precludes sign changes in W along streamlines of \mathbf{w} .

This leads to one of our central results: *the singularities of \mathbf{w} are needed to create the negativities of W , i.e., they are needed to create quantum coherences* (Section 2.6.1).

2.7.1 The phase space velocity w is non-linear in W

In general, an evolution equation with higher order derivatives does not allow for trajectory-based solutions since it is neither of first order in derivatives nor linear in W , see Section 2.3.1. Forcing such an equation into Lagrangian decomposition (2.15) leads to equations (2.16) which burden us with spurious non-linearities in W : while $\mathbf{J}(W_a) + \mathbf{J}(W_b) = \mathbf{J}(W_a + W_b)$, in general $\mathbf{w}(W_a) + \mathbf{w}(W_b) \neq \mathbf{w}(W_a + W_b)$ and left and right hand side of Eq. (2.15) are also non-linear in W . This argument carries over to evolution equations [86, 90] of other quantum phase space distributions.

2.8 Short time integration of Eulerian and Lagrangian evolution equations –an analytically solvable case–

We now demonstrate that application of the Lagrangian decomposition (2.15) creates misleading analytical and numerical results, whereas the Eulerian approach gives correct results.

We use the harmonic oscillator groundstate $W_0(\mathbf{r}) = (\hbar\pi)^{-1} \exp[-(x^2 + p^2/\hbar^2)]$ as a globally positive initial state for a quartic oscillator $V(x) = Kx^4$, $K > 0$. Since it is not an energy eigenstate and all states have at least one zero at infinity, it immediately develops negativities [41].

We find that even in this case, where initially singularities of \mathbf{w} and $\nabla \cdot \mathbf{w}$ are absent, the Lagrangian approach fails, see Fig. 2.1.

A first order difference approximation of continuity equation (2.11), using a finite value for Δt , applied to $W_0(\mathbf{r})$, according to the Eulerian equation (2.13) gives the

single-step propagation approximation

$$W(\mathbf{r}, \Delta t) \approx W_0(\mathbf{r}) - \Delta t \nabla \cdot \mathbf{J} \quad (2.20)$$

$$= \left[1 + \Delta t \left(-\hbar^2 K x \partial_p^3 + \{4K x^3 \partial_p - \frac{p}{M} \partial_x\} \right) \right] W_0(\mathbf{r}). \quad (2.21)$$

Eq. (2.21) is illustrated in Fig. 2.1 (a). It confirms the immediate formation of negativities and that even the single-step approximation of the Eulerian equation (2.13) gives tolerable results. Repeated iteration of Eq. (2.21) yields successively better approximations of the true dynamics, see Fig. 2.1 (b).

We now show that the growth of the magnitude $|\nabla \cdot \mathbf{w}|$, at small values of W (even if $W_0 > 0$ everywhere), is so explosive that it renders the Lagrangian approach misleading, for any non-zero time-step Δt . We repeat calculation (2.21) using the transport form (2.17). In this case, for the same initial state W_0 , we get the Lagrangian single-step propagation approximation

$$W(\mathbf{r}, \Delta t) \approx W_0(\mathbf{r} - \Delta t \mathbf{w}) [1 - \Delta t 8\hbar^{-2} K x p], \quad (2.22)$$

$$\text{where } \mathbf{w} = \begin{pmatrix} p/M \\ -4K x^3 + \hbar^2 K x W^{-1} \partial_p^2 W \end{pmatrix}. \quad (2.23)$$

Equation (2.22) is incorrect, see Fig. 2.1 (c), it puts the Wigner distribution's negative patches into the wrong sectors in phase space and creates deep gashes in them, see Fig. 2.1 (d); these violate probability conservation.

We cross-checked these results, see Fig. 2.1 (b), using standard numerical Schrödinger function solvers, the ‘QuTiP’ programming suite [42] and a split-operator technique [13], confirming that only the Eulerian equation (2.21), see Fig. 2.1 (a), and iterations thereof, see Fig. 2.1 (b), give acceptable results.

Fig. 2.1 (d) shows that even for our initially positive state W_0 , the behaviour of \mathbf{w} is responsible for the stark deviation of the ill-defined Lagrangian transport form (2.17) from the correct Eulerian continuity equation's solution.

2.9 Misconceptions associated with phase space trajectories

2.9.1 There are no Wigner trajectories

In reference [55] Lee and Scully consider energy eigenstates (of the Morse potential) and argue that “*In terms of the Wigner distribution, it means that each phase space point should move in such a way that the Wigner distribution does not change in time. This consideration leads to the concept of ‘Wigner trajectories’, trajectories along which phase space points of the Wigner distribution move. For the case under consideration, Wigner trajectories must be trajectories along the surfaces on which the Wigner distribution takes on the same value, i. e., trajectories along the equi-Wigner surfaces. These Wigner trajectories are ‘quantum-mechanical’ trajectories in the sense that they represent paths of phase space points that move according to the quantum-mechanical equation of motion. They describe the exact quantum-mechanical dynamics in a phase space, whereas classical trajectories obviously yield only an approximate description of quantum dynamics*”[55].

It has been suspected before that this concept might be flawed, see e.g. [77, 22], here we provide a simple proof and a counterexample.

To disprove Lee and Scully’s assertion that for energy eigenstates of quantum systems $\mathbf{J} \cdot \nabla W = 0$, note that for eigenstates $\nabla \cdot \mathbf{J} = -\partial_t W = 0$, so, with $\mathbf{w} = \mathbf{J}/W$

$$\nabla \cdot \mathbf{w} = \frac{W \nabla \cdot \mathbf{J} - \mathbf{J} \cdot \nabla W}{W^2} = -\frac{\mathbf{J} \cdot \nabla W}{W^2}. \quad (2.24)$$

Therefore Lee and Scully implicitly assume that the flow is Liouvillian which we showed previously [44] to imply that no quantum terms are present in Eq. (2.12) for \mathbf{J} . This is incorrect for the Morse oscillator they studied [55].

We confirm our conclusion by a plot of fieldlines of \mathbf{J} (to which the velocity field \mathbf{w} , where it exists, is tangential) in Fig. 2.2 (b). This shows that Wigner current crosses W ’s contours, in other words, $\mathbf{J} \cdot \nabla W \neq 0$.

2.9.2 The Non-Crossing Rules do not apply

We have shown in Section 2.7 that the non-crossing rules by Trahan and Wyatt are artefacts of the use of the Lagrangian form (2.15).

Daligault also seems to invoke non-crossing rules when he states that for a region V_0 where the Wigner distribution has negative polarity, and $\nabla \cdot \mathbf{w} < 0$, “*the*

trajectories lying in this volume would condense and eventually collapse into a volume of zero volume. From the practical viewpoint, the set of initial trajectories modelling the whole initial region V_0 would eventually describe a tiny volume.” [20]

Lee and Scully’s argument [55] for ‘Wigner trajectories’, see section 2.9.1 above, also amounts to invocation of a non-crossing rule.

Section 2.9.1 and Fig. 2.2 (b) prove assertions based on Liouvillian flow and non-crossing rules incorrect. Instead of trajectories-based on the velocity field \mathbf{w} , fieldlines of Wigner current \mathbf{J} should be used, they are singularity-free and cross zero-contours of W [83, 43].

2.9.3 Misconceptions due to incorrect decomposition of the continuity equation

In equation (2.12) for \mathbf{J} the $l = 0$ -term is the classical force term rendering the dynamics, if truncated here, Liouvillian ($\nabla \cdot \mathbf{w} = 0$). The classical form also is *degenerate* in the sense that the current is zero wherever W is zero [43].

In the anharmonic quantum case this is typically not the case, since (lines of) zeros of the Wigner distribution do not imply that the current stagnates. Instead, this degeneracy in \mathbf{J} is lifted due to the quantum terms, of order $l \geq 1$ [43]. This implies that zeros of W are zeros of J_x but not of J_p . The quantum terms in (2.12) shift the lines of zero of J_p away from those of J_x . Only where those lines intersect do stagnation points of the current exist [43], see Fig. 2.2 (b) and (c). The stagnation points of the current therefore straddle the boundaries of negative regions of W where the current gets inverted [83, 43]. These stagnation points have special importance because they are topologically protected [83], and they display very large local variations of the direction of the current for non-zero values of the momentum p , a feature alien to classical Hamiltonian flows. These aspects of the stagnation points of Wigner current were found recently [83, 43] although precursors were observed in quantum phase space studies of Husimi’s function [81].

Incorrect use of Newton trajectories In reference [12] continuity equation (2.11) is decomposed into its classical term [with \mathbf{v} from Eq. (2.7)] and quantum term Q

$$\partial_t W + \mathbf{v} \cdot \nabla W = -\partial_p J_p - \partial_p W \partial_x V = Q . \quad (2.25)$$

This is an incorrect decomposition, the correct Lagrangian decomposition is given in equation (2.15). The authors then formally integrate this equation propagating their solutions along classical Newtonian trajectories (2.6), supposedly fully taking into account all quantum effects [12, 79]. This is only correct for quantum-mechanical cases whose hamiltonians have potentials up to second order in position x [85, 76, 12, 83, 82], in which case $Q = 0$. In the anharmonic case, the approach of references [12, 79] does not allow for the directional modifications of the current that is so characteristic for quantum dynamics (see [83, 43] and Fig. 2.2): the Newton trajectory approach is incorrect.

Incorrect total derivative decomposition Carruthers and Zachariasen [15] decomposed Wigner current according to $\frac{dW}{dt} = -\partial_p J_p$, the correct expression is $\frac{dW}{dt} = -W\partial_p w_p$, see equation (2.15).

The $\dot{p} = \partial_p J_p / \partial_p W$ decomposition error Lee [52] and Lee and Scully [55, 56, 53] incorrectly decomposed \mathbf{J} using the analogy with classical physics. Imposing the Liouvillian form

$$\partial_t W + \frac{p}{M} \partial_x W + \dot{p} \partial_p W = 0, \quad (2.26)$$

they concluded that, in the quantum case, $\dot{p} = \partial_p J_p / \partial_p W$. Their formal integration of this equation leads to incorrect results such as those detailed in Section 2.9.1.

This decomposition was criticized by Daligault [20], criticized and yet adopted by Sala *et al.* [77] and by Henriksen *et al.* [36] (who later concluded though that, based on numerical work, “*These studies showed a fatal degradation of the distribution function*” [61]). Decomposition (2.26) was also adopted by, e.g., Muga *et al.* [63], Razavy [72, 73], Dias and Prata [21], Zhang and Zheng [94], and reported by Landauer [51].

2.9.4 Can the non-zero divergence of the current be transformed away?

In Reference [44] we established that Wigner current obeys Liouville’s theorem only for systems with potentials at most quadratic in x .

Daligault asks whether one can find a transformation “*that would render Hamiltonian [divergence-free] quantum fluid dynamics in phase space*” [20]. Reference [44] proves this is not possible. Here we give an additional argument:

The idea of ‘transforming away’ the divergence in \mathbf{w} amounts to transforming away the quantum terms in \mathbf{J} [44] and is ill-conceived: according to equation (2.19), a divergence-free velocity field would not allow for a change of the value of W along a fieldline of \mathbf{J} . Since fieldlines are defined in all of phase space, negativities and quantum coherences could never form.

Based on an analysis different from Daligault’s, Sala *et al.* [77] argue that the ‘Wigner trajectories’ of Lee and Scully, see section 2.9.1, exist, that these trajectories follow the contours of W , and that along them $\frac{dW}{dt} = 0$. They modify and reinforce this statement by saying that “*Liouville’s theorem in the form of area preservation of a given contour of moving phase points is obeyed as long as the defined contour does not touch any of the singularities. The singularities are not only responsible for “destruction” of trajectories. They can also “create” them.*”[77]

We found here that for anharmonic oscillators \mathbf{w} is divergence-free only on lines (of measure zero) in phase space, see Fig. 2.2 (c). In other words, quantum phase space dynamics of anharmonic systems is non-Liouvillian almost everywhere in phase space. We have (other than for harmonic oscillator eigenstates and high-temperature thermal states) not seen evidence of fieldlines of \mathbf{J} following W ’s contours. The reported observation of the “creation or destruction” of trajectories at a singularity of \mathbf{w} might be due to careless numerics using an adaptive integrator.

2.9.5 There are no quantum potentials in phase space

The concept of Wigner trajectories was also used for the introduction of the concept of a “quantum potential” \tilde{V} [52] or “quantum force” \tilde{F} [72, 73]. The underlying idea is to identify the term \dot{p} in Eq. (2.26) with $\dot{p} = \tilde{F} = -\partial_x \tilde{V}$. Being based on an erroneous identification of terms in Eq. (2.26), it gives rise to incorrect and peculiar results such as a force with singularities [72, 73].

2.9.6 What about positive phase space distributions?

Proof (2.19) applies to all phase space quantum distributions with negative values, i.e., to the entire continuum of gaussian smeared distributions of which Husimi’s Q-function is the (positive semi-definite) limit [38].

Certain technical issues are tamed by using positive distributions such as Husimi’s Q-function [40] or some thermal Wigner distributions, but we doubt it changes the fundamental inadmissibility of the trajectory concept for positive distributions: to use trajectories one would have to find a transformation that removes the quantum terms

in (2.12) in order to render the equations first order in their derivatives and linear in W (Section 2.7.1). But the quantum terms are always present for anharmonic systems [38, 86, 90].

Particular non-trivial anharmonic systems with special states and special symmetries, admitting transformations to Lagrangian forms that simplify treatment, might exist. In general (and in light of failed attempts to find such transformations for W [44]) suggestions [1] that evolution equations of non-negative quantum distributions for anharmonic systems might admit trajectory-based representations appear implausible.

2.10 Conclusions

Quantum phase space dynamics has frequently been cast into Lagrangian form in order to represent its transport along trajectories. For anharmonic quantum mechanical systems this leads to a phase space velocity field \mathbf{w} with singularities and singular divergence $\nabla \cdot \mathbf{w}$. For anharmonic quantum systems transport-solutions, using trajectories, are mathematically ill-defined: trajectory-based approaches have to be avoided.

The occurrence of singularities of $\nabla \cdot \mathbf{w}$ in the anharmonic quantum case is *needed and responsible* for the generation of negativities in Wigner's quantum phase space distribution and thus for the generation of quantum coherences. This realization provides a deeper understanding of the differences between quantum and classical phase space dynamics (for which $\nabla \cdot \mathbf{w} = 0$). It also explains the frequently reported poor performance of numerical schemes employing trajectories in phase space.

Instead of studying quantum phase space dynamics from a Lagrangian trajectory approach it should primarily be studied from an Eulerian approach centered on Wigner's quantum phase space current \mathbf{J} . \mathbf{J} -fieldlines always exist and they reveal intriguing detail [83, 43].

An interesting open question [1] is: how stable are entangled-trajectories methods [23, 24, 22]?

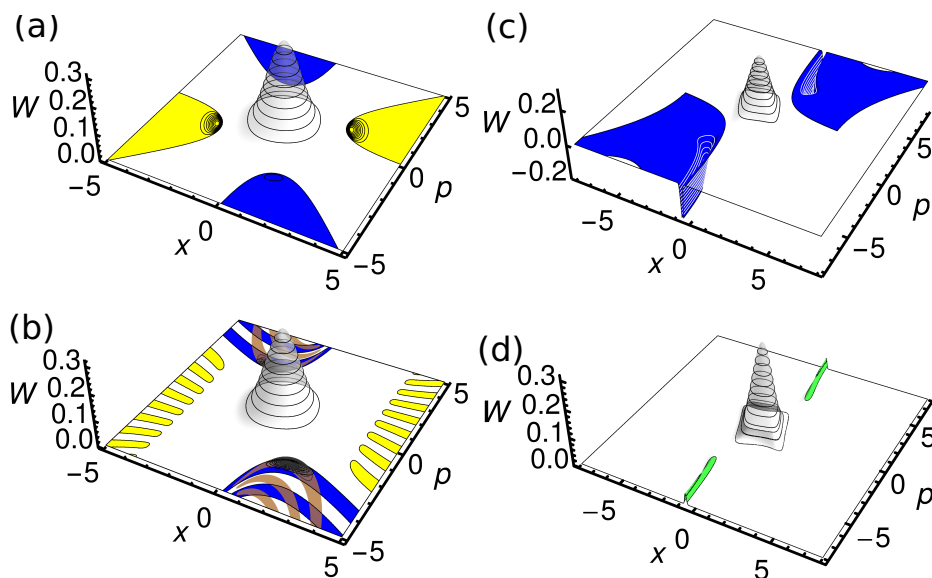


Figure 2.1: Initially positive Wigner distribution W evolved in Eulerian form (a) and (b) or Lagrangian form (c) and (d). (a), the single step propagation of W_0 with $\hbar = 1, M = 1, V = x^4$, and $\Delta t = 10^{-2}$, using the Eulerian solution (2.21), shows correct formation of negativities as blue patches in phase space. However, due to the crude nature of the first order difference approximation (2.20) of the Δt -step employed in this illustration, spurious negative classical transport patches form, shown in yellow. (c), essentially the same scenario as (a) (for explicitness we chose a longer time of $\Delta t = 5 \times 10^{-2}$) is displayed using the Lagrangian transport form (2.22): deep, unphysical gashes form due to the singularities in \mathbf{w} in (2.23). (b), using a twelve step iteration of the Eulerian solution (2.21), while reducing the time step per iteration to $10^{-2}/12$, we end up with a better approximation than in (a): W 's negativities (blue patches) persist and develop fringes, whereas the unphysical (yellow) classical patches recede. This is confirmed by an exact numerical integration (brown overlay). (d), the transport shift form (2.18), for the same scenario as (c), displays unphysical formation of humps highlighted in green, their positions confirm that the singularities of \mathbf{w} create the deep gashes in (c).

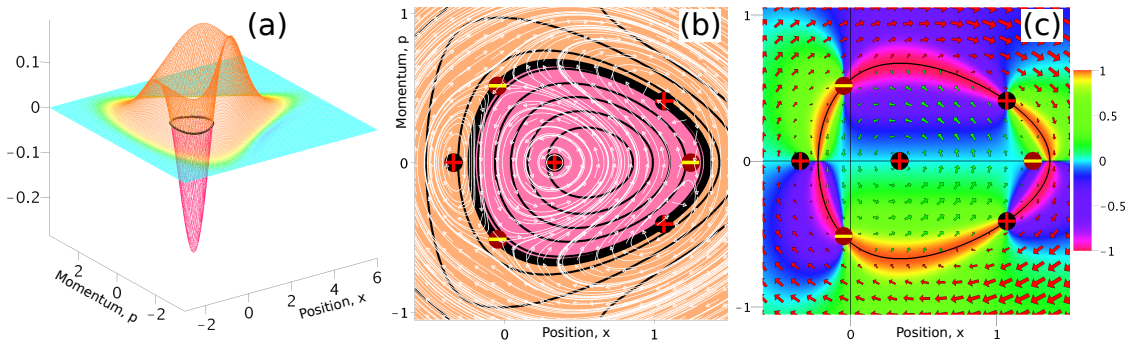


Figure 2.2: (a) The Wigner distribution for the first excited state of an anharmonic Morse oscillator [19] with potential $U(x) = 3(1 - \exp(-x/\sqrt{6}))^2$ (parameters: $\hbar = 1$ and $M = 1$) is depicted by its black contour lines in (b). W 's thick zero contour (black line in (a)) separates the negative central patch from the surrounding positive area in (b): Red crosses and yellow bars mark the locations of \mathbf{J} 's stagnation points, with Poincaré-Hopf indices [83] $\omega = +1$ and -1 , respectively. Integrated fieldlines of \mathbf{J} are depicted as thin white lines, displayed together with normalized current \mathbf{J}/J (white arrows). \mathbf{J} -fieldlines, cut across the Wigner distribution's contours and enter and leave the negative area. (c) shows $\frac{2}{\pi} \arctan |\nabla \cdot \mathbf{w}|$ and illustrates that \mathbf{w} is Liouvillian only on lines in phase space (cyan coloring) while featuring singular behaviour where $W = 0$ (thin black line). Red arrows depict regular and green arrows inverted [83] current \mathbf{J} .

Article 3

Structures far below sub-Planck scale in quantum phase space through superoscillations

by

M. Oliva, O. Steuernagel [65]

3.1 Abstract

In 2001, Zurek derived the generic minimum scale a_Z for the area of structures of Wigner's quantum phase distribution. Here we show by construction, using superoscillatory functions, that the Wigner distribution can locally show regular spotty structures on scales much below Zurek's scale a_Z . The price to pay for the presence of such structures is their exponential smallness. For the case we construct there is no increased interferometric sensitivity from the presence of patches with superoscillatory structure in phase-space.

3.2 Introduction

Based on the concept of interferences in phase-space [78], Zurek established that the minimum scale a_Z for the area of structures of quantum phase distributions can, for one-dimensional quantum systems, be as small as $a_Z \approx \hbar^2/A$, where A is the action representing the area of support of a system's Wigner distribution [91]. This was

surprising [97], since Heisenberg’s uncertainty principle was interpreted to limit the area of spots in phase-space to approximately $\hbar/2$.

When a bandwidth-limited signal contains segments which oscillate faster than what its spectrum suggests, it “superoscillates” [9].

Superoscillations have first been noticed in physics in the framework of weak measurement by Aharonov et al. [2], and then studied in detail by Aharonov et al. [3], Berry et al. [9, 11], and others [14]. They have since been used experimentally, for example in super-resolution microscopy [75].

Translated to quantum phase-space: Wigner distributions can show regular spotty structures much below Zurek’s scale a_Z ; but such states cannot obviously be exploited for higher resolution in measurements.

3.3 Zurek’s fundamental phase-space tiles

The Wigner distribution of a “Schrödinger’s cat” state of squeezed states $G(x, p) = (\pi\hbar)^{-1}e^{-x^2/\xi^2 - \frac{p^2\xi^2}{\hbar^2}}$, with squeezing parameter ξ , is

$$W(x, p) = \frac{G(x - \Delta x, p) + G(x + \Delta x, p)}{2} \quad (3.1a)$$

$$+ G(x, p) \cos\left(\frac{2p}{\hbar}\Delta x\right). \quad (3.1b)$$

Zurek’s compass state is a coherent sum of two Schrödinger’s cat states rotated by $\pi/2$ with respect to each other. Starting from such compass states, Fig. 3.1 (a), Zurek showed that “Wigner functions can, and generally will, develop phase-space structures on scales as small as, but not generally smaller than” [97]

$$a_Z = \frac{h}{P} \times \frac{h}{L} = \frac{h^2}{A}. \quad (3.2)$$

Here, P and L are the phase-space distances between the squeezed states along the momentum and position axes respectively.

The Zurek scale a_Z is, e.g., the phase-space area of one fundamental tile [97] (“Zurek tile”) associated with a compass state, highlighted in Fig. 3.1 (a).

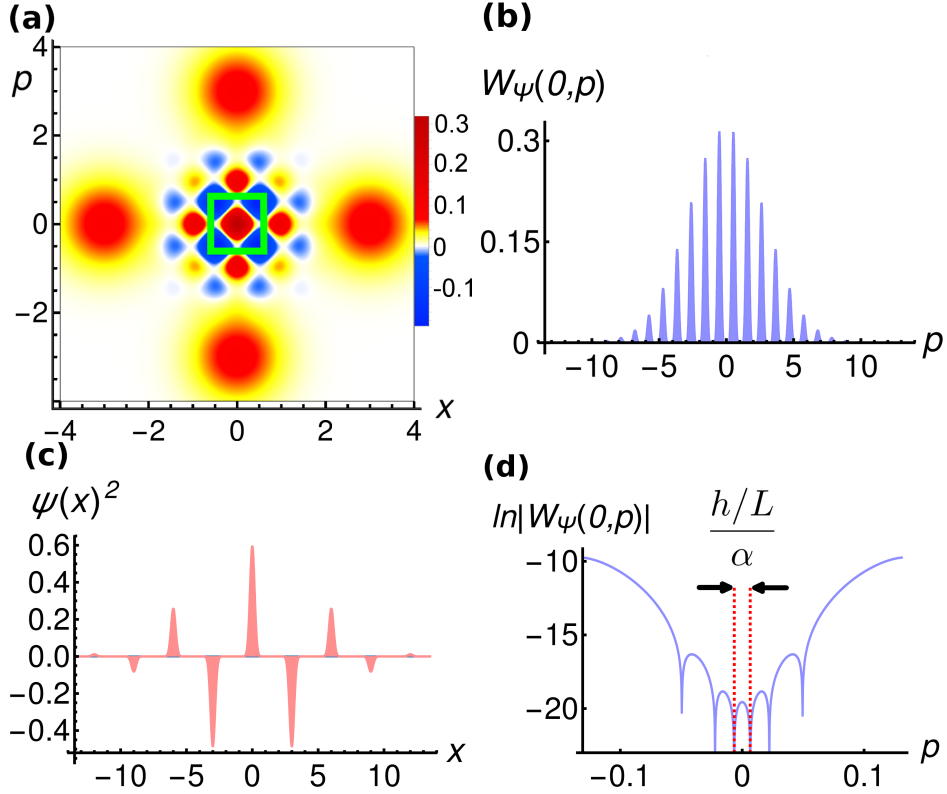


Figure 3.1: **(a)** shows a cross state [97] for $L = P = 6$ and $\xi = 1$ (atomic units [a.u.], $\hbar = 1$, are used in all figures), the green frame borders its Zurek tile with area a_Z . **(b)**, **(c)** and **(d)** are obtained using $N = 8$, $\alpha = 10$, $\xi = \frac{1}{4}$, $\Delta x = 3$ and $\hbar = 1$. **(c)** shows the squared wave function $\Psi(x)^2$ and its sign changes due to the complex coefficients in $\Psi(x)$ [Eq. (3.5)]. **(b)** shows $W_\Psi(0, p)$, and **(d)** the logarithm of $|W_\Psi(0, p)|$ near the origin, in a panel of width $h/L \approx 0.26$, in which the two red dashed lines bracket superoscillatory structure of length $\frac{h/L}{\alpha} = \frac{h/L}{10}$ [see Eq. (3.7)].

3.4 The superoscillating cross-state

Inspired by Zurek's compass state, we construct a "cross-state" featuring superoscillations in quantum phase-space. This state features small patches with regular structures on scales much smaller than a_Z , Fig. 3.2.

We use the superoscillating function [3, 9, 11]

$$f(x) = (\cos(x) + i\alpha \sin(x))^N, \quad \alpha > 1, \quad N \in \mathbb{N}. \quad (3.3)$$

For $\alpha = 1$, $f(x) = e^{iNx}$ is a regular plane wave. For $\alpha > 1$ and $N \gg 1$, $f(x)$ becomes superoscillatory [see Fig. 3.1 (d)]

$$f(x) = \sum_{j=0}^N C_j(N, \alpha) e^{i(N-2j)x}, \quad (3.4)$$

where $C_j(N, \alpha) = (-1)^j \binom{N}{j} (\alpha + 1)^{N-j} (\alpha - 1)^j / 2^N$ are the Fourier coefficients [3].

To map $f(x)$ of Eq. (3.4) into phase-space, we use a superposition of suitably pairwise-displaced squeezed states $S(x) = (\pi\xi^2)^{-1/4} e^{-x^2/(2\xi^2)}$ [see Eq. (3.1)], to form

$$\Psi(x) = \Phi_0(x) + \frac{1}{\sqrt{2}} \sum_{\substack{j=-N/2 \\ j \neq 0}}^{N/2} (-i)^j \Phi_j(x), \quad (3.5)$$

where $\Phi_j(x) = K_j S(x - j\Delta x)$, $K_j = \sqrt{|D_j| / \sum_{l=0}^{N/2} D_l}$

$$\text{and } D_j = \begin{cases} C_{N/2} & \text{if } j = 0 \\ C_{N/2+j} + C_{N/2-j} & \text{if } j \neq 0 \end{cases}.$$

Here, N is even and Ψ contains $N + 1$ spikes, see Fig. 3.1 (c). The associated Wigner distribution W_Ψ contains a suitable combination of plane wave terms [Eq. (3.1b)] to emulate $f(x)$ of Eq. (3.4), see Fig. 3.1 (d).

An incoherent sum of two such Wigner distributions, rotated by $\pi/2$ with respect to each other, forms the desired cross-state $W_+(x, p) = [W_\Psi(x, p) + W_\Psi(-p, x)]/2$. This balanced mixed state features superoscillatory structures within Zurek tiles, on sub-Zurek scales [Fig. 3.2 (a)-inset, (b) and (c)].

One could use a coherent sum to form a cross, but this would lead to greater complexity in Fig. 3.2, which is unnecessary to illustrate our construction.

3.5 Substructures within Zurek tiles

The area of sub-Planck structures of non-superoscillating states is limited by a_Z [97]. Now we show that regular structures on scales much smaller than a_Z can exist.

The local expansion of Eq. (3.3) around the origin has the local superoscillatory plane wave form

$$f(x) = e^{N \ln[\cos(x) + i\alpha \sin(x)]} \approx e^{iN\alpha x} e^{N\alpha^2 x^2/2}. \quad (3.6)$$

Therefore, the superoscillating Wigner distribution W_Ψ contains interference terms,

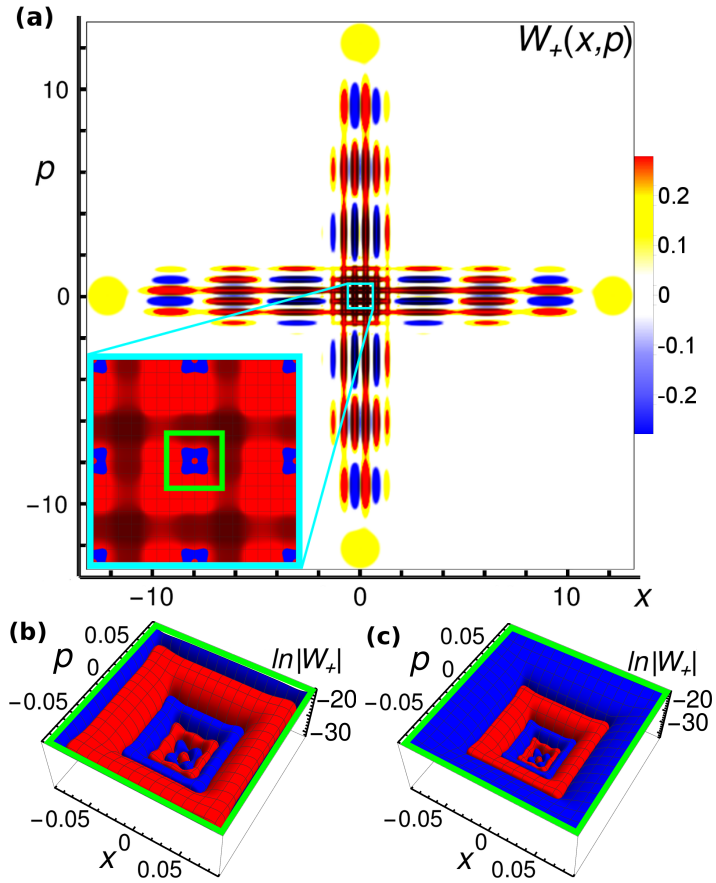


Figure 3.2: **(a)** Cross-state $W_+(x, p) = [W_\Psi(x, p) + W_\Psi(-p, x)]/2$ for $N = 4$, $\alpha = 6$, $\xi = 1$, and $\Delta x = 6$ ($\hbar = 1$, a.u.). In **(a)**'s inset and panels **(b)** and **(c)**, red (positive) and blue (negative) regions depict superoscillatory structures contained within Zurek tiles (green frames). **(b)** and **(c)** show $\ln |W_+(x, p)|$ and demonstrate the scaling with a_{SO} , see Eq. (3.7). State parameters $N = 12$, $\xi = \frac{1}{4}$, $\Delta x = 3$, with $\alpha = 10$ in **(b)**, and $\alpha = 16$ in **(c)**, respectively.

equivalent to expression (3.1b), proportional to $\cos(\frac{2p}{\hbar} \frac{N\Delta x}{2} \alpha) = \cos(p \frac{L}{\hbar} \alpha)$. Thus for W_+ , analogously to Zurek's scale a_Z in the cross state Fig. 3.1 **(a)**, superoscillatory structures with α -fold reduced length scales, Fig. 3.1 **(d)**, yielding areas on the scale of

$$a_{SO} \approx \frac{\hbar/P}{\alpha} \times \frac{\hbar/L}{\alpha} \approx \frac{a_Z}{\alpha^2} \quad (3.7)$$

arise.

For these superoscillatory structures to show, the 'overspill' from the two adjacent squeezed states Φ_{-1} and Φ_{+1} has to be so small that their Wigner distributions obey

$$W_{\Phi_{-1}}(0, 0) + W_{\Phi_{+1}}(0, 0) \ll |W_\Psi(0, 0)|. \quad (3.8)$$

3.6 Conclusion

We remind the reader of the fact that a quantum wave function cannot be *strictly* “bandwidth-limited”, simultaneously in position and momentum. Our Wigner distributions are confined by a finite area A in phase-space, yet they feature regular sub-Zurek scale structures, in this sense they are superoscillating.

Zurek’s compass states provide interferometric sensitivity at the Heisenberg limit. As Fig. 3.1 (c) illustrates, our superoscillating states change, under tiny displacements in x , p and t , in essentially the same way as regular compass states; they therefore do not perform better at the detection of small shifts or rotations.

At this stage, the formation of structures below the Zurek scale using superoscillations in phase-space is primarily a surprising curiosity. Superoscillating regions are known to be tiny in extent and amplitude [11, 3, 14]. This is why our superoscillating states cannot show sensitivity below the Heisenberg limit.

We have shown, to paraphrase Zurek’s statement cited above, that phase-space structures are frequently as small as, but not generally smaller than a_Z . Yet, superoscillating states can generate localized small patches with regular structures on very much smaller scales.

An interesting open question raised by the existence of sub-Planck and sub-Zurek scale phase-space structures concerns their potential effects on simulations. Possibly, grids finer than commonly assumed for numerical calculations [48] have to be used.

Article 4

Dynamical shear suppression in quantum phase space

by

M. Oliva, O. Steuernagel [67]

4.1 Abstract

Classical phase space flow is inviscid. Here we show that in quantum phase space Wigner's probability current \mathbf{J} can be effectively viscous. This results in shear suppression in quantum phase space dynamics which enforces Zurek's limit for the minimum size scale of spotty structures that develop dynamically. Quantum shear suppression is given by gradients of the quantum terms of \mathbf{J} 's vorticity. Used as a new measure of quantum dynamics applied to several evolving closed conservative 1D bound state systems, we find that shear suppression explains the saturation at Zurek's scale limit and additionally singles out special quantum states.

4.2 Main text

The differences between quantum and classical evolution are best investigated in phase space [29]. It is known that quantum evolution in phase space does not obey Liouville's theorem of volume conservation [62, 68] and that there is no velocity field in quantum phase space [68] (and therefore no flow). It is less clear why there is no quantum chaos [98, 16, 99, 29, 28].

Here we show that the effective viscosity of quantum phase space dynamics entails a shear suppression mechanism which fundamentally differentiates quantum from classical dynamics. This observation explains, amongst other things, the absence of quantum chaos.

We consider dynamics in 1D closed conservative systems with spatial coordinate x and momentum p . As initial states we use displaced Gaussians

$$W_0(x, p, x_0, p_0) = (\pi\hbar)^{-1} \exp[-(x - x_0)^2 - (p - p_0)^2/\hbar^2]$$

which are positive [41] and therefore ‘classical’.

A classical probability distribution $\rho(x, p, t)$ evolves, after sufficient time t , thinly stretched out threads, see Fig. 4.1 (c). Generally, structures of ρ become progressively finer as time progresses [97], particularly chaotic systems develop very fine structures quickly [10, 97, 64, 18].

Wigner’s quantum phase space distribution $W(x, p, t)$ [91, 38] is the closest quantum analogue [97, 68] of the classical phase space distribution ρ . Quantum evolution creates negative regions (blue, delineated by dashed lines at $W = 0$, see Fig. 4.1) [in all figures atomic units $\hbar = 1$ and $M = 1$ are used (see Section 4.3.5)]. These negative regions represent the existence of quantum coherences [25, 57, 97, 68] and Section 4.3.6.

Interference in phase space [78] is a property built into quantum phase space functions, such as W , through the Wigner-Moyal mappings [91, 62] between Hilbert space operators and their quantum phase space images [71, 33]. This interference limits the fineness of spotty structures that W can have to Zurek’s phase space area scale [97]

$$a_Z = \frac{\hbar}{P} \frac{\hbar}{L} = \frac{2\pi}{K_x} \frac{2\pi}{K_p} \quad (4.1)$$

(see Fig. 4.1 (b) and Fig. 4.1 (d)). Here \hbar is Planck’s constant, and length L and momentum P are W ’s spread in phase space and thus the area LP (measured in units of action) to which it is confined. The maximal wave-numbers associated with W ’s structures in x and p are, respectively, $K_x = P/\hbar$ and $K_p = L/\hbar$ [97] (see Ref. [65] for exceptions). Over time states develop spotty structures which saturate on the Zurek scale a_Z [97].

Here we show that the adherence to Zurek’s scale limit in the evolution is best understood in terms of the viscosity of the Wigner current \mathbf{J} [91, 83, 44, 68].

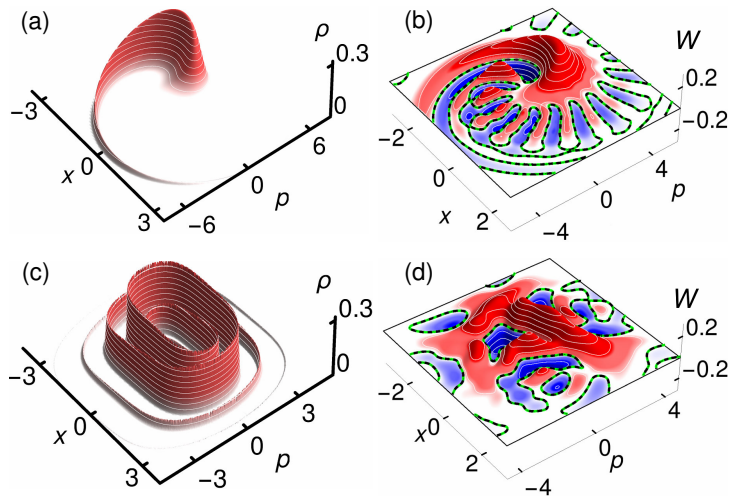


Figure 4.1: *Comparison between classical and quantum distributions in phase space.* For short times quantum evolution resembles classical evolution, compare (b) to (a). But for long times, since quantum evolution creates less fine structures than classical evolution [8, 97], their outcomes differ very substantially, contrast (d) with (c). A weakly excited initial state $W_0(x, p, 1.5, 0)$ is propagated in the soft potential $V_V = 31x^2/10 - x^4/81$ for time $t = 50$, under, (a), classical evolution and, (b), quantum evolution. Similarly, the state $W_0(x, p, 2, 0)$ is propagated in the hard potential $V_U = (x/2)^4$ for time $t = 25$, under, (c), classical and, (d), quantum evolution.

\mathbf{J} is the quantum analogue of the classical phase space current $\mathbf{j} = \rho \mathbf{v}$ which transports the probability density $\rho(x, p, t)$ according to Liouville's continuity equation $\partial_t \rho = -\nabla \cdot \mathbf{j}$. Here \mathbf{v} is the classical phase space velocity $\mathbf{v} = (p/M, -\partial_x V(x))$, M the mass of the particle and $V(x)$ the potential.

Over time ρ gets sheared since \mathbf{v} creates non-zero gradients of its angular velocity across energy shells. The classical Hamiltonian phase space flow is inviscid as \mathbf{v} is independent of ρ . Thus no terms suppress the effects of the angular velocity gradients, and so, as time progresses, non-singular probability distributions in phase space get sheared into ever finer filaments (see Fig 4.1 (c)).

We define classical phase space shear as (see Section 4.3.5)

$$s(x, p; H) = \partial_{\widehat{\nabla}_H} (-\nabla \times \mathbf{v}) = \partial_{\widehat{\nabla}_H} (\partial_p v_x - \partial_x v_p), \quad (4.2)$$

using the directional derivative across energy shells $\partial_{\widehat{\nabla}_H}$, formed from the normalized gradient $\widehat{\nabla}_H = \nabla H / |\nabla H|$ of the Hamiltonian H .

The sign convention with the negative curl in s in Eq. (4.2) was chosen to yield a positive sign for *clockwise* orientated fields since this is the prevailing direction of the classical velocity field \mathbf{v} . This choice yields $s > 0$ for hard potentials (potentials

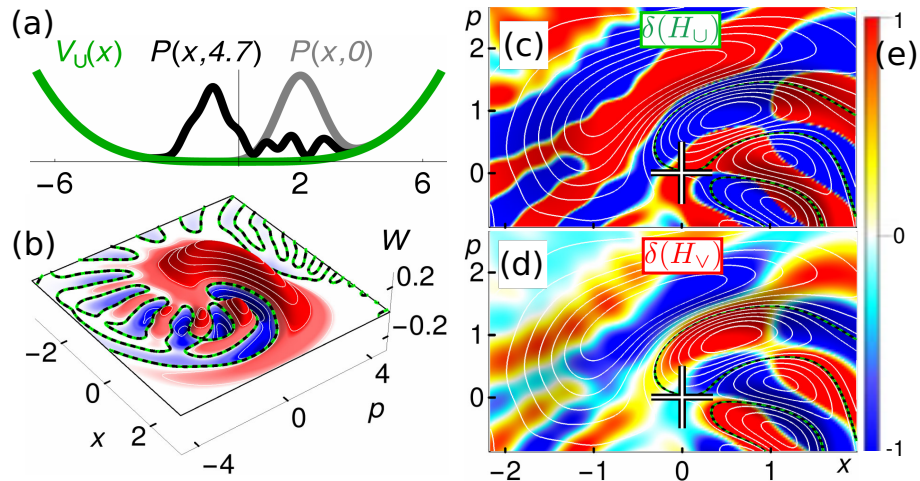


Figure 4.2: *Polarization of the vorticity δ and inversion of this polarization.* The comparison between (c) and (d) shows polarization inversion. (a), sketch of hard potential $V_U = (x/2)^4$ together with probability distributions $P(x, t) = |\Psi(x, t)|^2$ (black curve) of state evolved in V_U from initial Gaussian state $P(x, 0)$ (grey curve) at initial center position $x = 2$. The Wigner distribution W of a Glauber coherent state $\Psi(x, 4.7)$ in (a) is shown in (b). White contours of W [the origin $(x, p) = (0, 0)$ is labelled by a white cross] are overlaid with colors [legend given in sidebar (e)] representing values of $\text{Tanh}[50 \delta(H_U)]$, (c), and $\text{Tanh}[50 \delta(H_V)]$, (d). For the hamiltonians H_V and H_U the same potentials as in Fig. 4.1 are used.

for which the magnitude of the force increases with increasing amplitude), since they induce *clockwise* shear, see Fig. 4.1 (c), $s = 0$ for harmonic oscillators and free particles, and $s < 0$ for soft potentials (potentials for which the magnitude of the force decreases with increasing amplitude), since they induce *anti-clockwise* shear, see Fig. 4.1 (a).

The quantum continuity equation is [91, 68]

$$\partial_t W = -\nabla \cdot \mathbf{J} = -\partial_x J_x - \partial_p J_p, \quad (4.3)$$

where $\nabla = (\partial_x, \partial_p)$ is the gradient operator. Wigner's current \mathbf{J} does not factorize like \mathbf{j} [68]. It has an integral representation, see [91, 44] and Section 4.3.4. If the potential $V(x)$ is smooth such that it can be expanded into a Taylor series, the

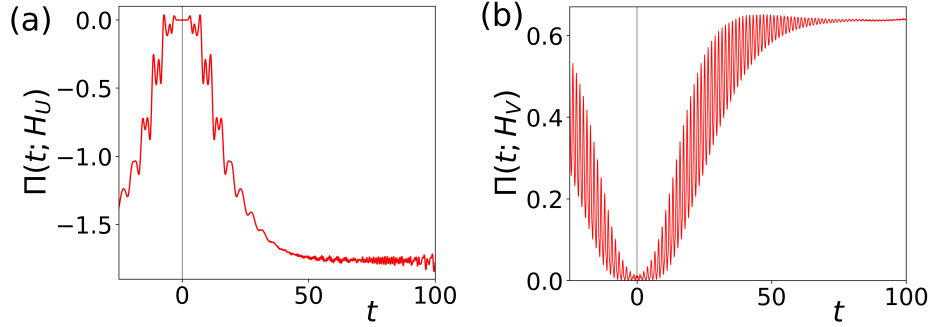


Figure 4.3: $\Pi(t; H)$ levels off over time as systems saturate. Π 's time evolution for, (a), initial state $W_0(x, p, 9, 0)$, for the hard potential $V_U = x^4/500$, and, (b), $W_0(x, p, 3, 0)$, for the soft potential $V_V = 31x^2/10 - x^4/81$. In accord with our sign-convention for Eq. (4.2) $\Pi(t; H_U)$ drops over time whereas $\Pi(t; H_V)$ rises, until the system saturates.

integral for \mathbf{J} can be determined explicitly as [91, 31, 62]

$$\mathbf{J}(x, p, t) = \mathbf{j} + \mathbf{J}^Q = W\mathbf{v} + \begin{pmatrix} 0 \\ J_p - j_p \end{pmatrix} \quad (4.4)$$

$$= W \begin{pmatrix} \frac{p}{M} \\ -\partial_x V \end{pmatrix} + \begin{pmatrix} 0 \\ -\sum_{l=1}^{\infty} \frac{(i\hbar/2)^{2l}}{(2l+1)!} \partial_p^{2l} W \partial_x^{2l+1} V \end{pmatrix}. \quad (4.5)$$

\mathbf{J} 's zeroth-order term in l is the classical term $\mathbf{j} = W\mathbf{v}$ (e.g. $J_p|_{l=0} = -W\partial_x V$). Terms of order $l \geq 1$ are the quantum correction terms $\mathbf{J}^Q = \mathbf{J} - \mathbf{j}$. They are only present for anharmonic potentials [44], which is why only anharmonic potentials create coherences. Harmonic systems' phase space dynamics is classical, see [68, 44] and Section 4.3.6.

The reaction of quantum dynamics to classical shear s has to reside in \mathbf{J}^Q . To extract it we form the vorticity of \mathbf{J}^Q

$$\delta(x, p, t; H) = -\nabla \times \mathbf{J}^Q = \partial_p J_x^Q - \partial_x J_p^Q. \quad (4.6)$$

δ 's sign distribution shows a pronounced polarization pattern, see for example Fig. 4.2 (c): specifically, on the positive main ridge of W (Fig. 4.2 (d)) δ tends to be positive on the inside (towards the origin) and negative on the outside. Because of this the outside is being slowed down while the inside speeds up. This polarized distribution of δ therefore counteracts the classical shear ($s_{V_U} > 0$) and can suppress it altogether.

The same applies to other positive regions of W , whereas for its negative regions the current \mathbf{J} tends to be inverted [83, 43] just as δ 's polarization pattern.

Switching the governing potential from hard, V_U , to soft, V_V (using the same state but different dynamics), reverses the classical shear, see Fig. 4.1. Accordingly, a reversal of the polarization pattern of Fig. 4.2 (c) occurs in Fig. 4.2 (d).

The distribution of δ 's polarization can be picked up with the directional derivative $\partial_{\nabla_H} \delta(t; H)$. This we multiply with W , because negative regions of W invert the current \mathbf{J} [83], and because we want to weight it with the local contribution of the state. The resulting measure for weighted shear polarization is $\pi(x, p, t; H) = W(t) \partial_{\nabla_H} \delta(t; H)$. Its average across phase space is W 's shear polarization

$$\Pi(t; H) = \langle\langle \pi(t; H) \rangle\rangle = \iint_{-\infty}^{\infty} dx dp \pi(x, p). \quad (4.7)$$

Initially $|\Pi(t)|$ rises on average and after a while levels off and settles, see Fig. 4.3.

We emphasize that the levelling-off behaviour of $\Pi(t)$ is in marked contrast to the classical case: in simple bound state systems the states never saturate, instead, for long enough times $\langle\langle \partial_{\nabla_H} (-\nabla \times \mathbf{j}) \rangle\rangle \propto t$ since $\rho(t)$ gets stretched out linearly into ever finer threads, see Fig. 4.1 (a) and Section 4.3.9.

In the quantum case the evolution's shear shrinks structures of W in size, but W 's minimal structures are forced to saturate due to the existence of Zurek's scale.

When a state saturates, the gradients in the quantum terms of \mathbf{J} become so large that they strongly quantum-suppress the classical shear inherent in \mathbf{J} . Where minimal structures of W have formed, this quantum shear suppression prevents finer minimal structures from developing: \mathbf{J} 's effective viscosity enforces the saturation of states at the Zurek scale.

When this happens $\Pi(t)$ has settled, see Figs. 4.3, 4.4 and 4.6.

To make explicit the connection between shear suppression $\Pi(t)$ and the saturation of systems at the Zurek scale we define W 's spatial frequency contents Ω as

$$\Omega(t) = \frac{\iint dk_x dk_p |\tilde{W}(k_x, k_p, t) k_x k_p|}{\iint dk_x dk_p |\tilde{W}(k_x, k_p, t)|} < 2K_X K_P, \quad (4.8)$$

where $\tilde{W}(k_x, k_p)$ is the 2D Fourier transform of $W(x, p)$. Since a state cannot only consist of structures at the Zurek scale Eq. (4.8) obeys the inequality $\Omega < \Omega_{\max} = \frac{8\pi^2}{a_z} = 2K_X K_P$, compare Eq. (4.1) and Section 4.3.8.

Fig. 4.4 demonstrates that for simple systems changes of the shear polarization $\Pi(t)$ can go hand-in-hand with those of the spatial frequency contents $\Omega(t)$. This estab-

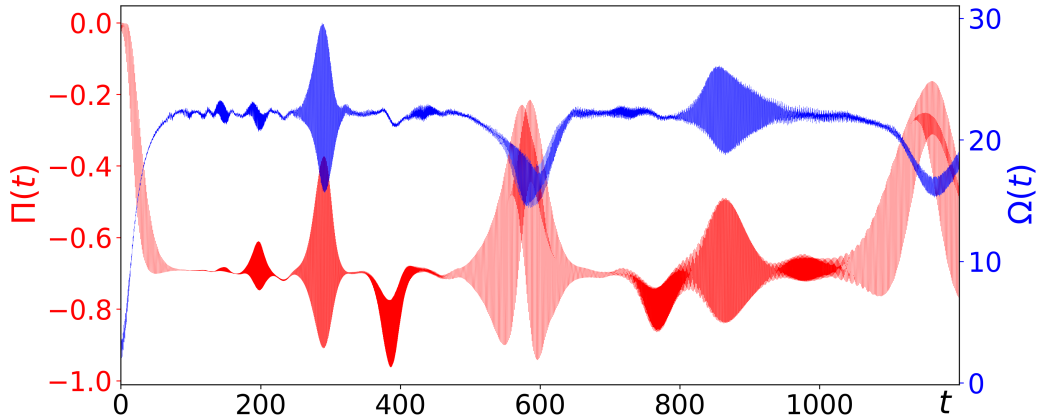


Figure 4.4: *Shear suppression $\Pi(t)$ and frequency contents $\Omega(t)$ can evolve similarly.* A gaussian state $W_0(x, p, 3, 0)$ is evolved in a hard potential $V_U = 31x^2/10 + x^4/81$. While $\Omega(t)$ rises (here, $\Omega_{\max} = 182.5$), as W develops fine structure, $\Pi(t)$ drops, since we consider a hard potential V_U . Both curves $\Pi(t)$ and $\Omega(t)$ level off at the time where W 's fine structures saturate at the Zurek scale. Here the oscillations around the respective mean values for saturated systems are due to the formation of special (partial revival) states [4, 74], for details see Fig. 4.6 and Section 4.3.3.

lishes that shear suppression constitutes the mechanism by which quantum dynamics conforms with interference in phase space.

Interestingly, both measures single out special states: those states for which the values of Π and Ω deviate from the typical saturated system states' values. In the case of weakly excited single well bound state systems the special states happen to be partial-revival states [4, 74], see Fig. 4.6. Some details of Fig. 4.4 can be understood from the observation that even partial-revival states feature more symmetric interference patterns, which lowers their frequency contents Ω , when compared with odd partial-revival states.

We emphasize that Π and Ω can measure aspects of the dynamics very differently from each other, see Section 4.3.11 for an illustration.

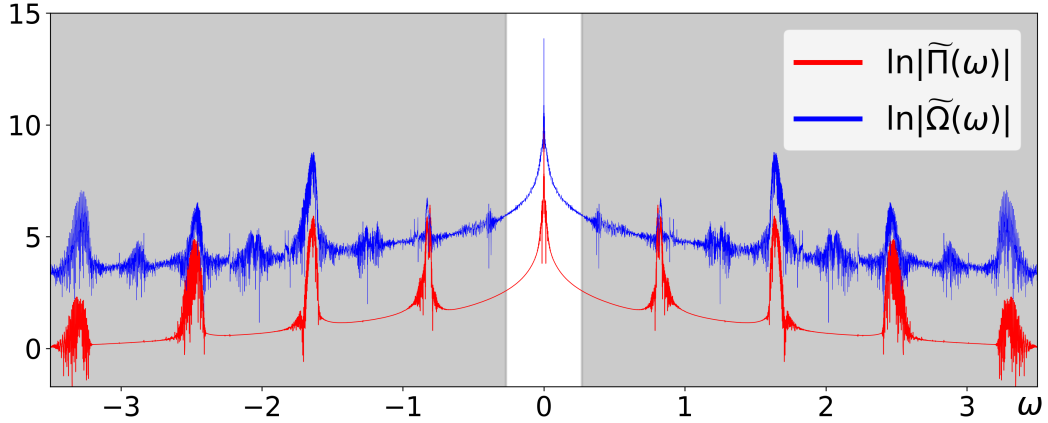


Figure 4.5: *Fourier spectra $\tilde{\Pi}(\omega)$ and $\tilde{\Omega}(\omega)$ of the time series $\Pi(t)$ and $\Omega(t)$ in Fig. 4.4. Note that $\Pi(t)$ provides a smoother spectrum than $\Omega(t)$. Cutting out $\tilde{\Pi}$'s central band ($\tilde{\Pi}_0$ within white corridor) allows us to smooth $\Pi(t)$; see Fig. 4.6.*

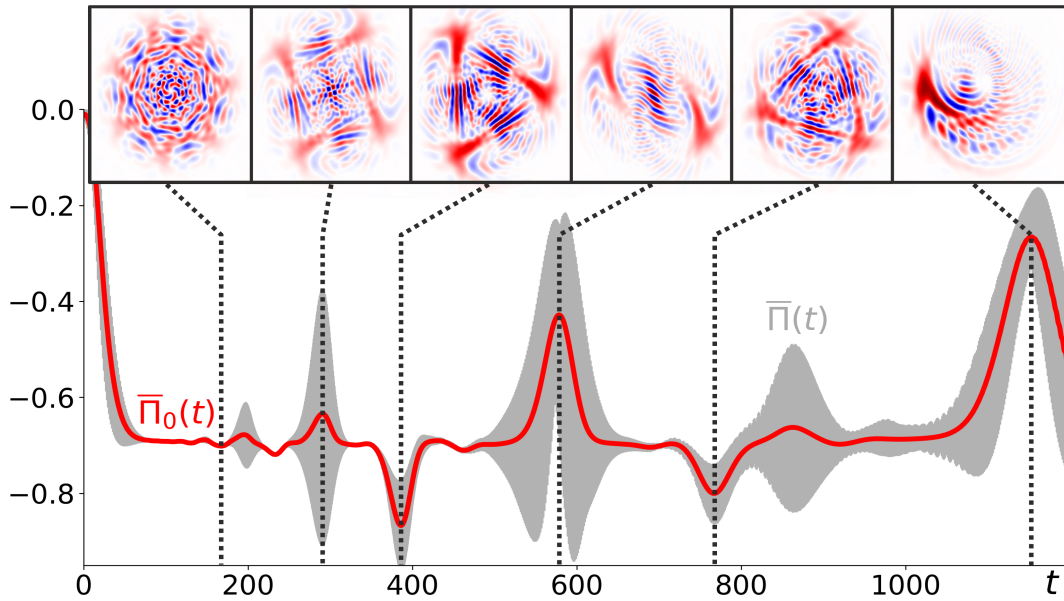


Figure 4.6: *Smoothed $\Pi(t)$ picks out special states. The inverse Fourier transform of the central band $\tilde{\Pi}_0(\omega)$ (highlighted in Fig. 4.5) yields a (thick red) smoothed curve $\bar{\Pi}_0(t)$ of $\Pi(t)$ (gray curve). Deviations of $\bar{\Pi}_0(t)$ from the settled value (≈ -0.7) singles out ‘unsaturated’ special states: the evolution shows an approximate recurrence of the initial state at time $T \approx 1154$. Pronounced peaks and troughs at intermediate times identify fractional revival states, see [4] and Section 4.3.3, with special n -fold symmetries.*

The spectrum $\tilde{\Pi}(\omega)$ of $\Pi(t)$ is smoother than the spectrum $\tilde{\Omega}(\omega)$ of $\Omega(t)$, see Fig. 4.5. Valuable information is more easily accessible through Π than Ω since this smoothness allows us to cut out frequency bands without sensitive dependence on

the cut location. Additionally, Π provides information more readily than the typically used wave function overlap $\mathcal{P}(t) = |\langle \Psi_0 | \Psi(t) \rangle|^2$. This is because $\mathcal{P}(t)$ depends sensitively on its initial state Ψ_0 but also because the spectrum of $\mathcal{P}(t)$ is noisier and does not have a central peak that provides accessible information in the manner that $\tilde{\Pi}_0$ does, see Section 4.3.2 for details

Our theory can be applied to Kerr-Hamiltonians, driven and dissipative systems [27] and higher-dimensional continuous systems [91]; it remains to be seen whether it can be applied to discrete systems [87].

To conclude, quantum dynamics in phase space can be effectively viscous; we have traced this back to the behaviour of the quantum corrections in Wigner's phase space current \mathbf{J} . Quantum suppression of classical shear generates shear polarization patterns that characterize the difference between quantum and classical phase space dynamics. \mathbf{J} 's viscosity limits the fineness of structures formed in quantum phase space dynamics. The quantification of shear polarization patterns using $\Pi(t)$ provides new insight into the character of quantum phase space dynamics. Additionally, studying the time series of Π we find that it sensitively displays features of the dynamics, picks out special quantum states, does not rely on arbitrarily chosen reference states, can be frequency filtered and provides information on the dynamics in a robust way.

For the study of the dynamics of continuous quantum systems we expect that the shear suppression polarization $\Pi(t)$ will prove to be a valuable alternative to the wave function overlap probability $\mathcal{P}(t)$.

4.3 Supplementary material

4.3.1 Fast oscillations and frequency filtering

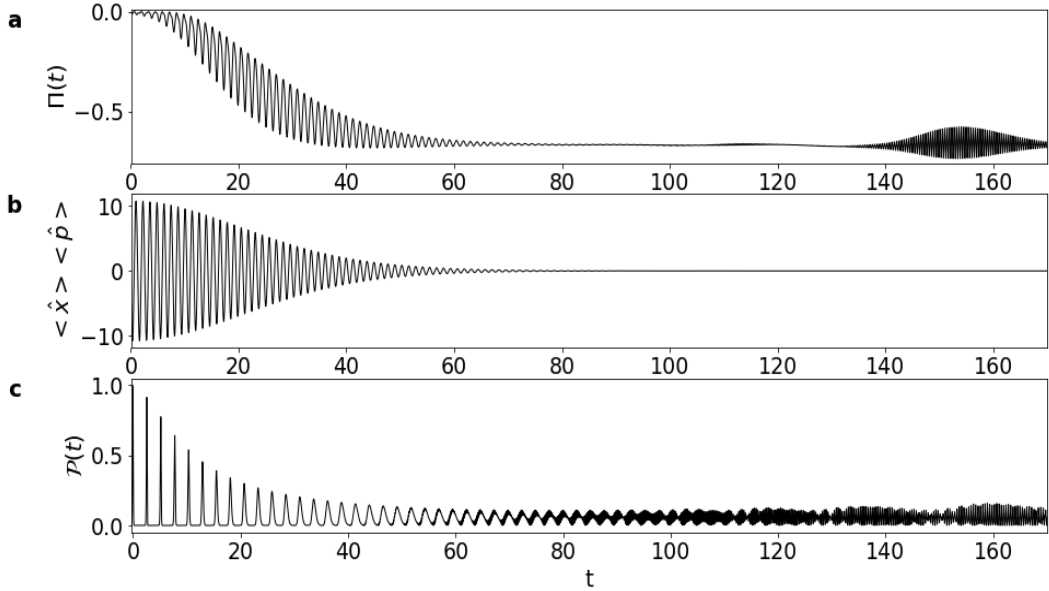


Figure 4.7: Frequencies for potential V_V with parameters of Fig. 4.3 (b). Panel (a), Π contains high frequency components at twice the frequency of the center-of-mass oscillation of the distribution W , as evidenced by comparison with panel (b) showing $\langle \hat{x} \rangle \langle \hat{p} \rangle$ and panel (c) showing the overlap probability $\mathcal{P}(t)$. For times greater than 130 the dispersion of the state into a distribution with several humps creates higher harmonics frequency side-bands $\tilde{\Pi}_n$, compare Figs. 4.9 and 4.6 (b).

4.3.2 Comparison of shear polarization Π with overlap \mathcal{P}

In Figs. 4.9-4.12 we apply essentially the same filtering procedure as was used to generate Fig. 4.6 (e). Comparing the respective spectra explains differences between $\tilde{\Pi}(\omega)$ versus $\tilde{\mathcal{P}}(\omega)$, and thus $\bar{\Pi}(t)$ versus $\bar{\mathcal{P}}(t)$:

The $\bar{\mathcal{P}}_n(t)$ -curves show that characterization of the behaviour of the system's dynamics is easier to achieve using $\bar{\Pi}_n(t)$ than $\bar{\mathcal{P}}_n(t)$, compare Fig. 4.9 (b) (and 4.6 (e)) with 4.10 (b), or Fig. 4.11 (b) (and 4.13 (e)) with 4.12 (b).

The reason for this observation is the presence of structure in the zero-frequency band $\tilde{\Pi}_0(\omega)$, highlighted in Figs. 4.6 (d) and 4.13 (d); this structure can provide us with a useful smoothed signal $\Pi_0(t)$, see Figs. 4.6 (e) and 4.13 (e). In contrast to $\tilde{\Pi}_0(\omega)$, $\tilde{\mathcal{P}}_0(\omega)$ is mostly concentrated into a single isolated peak, see Figs. 4.10 (a) or 4.12 (a), and, as a consequence, $\bar{\mathcal{P}}_0(t)$ flatlines, see Figs. 4.10 (b) or 4.12 (b).

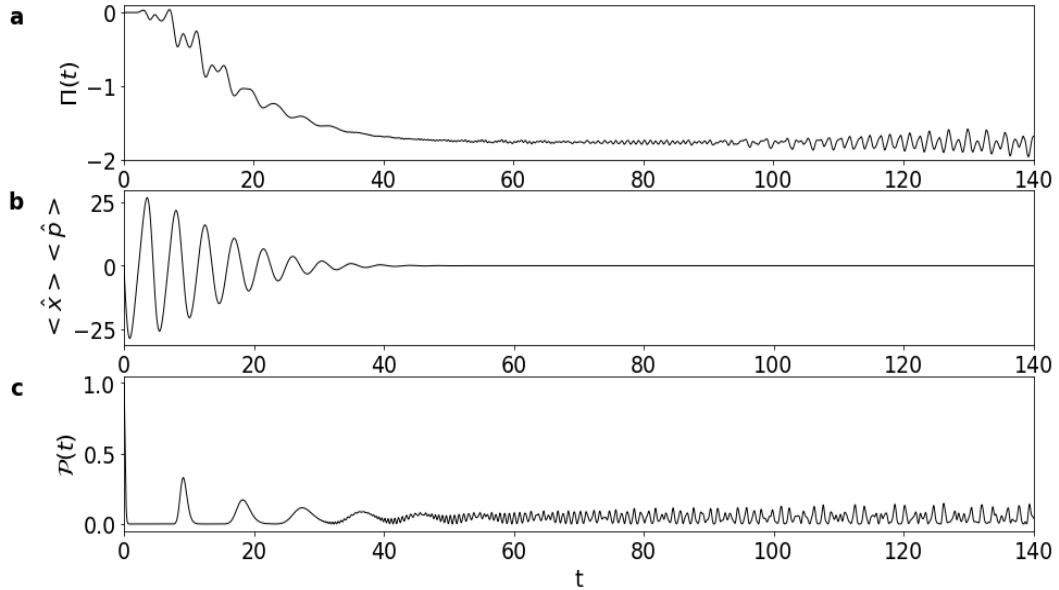


Figure 4.8: Frequencies for potential V_U with parameters of Fig. 4.3 (a). Panel (a), Π contains high frequency components at twice the frequency of the center-of-mass oscillation of the distribution W , as evidenced by comparison with panel (b) showing $\langle \hat{x} \rangle \langle \hat{p} \rangle$ and panel (c) showing the overlap probability $\mathcal{P}(t)$, compare Fig. 4.13 (b).

Additionally, the weights of the spectral bands $\tilde{\Pi}_n(\omega)$ drop with increasing band index n , see Figs. 4.9 (b) (and 4.6 (b)), or Figs. 4.11 (b) (and 4.13 (b)). Higher order bands can be truncated without losing too much information. In contrast, the weights of the spectral bands $\tilde{\mathcal{P}}_n(\omega)$, see Figs. 4.10 (a) or 4.12 (a), remain similar across several frequency bands n . For useful information, bands with high index n have to be retained. Their associated time-signal therefore suffers from complexity-overload, contrast Fig. 4.10 (b) with 4.9 (b), or 4.12 (b) with 4.11 (b).

The signals $\tilde{\mathcal{P}}_n(t)$ display spurious negativities, see Figs. 4.10 (b) or 4.12 (b), because they are filtered before being back-transformed. The probabilities $\mathcal{P}(t)$ are of course positive at all times, see Figs. 4.7 (c) and 4.8 (c).

Case of soft potential V_V

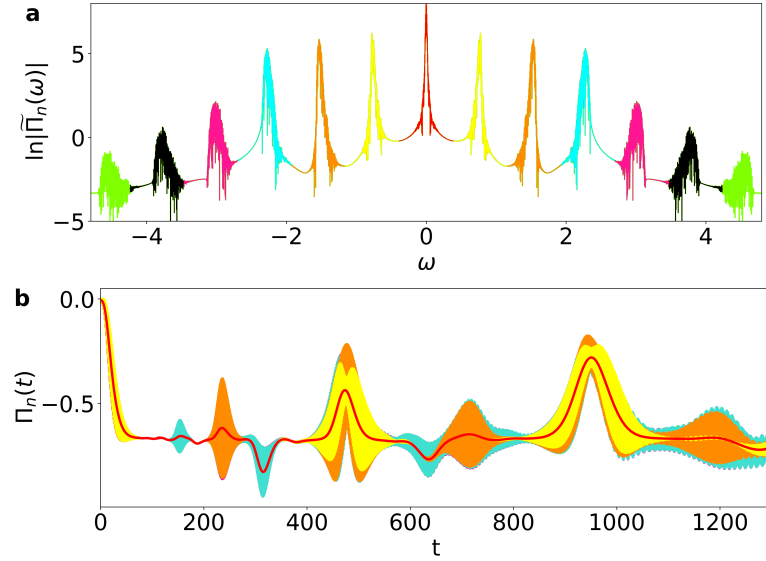


Figure 4.9: *Smoothing of $\Pi(t)$ through frequency filtering for potential V_V with parameters of Fig. 4.3 (b).* Panel (a), harmonic frequency bands of the Fourier image $\tilde{\Pi}(\omega)$ of $\Pi(t)$ are color-labelled. We progressively remove higher harmonics and retain only the n lower order bands $\tilde{\Pi}_n$ grouped in pairs around the central band $\tilde{\Pi}_0$ at zero (red color). (b), when back-transforming $\tilde{\Pi}_n$ we arrive at smoothed curves $\bar{\Pi}_n$ of Π , color-labelled by the highest retained frequency band in (a) above. Panel (b) shows that the $\bar{\Pi}_n$ -curves pick out special states of the corresponding recurrence order n at recurrence times T/n and their multiples, compare Fig. 4.6.

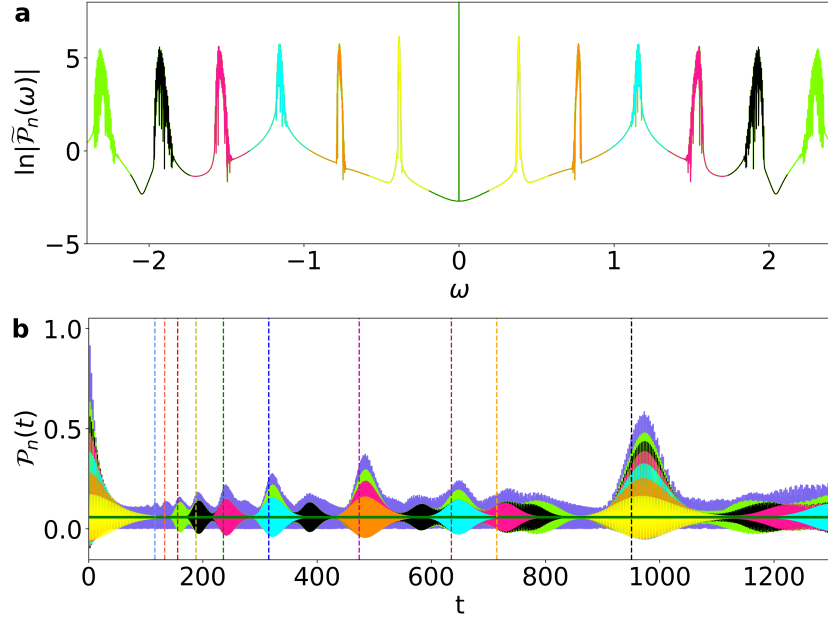


Figure 4.10: *Smoothing of $\mathcal{P}(t)$ through frequency filtering for potential V_V with parameters of Fig. 4.3 (b).* Panel (a), shows harmonic frequency bands of the Fourier image $\tilde{\mathcal{P}}(\omega)$ of $\mathcal{P}(t)$ and panel (b), the back-transformed images of $\tilde{\mathcal{P}}_n$, yielding smoothed curves $\bar{\mathcal{P}}_n$ of \mathcal{P} , compare Figs. 4.6, 4.9 and 4.13. (b), when back-transforming groups $\tilde{\mathcal{P}}_n(\omega)$ we arrive at smoothed curves $\bar{\mathcal{P}}_n(t)$ of $\mathcal{P}(t)$, color-labelled by the highest retained frequency band from (a) above; $\bar{\mathcal{P}}_0(t)$ flatlines. The dashed lines of panel (b) have been carried over from Fig. 4.6 (e). Their slight time offset is due to the fact that $\bar{\mathcal{P}}_n$ only measures the overlap with the initial state, whereas $\bar{\Pi}$ is a global measure.

Case of hard potential V_U

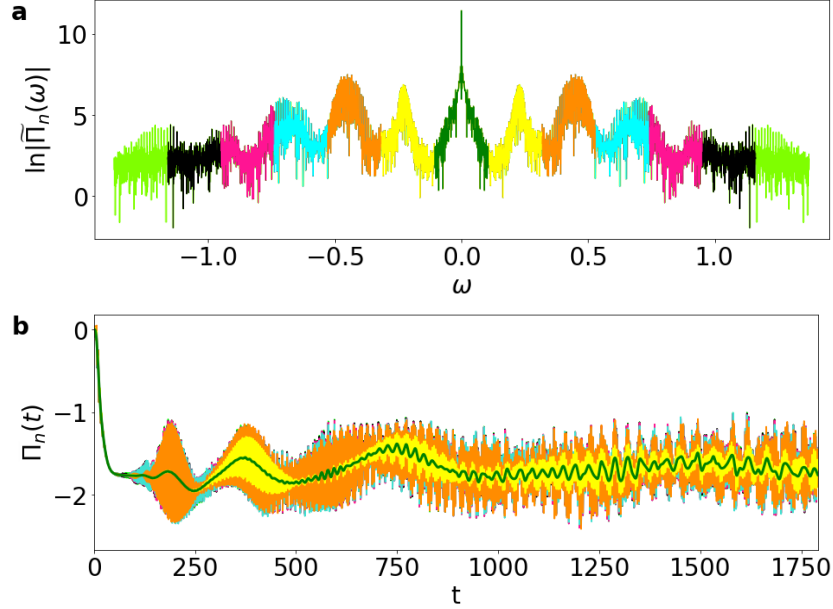


Figure 4.11: *Smoothing of $\Pi(t)$ through frequency filtering for potential V_V with parameters of Fig. 4.3 (b).* Panel (a), harmonic frequency bands of the Fourier image $\tilde{\Pi}(\omega)$ of $\Pi(t)$ are color-labelled. We progressively remove higher harmonics and retain only the n lower order bands $\tilde{\Pi}_n$ grouped in pairs around the central band $\tilde{\Pi}_0$ at zero (dark green color). (b), when back-transforming $\tilde{\Pi}_n$ we arrive at smoothed curves $\bar{\Pi}_n$ of Π , color-labelled by the highest retained frequency band in (a) above. Panel (b) shows that the $\bar{\Pi}_n$ -curves pick out special states of the corresponding recurrence order n at recurrence times T/n and their multiples, compare Fig. 4.13.

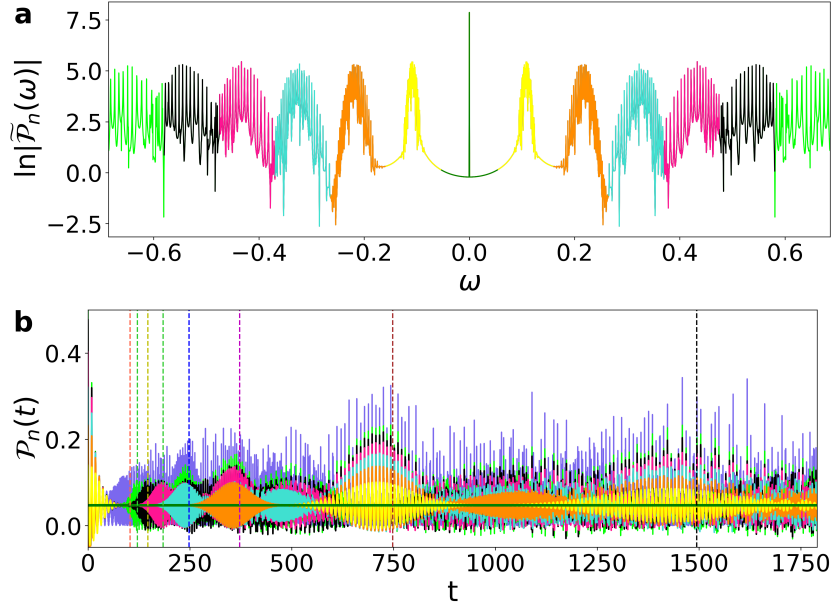


Figure 4.12: *Smoothing of $\mathcal{P}(t)$ through frequency filtering.* For the parameters of Fig. 4.3 (a) with hard potential V_U : (a), harmonic frequency bands of the Fourier image $\tilde{\mathcal{P}}(\omega)$ of $\mathcal{P}(t)$ are color-labelled. We progressively remove higher harmonic bands and retain the group $\tilde{\mathcal{P}}_n(\omega)$ of all n lower order bands. The smallest such group is the central band $\tilde{\mathcal{P}}_0(\omega)$ around zero (dark green colour). (b), when back-transforming groups $\tilde{\mathcal{P}}_n(\omega)$ we arrive at smoothed curves $\bar{\mathcal{P}}_n(t)$ of $\mathcal{P}(t)$, color-labelled by the highest retained frequency band from (a) above; $\bar{\mathcal{P}}_0(t)$ flatlines. The dashed lines of panel (b) have been carried over from Fig. 4.13 (e). Their slight time offset is due to the fact that $\bar{\mathcal{P}}_n$ only measures the overlap with the initial state, whereas $\bar{\Pi}$ is a global measure.

4.3.3 Identification of special states

Just like For the soft potential $V_V = 31x^2/10 - x^4/81$ the identification of special states, see Fig. 4.6, can be performed for the hard potential case, $V_U = x^4/500$, illustrated in Fig. 4.13 below:

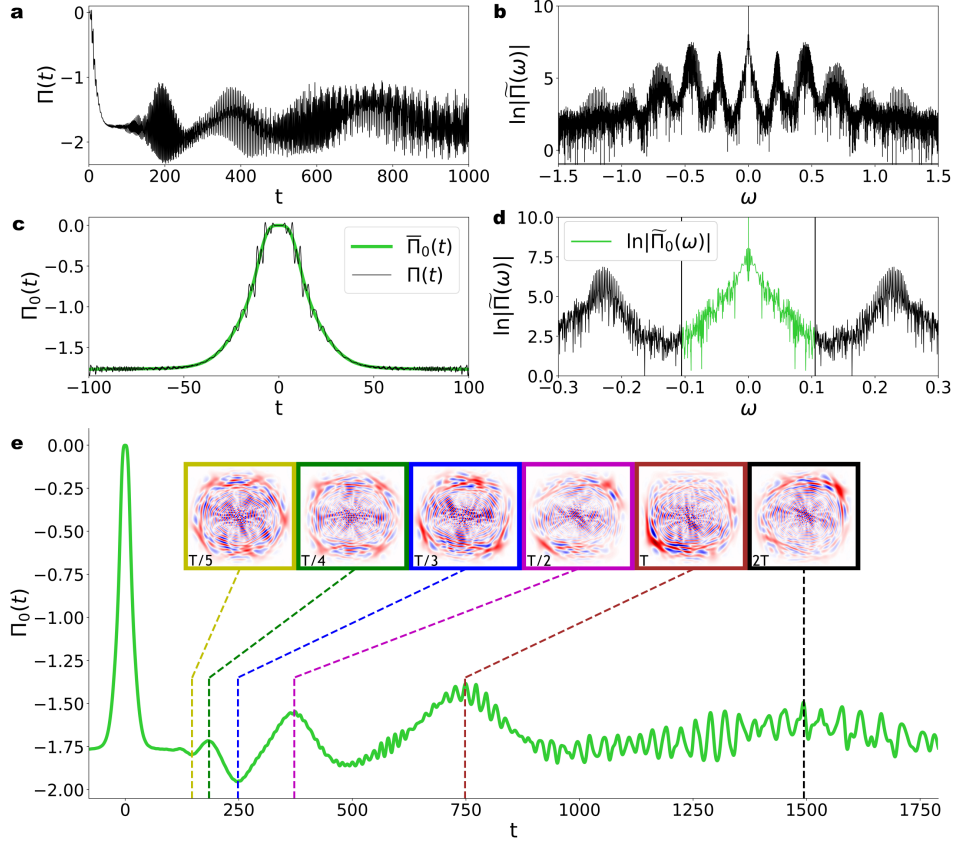


Figure 4.13: *Smoothed $\Pi(t)$, picks out special states.* For the same hard potential V_U and state, as in Fig. 4.3 (a): (a), $\Pi(t)$ contains high frequency components, (b), which are grouped into harmonic bands. (d), the central band (highlighted in green) is cut out and its inverse Fourier transform gives, (c) and (e), smoothed profiles $\bar{\Pi}_0(t)$ of $\Pi(t)$ in (a). (c), the close-up of $\Pi(t)$ and $\bar{\Pi}_0(t)$ near $t = 0$ shows the symmetry with respect to the ‘most unsettled’ initial state, compare Fig. 4.3 and main text. (e), when Π ’s value deviates most from the longtime average we find that the evolution has led to an approximate recurrence of the initial state at time $T \approx 750$. One observes several pronounced peaks and troughs at intermediate times where fractional revival states [4] with special n -fold symmetries are found.

4.3.4 Some properties of W and \mathbf{J}

Wigner's phase space quantum distribution [91, 38]

$$W_\varrho(x, p, t) \equiv \frac{1}{\pi\hbar} \int_{-\infty}^{\infty} dy e^{-\frac{2i}{\hbar}py} \langle x+y | \hat{\varrho}(t) | x-y \rangle \quad (4.9)$$

is real-valued and normalized $\iint_{-\infty}^{\infty} dx dp W(x, p, t) = 1$. W is set apart from other quantum phase space distributions [38] as the closest quantum analogue of the classical phase space distribution [57, 97], here we therefore only investigate W .

By construction W is non-local in y and subject to Fourier-limits; the same applies to the components of \mathbf{J} :

$$J_x = \frac{p}{M\pi\hbar} \int dy \varrho(x-y, x+y, t) e^{\frac{2i}{\hbar}py} = \frac{p}{M} W, \quad (4.10)$$

and its momentum component is

$$J_p = -\frac{1}{\pi\hbar} \int dy \left[\frac{V(x+y) - V(x-y)}{2y} \right] \times \rho(x-y, x+y, t) e^{\frac{2i}{\hbar}py} \quad (4.11)$$

4.3.5 Unit-free formulation of vorticity

To quantify the vorticity of \mathbf{v} in phase space, we form $-\nabla \times \mathbf{v} = \frac{\xi}{\tau} \frac{\partial}{\partial \mathcal{P}} v_{\mathcal{X}} - \frac{\tau}{\xi} \frac{\partial}{\partial \mathcal{X}} v_{\mathcal{P}} = \sqrt{MK} \frac{\partial}{\partial \mathcal{P}} v_{\mathcal{X}} - \frac{1}{\sqrt{MK}} \frac{\partial}{\partial \mathcal{X}} v_{\mathcal{P}}$. This form is firstly inspired by the curl operator and can secondly be justified by the fact that shear stress in classical fluids is proportional to its transverse velocity derivatives, see Chap. 41, Vol. II of [26]. In this second interpretation the minus sign arises from the symplectic structure of phase space.

We then use the coordinate transformations $x = (MK/\hbar^2)^{1/4} \mathcal{X} = \xi \mathcal{X}$ and $p = \tau \mathcal{P}$, where $\tau = 1/(\hbar\xi)$ to switch to unit-free systems ($\hbar = 1$, $M = 1$ and $K = 1$). This, e.g., maps a harmonic oscillator Hamiltonian, given in physical units, $\hat{\mathcal{H}} = -\frac{\hbar^2}{2M} \frac{\partial^2}{\partial x^2} + \frac{K}{2} \mathcal{X}^2$, to the isomorphic, unit-free system $\hat{H} = -\frac{1}{2} \frac{\partial^2}{\partial \mathcal{X}^2} + \frac{\mathcal{X}^2}{2}$ (with circular phase space trajectories [43]); applied to \mathbf{v} it yields Eq. (4.2).

4.3.6 Structure formation and coherences

We study one-dimensional systems, continuous in position x and momentum p , the generalization to higher dimensional continuous systems is straightforward [91].

It is known that forced oscillators with Hamiltonians of the form $\hat{\mathcal{H}} = -\alpha(t)\frac{\hbar^2}{2M}\frac{\partial^2}{\partial\mathcal{X}^2} + \gamma(t)\hat{\mathcal{X}} + \beta(t)\hat{\mathcal{X}}^2$, with real functions α, β and γ , have classical solutions in the sense that trajectories for the transport of their Wigner distribution can be given [85, 68]. This implies that systems described by such Hamiltonians cannot create or remove quantum coherences, or, what is the same [25, 57], they cannot create or remove [44, 68] Wigner distribution negativities.

Such systems can stretch and otherwise deform Wigner distributions through classical dynamics [50]. But, such changes do not concern us here since they do not create or modify coherences or negativities of the quantum state. The measures we devise here are designed to ignore classical-only [44, 68, 85] state transformations.

4.3.7 On the term ‘viscosity’

The fact that quantum dynamics does not generically allow for structure formation in phase space below Zurek’s scale a_Z is due to the fact that the quantum terms in \mathbf{J} somewhat suppress its shear.

We do not mean to imply that the dynamics is dissipative; even in classical, creeping Stokes flow the fluid’s dynamics is approximately reversible although it is dominated by its viscous behaviour.

Also, the quantum dynamics allows for fractional and full revivals, in this case structures are reversibly removed in phase space and the system becomes dynamically ‘unsettled’.

Partly, this is poorly captured by the term viscous, it should only be understood as a superficial description, yet we use the term viscous since no better term seems to exist.

4.3.8 Derivation of inequality for frequency content Ω in Eq. (4.8)

For states bound in a single well one can estimate W ’s extent in phase space according to Zurek’s arguments [97]:

assuming that W is spread over a spatial distance L and momentum distance P and is in its entirety structured at the associated Zurek scale as given by Eq. (4.1), it follows that its frequency spread in k_x is roughly $2K_x = 2P/\hbar$ and in k_p is roughly $2K_p = 2L/\hbar$; this is easily confirmed analytically.

Furthermore, assuming that $\tilde{W}(k_x, k_p)$ is confined to an ellipse with semi-axes K_x and K_p in phase space (rather than the exact energy contour associated with the

hamiltonian H) we can bound Ω by assuming that all the weight of $\tilde{W}(k_x, k_p)$ is concentrated on this elliptical rim alone. This yields the desired inequality

$$\Omega = \frac{\iint dk_x dk_p |\tilde{W}(k_x, k_p, t) k_x k_p|}{\iint dk_x dk_p |\tilde{W}(k_x, k_p, t)|} < \oint d\varphi |K_x \cos(\varphi) K_p \sin(\varphi)| = \Omega_{\max} = 2K_x K_p = \frac{8\pi^2}{a_Z}. \quad (4.12)$$

4.3.9 Remarks on measures δ , π and Π

The main structural difference between a classical shear measure such as s and the quantum measure π is, that the latter is based on the *difference* $\mathbf{J} - \mathbf{j}$.

The reason is somewhat subtle and deserves further discussion:

Classical shear s is only based on the hamiltonian and therefore distinguishes between hard and soft potentials, this case distinction does in general *not* carry over to the behaviour of the current \mathbf{j} .

After sufficiently long times quantum and classical distributions become stretched out such that they are sharply peaked in the direction perpendicular to their stretching. Thus large gradients result in the direction of $\widehat{\nabla}_H$, see Fig. 4.1, irrespective of which potential generated the distribution.

A measure such as δ therefore becomes dominated by the contribution from the derivatives due to the shape of the distribution and insensitive to the distinction between hard and soft potentials. Using the *difference* $\mathbf{J} - \mathbf{j}$ happens to reinstate the distinction between hard and soft potentials.

For the interested reader this is further explored in the next Subsection.

Classical current shear polarization scales with t^1

Consider the derivatives in $\sigma = \partial_{\widehat{\nabla}_H}(-\nabla \times \mathbf{j})$. For sufficiently long times and sufficiently smooth anharmonic potentials the terms containing second order derivatives of ρ become dominant and $\iint \sigma dx dp \sim t$, where the proportionality constant is positive in the case of bound systems since it is given by an average over the hamiltonian's gradient (which in bound systems is positive):

For long times the state stretches into a filament that grows linearly in length with time, since in the conservative case the 'angular' velocity difference between two energy shells is constant; additionally narrowing the filament's width inversely with time this scales up curvatures, associated with the second derivatives of ρ in σ , quadratically in time. This growth with t^3 , upon integration, is compensated for by

the narrowing in width $\propto t^{-1}$ which in turn has the side effect of picking up a linearly shrinking sample $\propto t^{-1}$ of the (smooth) variation of $H(x, p)$ (its averaged gradient) across energy shells. The upshot of this is that the above integral is linear in t ; this can be confirmed numerically.

With the proportionality constant positive, we find, that the distinction between hard and soft potentials disappears for classical shear measures such as $\sigma(\mathbf{j}) = \sigma(\rho\mathbf{v})$ as well as their quantum counterpart $\sigma(\mathbf{J})$ which is why we use

$$\pi(x, p, t; H) = W(t) \partial_{\widehat{\nabla}_H} \delta(t; H)$$

which is a function of $\mathbf{J}^Q = \mathbf{J} - \mathbf{j}$, this choice reinstates the distinction between hard and soft potentials.

4.3.10 Comparing polarization patterns for ‘hard’ and ‘soft’ potentials

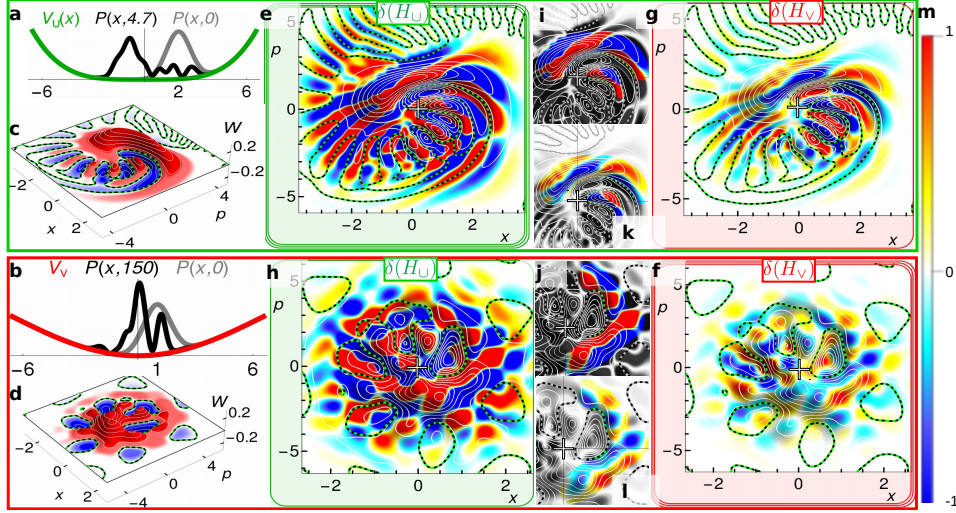


Figure 4.14: *Polarization of deviation vorticity δ .* (a), sketch of hard [$V_U = x^4/16$] and, (b), soft potential [$V_V = 31x^2/10 - x^4/81$] together with probability distributions $P(x, t) = |\Psi(x, t)|^2$ (black curves) of states evolved under these potentials from initial Gaussian states $P(x, 0)$ (grey curves) at initial center positions, (a), $x = 2$ and, (b), $x = 1$, respectively. The Wigner distributions associated with $\Psi(x, t)$ in (a) and (b) are shown in (c) and (d), respectively. (e)-(h), contours of the Wigner distributions of (c) or (d) overlaid with a color bar with (m)’s colors representing values of $\text{Tanh}[50 \delta(H)]$, where $\delta(H)$, see Eq. (4.6), is specified in the head of each framed panel. Small panels (i)-(l) highlight two regions where $W > 0$ [using color while the non-highlighted background is kept gray] to highlight polarization inversion when the Hamiltonian is switched [see main text after Eq. (4.6)]. For reference, the origin $(x, p) = (0, 0)$ is labeled by a white cross.

We note that our soft potential, $V_V = 31x^2/10 - x^4/81$, used in Figs. 4.1 and 4.3, is formally open for large values of x but we restrict its use to ‘safe’ values $|x| < 10$ which allows us to ignore quantum tunneling out of its central well.

4.3.11 $\Pi(t)$ and $\Omega(t)$ can evolve differently from each other

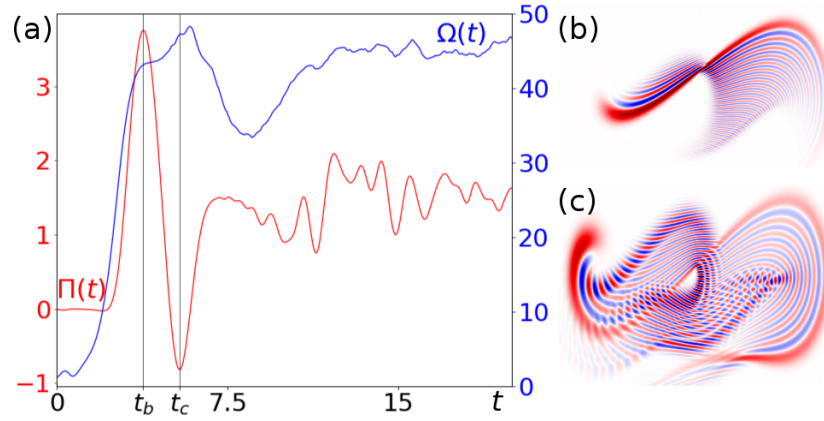


Figure 4.15: For a system more complicated than the single well potentials considered in the main text, shear suppression $\Pi(t)$ and frequency contents $\Omega(t)$ can evolve differently. For a double well potential $V_W = -\frac{x^2}{2} + \frac{x^4}{200}$ with an initial Gaussian state W_0 located at $(x_0, p_0) = (-9.9, 0)$ $\Pi(t)$ shows a pronounced maximum and minimum at times $t_b \approx 3.7$ and $t_c \approx 5.4$. $\Omega(t)$ is insensitive to this system's special dynamic behaviour.

Article 5

Quantum Kerr oscillators’ evolution in phase space: Wigner current, symmetries, shear suppression and special states

by

M. Oliva, O. Steuernagel [66]

5.1 Abstract

The formation of quantum coherences is of central importance in the study of quantum systems and their dynamics.

Here we consider closed 1D Kerr-type oscillators. These are anharmonic and can therefore create coherences [44]. Additionally, their dynamics has circular symmetry in phase space. This makes them the simplest continuous system to create coherences. Therefore, they are particularly suited to help us understand aspects of non-classical effects in quantum dynamics.

Wigner’s distribution W [91, 38] is the closest quantum analog [97, 68, 38, 57, 87] of the classical phase space distribution ρ . In continuous 1D systems the creation of quantum coherences is represented by the creation of negative regions of the Wigner distribution [35, 25, 57, 97, 68]. The formation of such negative regions in the Wigner distribution is easily monitored numerically.

The evolution of W is governed by the associated Wigner phase space current \mathbf{J}

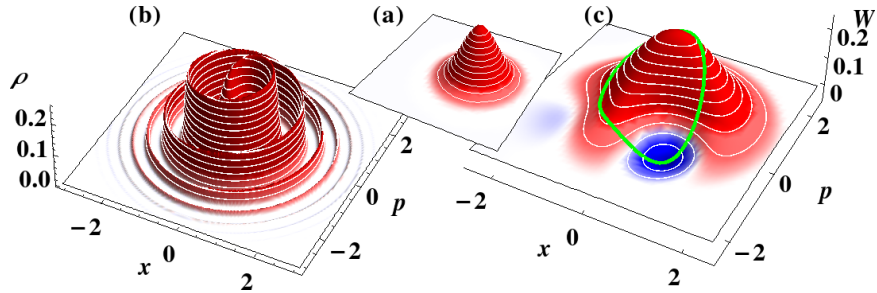


Figure 5.1: *Probability distributions in phase space.* (a), we start from a weakly excited coherent state $|\alpha\rangle = |7/12\rangle$ which is positive everywhere. (b), after time $t = 60$ under classical time evolution, $\rho(t)$ has formed a highly sheared and tight spiral. (c), after the same time the quantum evolution yields a Wigner distribution $W(t)$ which has much less fine detail but negativities (blue). The green line superimposed on panel (c) traces out the Wigner distribution profile on a ring around the origin with radius $r = 1$ which passes through an area with pronounced negativity. Fig. 5.2 displays evolution on this ring [$\Lambda = \frac{1}{2}$, see Eq. (5.4); in all figures $\hbar = 1$, $M = 1$ and $k = 1$].

(strictly speaking \mathbf{J} is a probability current density). Generally, phase space-based approaches are suitable for comparison of quantum with classical dynamics [8, 97, 67]. Specifically, \mathbf{J} allows us to adopt a geometric approach[83, 43, 44, 68, 67] to studying quantum dynamics.

We introduce Kerr oscillators, their Wigner distribution W , and their associated Wigner current \mathbf{J} in section 5.2. In Section 5.3 we show that there are no trajectories and no phase space flow for anharmonic systems such as Kerr oscillators. In Section 5.4 we investigate how pulses in phase space smear out classical spirals [Fig. 5.1 (b)]. We find that pulses in phase space steepen and lengthen dynamically. This analysis is aided by the system’s circular symmetry and the fact that the probability on circles in phase space is conserved. In Section 5.5 we show that using Wigner current \mathbf{J} ’s effective ‘viscosity’ [67] allows us to contrast classical with quantum dynamics and pick out special quantum states.

5.2 Wigner distributions and Wigner current of Kerr oscillators

A one-dimensional system’s Wigner distribution $W_\rho(x, p, t)$ [91, 38] (x denotes position, p the associated momentum, and t time), for a quantum state described by a density matrix $\hat{\rho}$, is defined as the Fourier transform of its off-diagonal coher-

ences $\varrho(x + y, x - y, t)$ (parameterized by the shift y)

$$W_\varrho(x, p, t) = \frac{1}{\pi\hbar} \int_{-\infty}^{\infty} dy \langle x + y | \hat{\varrho}(t) | x - y \rangle e^{-\frac{2i}{\hbar}py}, \quad (5.1)$$

where $\hbar = h/(2\pi)$ is Planck's constant. By construction W is normalized and non-local (through y). Unlike $\hat{\varrho}$, W is always real-valued but, generically, W features negativities [91]. Since W_ϱ is $\hat{\varrho}$'s Fourier transform, W and $\hat{\varrho}$ are isomorphic to each other, allowing us to describe all aspects of the quantum system's state and its dynamics using the Wigner representation of quantum theory [95].

Time evolution of the Wigner distribution

For conservative Kerr systems the time development of W is given by the Moyal-bracket $\{\{.,.\}\}$ [62, 95]

$$\partial_t W(x, p, t) = \{\{H, W\}\} \quad (5.2)$$

$$\equiv \frac{2}{\hbar} H(x, p) \sin\left(\frac{\hbar}{2}(\overleftarrow{\partial}_x \overrightarrow{\partial}_p - \overleftarrow{\partial}_p \overrightarrow{\partial}_x)\right) W(x, p, t). \quad (5.3)$$

Here, $\partial_x = \frac{\partial}{\partial x}$, etc.; the arrows over the derivatives indicate whether they act on (point towards) Hamiltonian or Wigner distribution.

The Hamiltonian of anharmonic single-mode oscillators of the Kerr type has the form

$$\hat{H}_\Lambda = \left(\frac{\hat{p}^2}{2M} + \frac{k}{2}\hat{x}^2\right) + \Lambda^2 \left(\frac{\hat{p}^2}{2M} + \frac{k}{2}\hat{x}^2\right)^2, \quad (5.4)$$

with the oscillator mass M and spring constant k . Such Hamiltonians describe electromagnetic fields subjected to Kerr non-linearities $\chi^{(3)}$ (here $\Lambda^2 \propto \chi^{(3)}$) [96, 69, 59, 70]. This system is fully solvable since wave functions of the harmonic oscillator are solutions to the Kerr Hamiltonian with eigen-energies $E_n = \hbar\sqrt{\frac{k}{M}}[(n + \frac{1}{2}) + \Lambda^2(n + \frac{1}{2})^2]$. Its quantum recurrence time is

$$T_\Lambda = \frac{\pi}{|\Lambda|^2}. \quad (5.5)$$

Following Wigner [91], we cast expression (5.3) in the form of the phase space continuity equation

$$\partial_t W + \nabla \cdot \mathbf{J} = 0, \text{ where } \nabla = \begin{pmatrix} \partial_x \\ \partial_p \end{pmatrix} \text{ is the gradient, and } \mathbf{J} = \begin{pmatrix} J_x \\ J_p \end{pmatrix} \quad (5.6)$$

denotes the Wigner current in phase space [83]. \mathbf{J} is the quantum analog [23, 7] of the classical phase space current $\mathbf{j} = \rho \mathbf{v}$ [64] which transports the classical probability density $\rho(x, p, t)$ according to Liouville's continuity equation $\partial_t \rho = -\nabla \cdot \mathbf{j}$.

\mathbf{J} reveals details [83, 43] about quantum systems' phase space dynamics previously thought inaccessible due to the supposed 'blurring' by Heisenberg's uncertainty principle. From now on we will consider $M = k = 1$ only. Then [for a derivation see Eqns. (5.22) and (5.23) in the Appendix 5.6], with $\mathbf{r} = (x, p) = r(\cos \theta, \sin \theta)$, $r = \sqrt{x^2 + p^2}$ and $\Delta = \partial_x^2 + \partial_p^2$, \mathbf{J} can be written as

$$\begin{aligned} \mathbf{J} &= \begin{pmatrix} p \\ -x \end{pmatrix} \left[1 + \Lambda^2 \left(x^2 + p^2 - \frac{\hbar^2}{4} \Delta \right) \right] W \\ &= \begin{pmatrix} r \sin \theta \\ -r \cos \theta \end{pmatrix} \left[1 + \Lambda^2 \left(r^2 - \frac{\hbar^2}{4} (\partial_r^2 + \frac{1}{r} \partial_r + \frac{1}{r^2} \partial_\theta^2) \right) \right] W. \end{aligned} \quad (5.7)$$

\mathbf{J} is tangent to circles concentric with the origin of phase space. This *circular symmetry* allows us to consider an approximation of the dynamics on such individual circles, an observation we make use of below. For future reference we split \mathbf{J} into its classical \mathbf{j} and quantum terms \mathbf{J}^Q

$$\mathbf{J} = \mathbf{j} + \mathbf{J}^Q = W \mathbf{v} - \begin{pmatrix} p \\ -x \end{pmatrix} \left(\frac{\hbar^2 \Lambda^2}{4} \Delta \right) W, \quad (5.8)$$

here $\mathbf{v} = \begin{pmatrix} p \\ -x \end{pmatrix} (1 + \Lambda^2 r^2)$ is the classical phase space velocity. The quantum terms \mathbf{J}^Q are only present for anharmonic potentials [44], which is why only anharmonic potentials create coherences. Harmonic systems' phase space dynamics follows \mathbf{v} and is classical, see Refs. [68, 44].

5.3 No trajectories or flow in quantum phase space

Inspired by classical mechanics, there have been several attempts to treat quantum phase space evolution as a flow along trajectories [68]. Such attempts are ill-fated [68] as we will explain now. They use the formal factorization $\mathbf{J} = W \mathbf{w}$ to define a 'quantum phase space velocity' $\mathbf{w} = \mathbf{J}/W$, then the continuity equation (5.6) assumes the form [89, 20, 68]

$$\partial_t W + \mathbf{w} \cdot \nabla W + W \nabla \cdot \mathbf{w} = 0. \quad (5.9)$$

Here the convective term $\mathbf{w} \cdot \nabla W$ describes the transport that carries W along with the current (following fieldlines in phase space) without changing its values. In contrast, the current divergence term $W \nabla \cdot \vec{w}$ changes values of W . This is best seen by formally rearranging Eq. (5.9) for the total derivative

$$\frac{dW}{dt} = \partial_t W + \mathbf{w} \cdot \nabla W = -W \nabla \cdot \mathbf{w} . \quad (5.10)$$

Treating a continuity equation in this form is known as its *Lagrange decomposition*. This decomposition has to be treated with extreme caution, since it essentially splits the well behaved and finite term $\nabla \cdot \mathbf{J}$ into the two individually singular terms $\mathbf{w} \cdot \nabla W$ and $W \nabla \cdot \mathbf{w}$. Some implications are discussed below. For the Kerr system this total derivative is

$$\begin{aligned} \frac{dW}{dt} &= -\frac{\Lambda^2 \hbar^2}{4} \left[p \left(\frac{(\partial_x W)}{W} - \partial_x \right) - x \left(\frac{(\partial_p W)}{W} - \partial_p \right) \right] \Delta W \\ &= -\frac{\Lambda^2 \hbar^2}{4} W \partial_\theta \left(\frac{\Delta W}{W} \right), \end{aligned} \quad (5.11)$$

and the convective transport term in Eq. (5.10) is

$$\mathbf{w} \cdot \nabla W = \left(\Lambda^2 \left[-r^2 + \frac{\hbar^2}{4W} \Delta W \right] - 1 \right) \partial_\theta W. \quad (5.12)$$

Since the divergence $\nabla \cdot \mathbf{w}$ is non-zero, the quantum evolution does not preserve phase space volumes [62, 44, 68].

One could still describe quantum evolution by phase space transport if the magnitude of this divergence were finite across the entire phase space [68]. Indeed, modelling quantum phase space dynamics through such transport along trajectories has been attempted many times; in this context it has been considered an undesirable feature of \mathbf{w} that it is a singular quantity when W is zero (see Ref. [68] for details). But zeros in W are unavoidable [41]:

The singularities in $\nabla \cdot \mathbf{w}$ are a fundamental and necessary feature to create negative regions in W and thus to create quantum coherences. Such singularities are not a flaw. A velocity field \mathbf{w} with positive divergence that is bounded from above, $B > \nabla \cdot \mathbf{w} > 0$, will by itself not be able to generate negativities. The associated expansion of phase space volumes can only reduce the initial value $W(0) > 0$ of a

density towards zero, since Eq. (5.10) implies that [89, 68]

$$W(t)|_{\text{comoving}} > W(0) \exp(-Bt) > 0 \quad (5.13)$$

for all times. Trahan and Wyatt noticed this and concluded that “*the sign of the density riding along the trajectory cannot change*” [89].

But this interpretation is incorrect. When $W = 0$ the velocity \mathbf{w} and its divergence is singular, Eq. (5.11) cannot be integrated since \mathbf{w} 's singularities render integrals and associated bounds such as (5.13) ill-defined [68]. Therefore, in anharmonic quantum systems neither trajectories nor transport along flow lines exist [68] (References [7] and [83], refer to Wigner ‘flow’ but were written before this was realized).

Because of the singular volume changes associated with Eq. (5.11), we feel the quantum *Liouville* equation (5.6) should be called Wigner’s continuity equation instead.

We are forced to conclude that a trajectory-based approach to quantum phase space evolution creates contradictions such as singular \mathbf{w} and singular phase space volume changes. This highlights the stark differences between classical and quantum dynamics in an illuminating manner. The singularities in \mathbf{w} and phase space volume changes are needed to violate inequality (5.13) thus allowing for the creation of quantum coherences and negative regions in W [44, 68].

5.4 Pulses in Quantum phase space

In the classical case the probability (of ρ) on a classical trajectory of a conservative system is conserved over time. It can be checked that the probability (of W) on a classical trajectory is not conserved for typical anharmonic quantum systems.

The quantum Kerr system is an exception as its evolution preserves probability on rings around the origin:

$$\oint d\theta \partial_t W = - \oint d\theta \nabla \cdot \mathbf{J} = 0, \quad (5.14)$$

since $\nabla \cdot \mathbf{J} = r\partial_\theta([v(r) - \Lambda^2 \frac{\hbar^2}{4} \Delta]W)$. Additionally to the circular symmetry displayed in Eq. (5.7), this probability conservation on circles is the primary reason why considering the Kerr dynamics on circles is suitable.

The classical velocity profile $v(r)$ leads to the formation of fine detail in the classical evolution: in the case of a Gaussian initial state, the state becomes wrapped into

a single tightly wound spiral, see Fig. 5.1 *b*. The quantum evolution shows this tendency of spiral wrapping as well, but while the formation of fine detail is suppressed through “viscous” behaviour (see Section 5.5), negativities of the Wigner distribution emerge.

To study this in more detail, consider W on a ring of radius r , as displayed in Fig. 5.2.

The quantum ‘cross-talk’ terms $\partial_r^2 + \frac{1}{r}\partial_r$ in Eq. (5.7) couple the current on adjacent rings. We can cast these terms aside if we may assume that the Wigner distribution’s azimuthal curvature $\partial_\theta^2 W$ is much greater than its radial curvature and gradient. Making this assumption temporarily, the velocity on a ring is approximately

$$w(r, \theta) \approx r \left[1 + \Lambda^2 \left(r^2 - \frac{\hbar^2}{4r^2} \frac{1}{W} \partial_\theta^2 W \right) \right]. \quad (5.15)$$

This approximation is obviously poor when $W \approx 0$, but Eq. (5.15) is still useful for the discussion that follows.

In Figs. 5.2-5.4 the full evolution is portrayed, not its approximate behaviour of Eq. (5.15). The axis ‘ $-\theta$ ’ is chosen in Figs. 5.2-5.4 since classical evolution proceeds clockwise, in the direction of negative values of θ .

The effect of the θ -curvature term, retained in Eq. (5.15), is primarily twofold: for a Wigner distribution on a circle, forming a hump, the hump’s leading and trailing edges, having positive curvature, get delayed. Conversely, the negative curvature of the peak of the hump accelerates its center, see Fig. 5.2. This lengthens the pulse, making the tail trail, and sharpens its front since the center catches up with the front, see Fig. 5.2. This sharpening in turn spawns oscillations that project forward from the pulse, see Fig. 5.2 and discussion in Ref. [27].

A narrower pulse, as portrayed in Fig. 5.3, develops more pronounced oscillations. Additionally, in Fig. 5.3, Λ is chosen formally complex such that $\Lambda_-^2 < 0$. This creates “backwards” dynamics when contrasted with a positive Kerr-nonlinearity, compare Figs. 5.2 and 5.3: in Fig. 5.3 the pulse lengths to the ‘right’ and steepens and spawns oscillations to the ‘left’; in ‘reverse’ to Fig. 5.2.

In Fig. 5.4, two pulses on a ring interfere with each other. Here, like in Fig. 5.2, the overall effect is that the quantum terms speed the pulses up.

5.5 \mathbf{J} 's viscosity and special states

In the preceding Section 5.4 we discussed motion on a ring. Here we consider cross talk between motion on neighbouring rings.

Over time classical Hamiltonian phase space flow shears ρ since \mathbf{v} creates non-zero gradients of its angular velocity across energy shells. This flow is inviscid as \mathbf{v} is independent of ρ , thus no terms suppress the effects of the angular velocity gradients, and, as time progresses, non-singular probability distributions in phase space get sheared into ever finer filaments [see Fig 5.1 (b)].

The associated classical phase space shear has been derived in Ref. [67] as

$$s(x, p; H) = \partial_{\widehat{\nabla}_H}(-\nabla \times \mathbf{v}) = \partial_{\widehat{\nabla}_H}(\partial_p v_x - \partial_x v_p). \quad (5.16)$$

Here the directional derivative across energy shells $\partial_{\widehat{\nabla}_H}$, is formed from the normalized gradient $\widehat{\nabla}_H = \nabla H / |\nabla H|$ of the Hamiltonian H . Because of the Kerr system's circular symmetry $\widehat{\nabla}_H = \partial_r$.

The sign convention using the negative curl in s in Eq. (5.16) is designed to yield a positive sign for *clockwise* orientated fields since this is the prevailing direction of the classical velocity field \mathbf{v} . This choice yields $s > 0$ for hard potentials [potentials for which the magnitude of the force increases with increasing amplitude, i.e., $\Lambda^2 > 0$], since they induce *clockwise* shear, see Fig. 5.1 (b). $s = 0$ for harmonic oscillators [i.e., $\Lambda = 0$], and $s < 0$ for soft potentials [for which the magnitude of the force decreases with increasing amplitude, i.e., $\Lambda^2 < 0$] since they induce *anti-clockwise* shear.

The reaction of quantum dynamics to classical shear s has to reside in \mathbf{J}^Q of Eq. (5.8). To extract it we form the vorticity of \mathbf{J}^Q [67]

$$\delta(x, p, t; H) = -\nabla \times \mathbf{J}^Q = \partial_p J_x^Q - \partial_x J_p^Q. \quad (5.17)$$

δ 's sign distribution shows a pronounced polarization pattern, see Fig. 5.5.

Specifically, for a system with clockwise shear Fig. 5.5 (b) illustrates that $\delta(H_{\Lambda_+})$ [with $\Lambda_+^2 = +(1/4)^2$] tends to be positive on the inside [towards the origin] and negative on the outside of the positive main ridge of W [see inset of Fig. 5.5 (a)]. Because of this, the outside is being slowed down while the inside speeds up. This polarized distribution of δ therefore counteracts the classical shear [$s_{H_{\Lambda_+}} > 0$] and can suppress it altogether [67]. The same applies to other positive regions of W , whereas for its negative regions the current \mathbf{J} tends to be inverted [83, 43] inverting δ 's polarization pattern, see Ref. [67] and Fig. 5.5 (b).

When the same state W is governed by a Hamiltonian H_{Λ_-} with anti-clockwise shear [67] [i.e. $(\Lambda_-)^2 < 0$] $\delta(H_{\Lambda_-})$ tends to be the sign-inverted form of $\delta(H_{\Lambda_+})$ (for Kerr systems we find $\delta(H_{\Lambda_+}) = -\delta(H_{\Lambda_-})$ if $|\Lambda_+| = |\Lambda_-|$). This is illustrated in Fig. 5.5 (c), where $\Lambda_-^2 = -(1/4)^2$ is negative, whereas in Fig. 5.5 (b) $\Lambda_+^2 = +(1/4)^2$ is positive.

The distribution of δ 's polarization can be picked up with the directional derivative $\partial_{\nabla_H} \delta(t; H) = \partial_r \delta(t; H)$. This we multiply with W , because negative regions of W invert the current \mathbf{J} [83], and because we want to weight it with the local contribution of the state. The resulting local measure for weighted shear polarization is [67] $\pi(x, p, t; H) = W(t) \partial_r \delta(t; H)$. Its average across phase space is W 's shear polarization [67]

$$\Pi(t; H) = \langle\langle \pi(t; H) \rangle\rangle = \iint_{-\infty}^{\infty} dx dp \pi(x, p, t; H). \quad (5.18)$$

Fig. 5.6 illustrates that $\Pi(t)$ initially drops and after a while levels off.

We emphasize that the levelling-off behaviour of $\Pi(t)$ is in marked contrast to the classical case: for long enough times, in simple bound state classical systems non-singular states $\rho(t)$ get stretched out linearly [67] into ever finer threads, see Fig. 5.1 (b), therefore $\langle\langle \partial_r(-\nabla \times \mathbf{j}) \rangle\rangle \propto t$ [67]. The quantum evolution counteracts this classical shear s resulting in values of the shear suppression Π which are opposite in sign to those of s [67] (for the Kerr system $\text{sign}[s]=\text{sign}[\Lambda^2]$).

Moreover, starting from an initial Gaussian state, the magnitude $|\Pi(t)|$ initially grows the more the evolution stretches out the state into finer structures. Eventually quantum shear suppression stops classical shear from creating finer structures in phase space [67]: $|\Pi(t)|$ levels off.

In other words, the quantum evolution is effectively 'viscous'. This 'viscosity' is the mechanism by which quantum evolution enforces that W can typically not form structures below the size scale identified by Zurek [97]. Therefore $\Pi(t)$ settles when the state has formed structures at the Zurek scale. This can e.g. be quantified by monitoring the phase-spatial frequency content of W as a function of time, for details see [67].

Yet, quantum evolution is not truly viscous, it allows for revivals. Interestingly, these are picked up by the *deviation* of $\Pi(t)$ from the local time average. For the Kerr system, the special states for which this deviation is largest are (fractional) revival states [74, 70], see Fig. 5.6.

We emphasize that such revival states are traditionally picked up through the

overlap of the evolved state with a suitably chosen reference state (such as a Gaussian initial state) [74], instead, our measure $\Pi(t)$ does not depend on a reference state, this makes it more versatile than the use of wave function overlaps.

We note that graphs of $\Pi(t)$ for anharmonic systems that do not have the symmetry of the Kerr system carry high frequency oscillations [67], whereas, due to the symmetry of the Kerr system, such oscillations are absent here. Generally, for other anharmonic systems without circular symmetry, graphs as smooth as those for $\Pi(t)$ obtained in Fig. 5.6 require frequency filtering [67].

Additionally to the symmetries identified above, also in this regard are Kerr oscillators the simplest possible continuous quantum systems that alter quantum coherences.

To conclude, quantum dynamics that generates coherences in continuous systems is most easily studied in phase space and using Kerr systems, since these have special symmetries. The two new symmetries we have identified are circular phase space current \mathbf{J} , Eq. (5.7), and probability conservation for W on rings, Eq. (5.14). These imply the absence of high-frequency components in $\Pi(t)$ of Eq. (5.18), see Fig. 5.6. We also have identified a quantum speed-up of the propagation of wave function pulses in phase space and we demonstrate that the dynamics of the Kerr system is ‘effectively viscous’. This can be quantified, explains the emergence of Zurek’s scale for the formation of minimum structures in quantum phase space, and can be used to pick out special quantum states.

The geometric nature of our approach helps us to guide the understanding of the generation of coherences in quantum dynamics and the formation of negativities of W and will hopefully help pave the way to devise new strategies to protect coherences, for related ideas see Ref. [27].

5.6 Appendix

The Hamiltonian of anharmonic single-mode oscillators of the Kerr type has the form (5.4)

$$H_\Lambda = \left(\frac{p^2}{2M} + \frac{k}{2}x^2 \right) + \left(\Lambda \frac{p^2}{2M} + \lambda \frac{k}{2}x^2 \right)^2, \quad (5.19)$$

with $\Lambda = \lambda$. Here we keep the two parameters Λ and λ distinct to allow us to tune the system’s non-linearities independently and help with keeping track of terms in

the derivation of the form of \mathbf{J} .

The Wigner distribution of the Kerr oscillator obeys the phase space continuity equation (5.3) [84, 59, 45]

$$\begin{aligned} \partial_t W(x, p, t) &= \{\{H, W\}\} = \frac{2}{\hbar} H(x, p) \sin\left(\frac{\hbar}{2}(\overleftarrow{\partial}_x \overrightarrow{\partial}_p - \overleftarrow{\partial}_p \overrightarrow{\partial}_x)\right) W(x, p, t) \quad (5.20) \\ &= \left(\left[-\Lambda^2 \frac{\hbar^2}{4M^2} p \partial_x^3 + \lambda^2 \frac{\hbar^2 k^2}{4} x \partial_p^3 - \left\{ \Lambda \lambda \frac{kxp^2}{M} + \lambda^2 k^2 x^3 \right\} \partial_p \right. \right. \\ &\quad \left. \left. - \Lambda \lambda \frac{\hbar^2 k}{4M} p \partial_x \partial_p^2 + \Lambda \lambda \frac{\hbar^2 k}{4} x \partial_p \partial_x^2 + \left\{ \Lambda^2 \frac{p^3}{M^2} + \Lambda \lambda \frac{kx^2 p}{M} \right\} \partial_x \right] \right. \\ &\quad \left. + \frac{p}{M} \partial_x - kx \partial_p \right) W(x, p, t). \quad (5.21) \end{aligned}$$

The square brackets bracket the terms arising from the Kerr Hamiltonian's anharmonic part whereas the terms $\frac{p}{M} \partial_x - kx \partial_p$ stem from the harmonic oscillator contribution $p^2/(2M) + kx^2/2$.

The associated Wigner current components (5.6) are

$$J_x = \left[\hbar^2 \left(-\Lambda^2 \frac{1}{4M^2} p \partial_x^2 - \Lambda \lambda \frac{k}{4M} p \partial_p^2 \right) + \left\{ \Lambda^2 \frac{p^3}{M^2} + \Lambda \lambda \frac{kx^2 p}{M} + \frac{p}{M} \right\} \right] W(x, p, t) \quad (5.22)$$

$$\text{and } J_p = \left[\hbar^2 \left(\lambda^2 \frac{k^2}{4} x \partial_p^2 + \Lambda \lambda \frac{k}{4M} x \partial_x^2 \right) - \left\{ \lambda^2 k^2 x^3 + \Lambda \lambda \frac{kxp^2}{M} + kx \right\} \right] W(x, p, t). \quad (5.23)$$

The curly brackets in Eqns. (5.22) and (5.23) contain the classical Hamiltonian current terms, the round brackets the quantum terms.

To justify this assignment, note that the first term in J_p is of the form $\frac{\hbar^2}{4 \cdot 3!} \partial_x^3 V \partial_p^2 W$ [91, 83] and thus has to be assigned to J_p , while the first term of J_x is its 'partner' term for the position case. What remains somewhat ambiguous is whether the second terms in (5.22) and (5.23) have been assigned correctly. To highlight this ambiguity consider

$$J_x^{(\sigma)} = J_x + \sigma \Lambda \lambda \frac{\hbar^2 k}{4M} [x \partial_p \partial_x + p \partial_p^2] W(x, p, t) \quad (5.24)$$

$$\text{and } J_p^{(\sigma)} = J_p - \sigma \Lambda \lambda \frac{\hbar^2 k}{4M} [x \partial_x^2 + p \partial_x \partial_p] W(x, p, t), \quad (5.25)$$

parameterized by the interpolation parameter σ with $0 \leq \sigma \leq 1$. This interpolation fulfills the continuity equation (5.6) since the σ -dependent terms are divergence-free for $0 \leq \sigma \leq 1$.

To remove the ambiguity we can use Wigner current plots. We notice that the field plots of $\mathbf{J}^{(\sigma \neq 0)}$ do not ‘make sense’, see Fig. 5.7: $\mathbf{J}^{(\sigma=0)}$ of Eqns. (5.22) and (5.23), or (5.7) is the correct Wigner current expression.

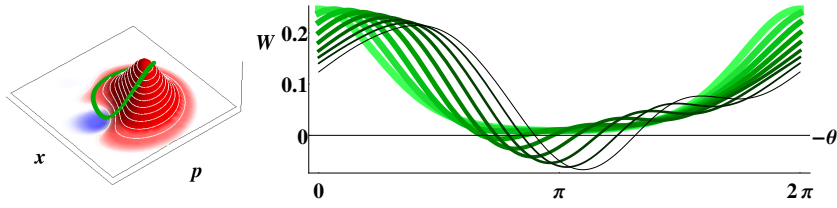


Figure 5.2: *Time evolution of $W(\theta)$ on a ring with fixed radius $r = 1.0$ for initial coherent state $|\alpha\rangle = |7/12\rangle$ over time $t = 0$ to $T_{\Lambda}/4 = 4\pi = 12.56$ [$\Lambda = \frac{1}{4}$]. The darker and thinner the curves, the more time has elapsed. The curves move clockwise on the ring, towards increasing values of ‘ $-\theta$ ’. The quantum evolution leads to a speed-up over the classical evolution (the classical phase angle vt is subtracted). Additionally, under quantum evolution the pulse widens and steepens at the front, this triggers the formation of oscillations with negative regions in front of the pulse which eventually catch up with the main pulse from ‘behind’.*

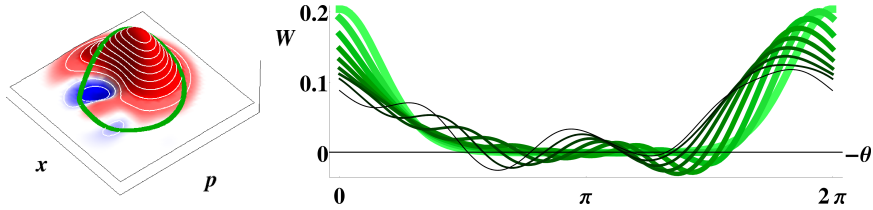


Figure 5.3: *Time evolution of $W(\theta)$ on a ring with fixed radius $r = 1.6$ for initial coherent state $|\alpha\rangle = |5/4\rangle$ over time $t = 0$ to $T_{\Lambda_-}/4 = 12.56$. Here the Kerr-nonlinearity is *negative*, $\Lambda_-^2 = -1/16$, therefore the Wigner distribution is wrapped *anti-clockwise* and the center-of-gravity of the pulse falls *behind* the classical motion (vt has been subtracted). Contrast with Fig. 5.2.*

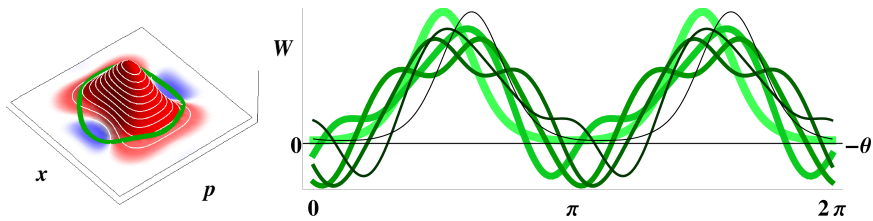


Figure 5.4: *Time evolution of $W(\theta)$ on a ring with fixed radius $r = 1.6$ for initial squeezed vacuum state (squeezing parameter = $1/3$) over time $t = 0$ to $T_{\Lambda_+} = \frac{\pi}{4} = 0.785$. Here the Kerr-nonlinearity is *positive*, $\Lambda_+^2 = 1$, therefore the Wigner distribution’s center-of-gravity moves *ahead* of the classical motion (vt has been subtracted): at time $t = \frac{T_1}{4}$ (its recurrence time is shortened by $\frac{T_1}{4}$ because the squeezed state is symmetric w.r.t. the origin) the original pulse reforms and is rotated forward, similar to Fig. 5.2.*

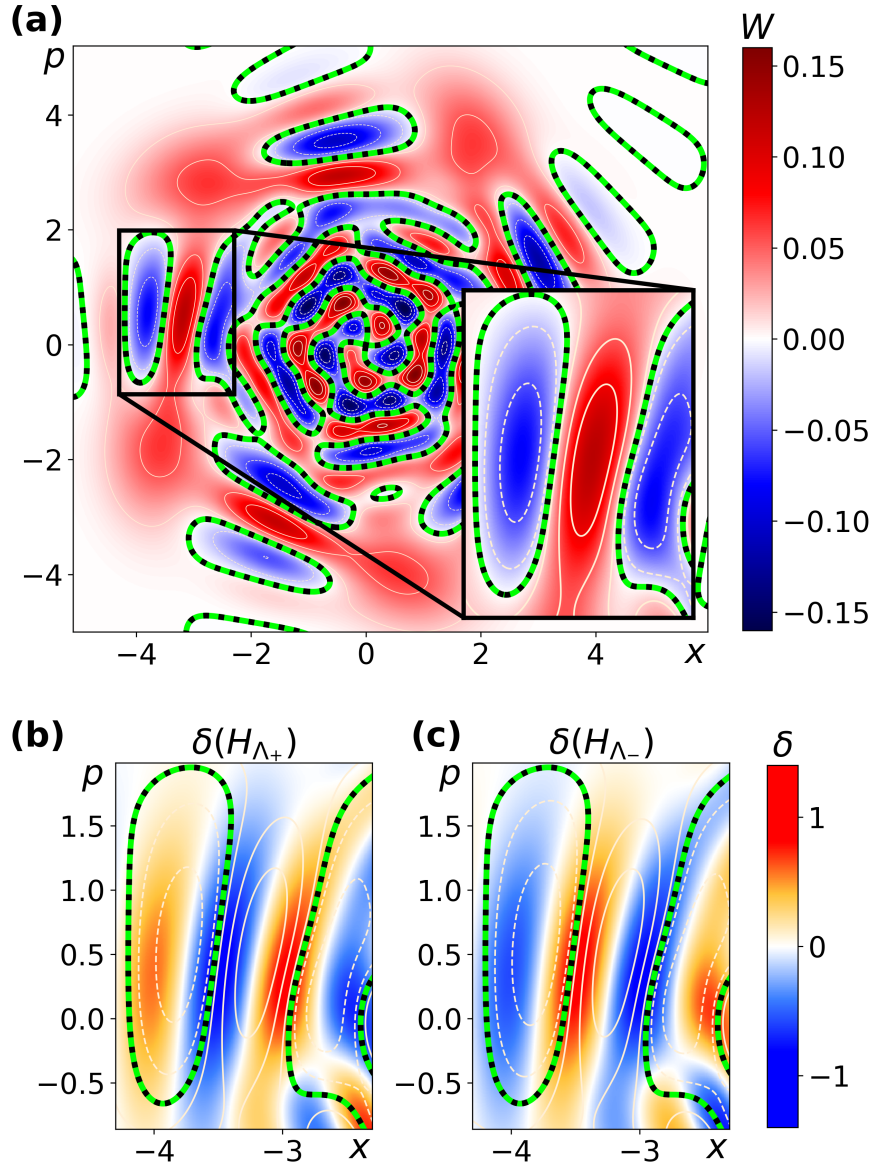


Figure 5.5: *Polarization of the vorticity δ and inversion of this polarization.* (a), the Wigner distribution W of a Gaussian initial state centered on $x = -4$, $p = 0$ and evolved to $t = 40$ using $\hat{H}_{\Lambda_+} = \hat{H}_{1/4}$. Its contours, for emphasis the zero contour is shown as black-green dashed lines, are also employed in (b) and (c). The inset for W in (a) is reproduced showing the effects of, (b), clockwise shear $[\delta(H_{\Lambda_+})]$ and, c, anticlockwise shear $[\delta(H_{\Lambda_-})]$. Comparing (b) with (c) demonstrates polarization inversion of δ associated with shear inversion of the system, here $\Lambda_+^2 = +(1/4)^2 = -\Lambda_-^2$.

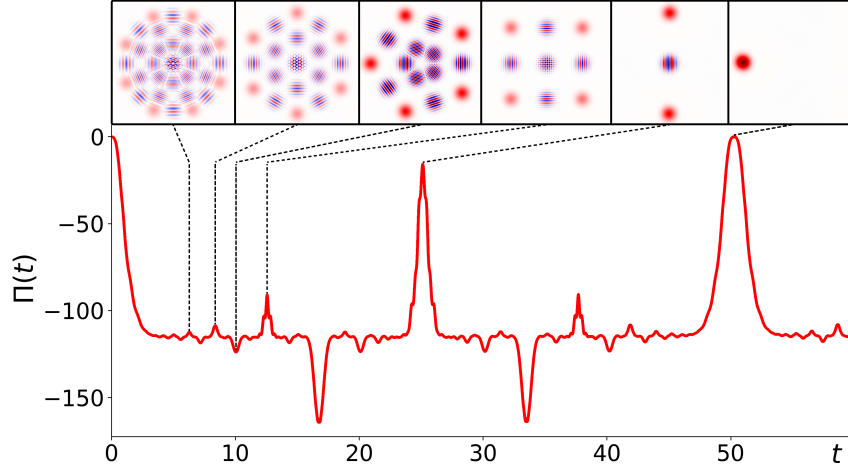


Figure 5.6: $\Pi(t)$ picks out special states. Deviations of $\Pi(t)$ from the settled value (≈ -115) single out special states: the evolution shows recurrence of the initial state at time $T_{\Lambda_+} = 16\pi \approx 50.3$ ($\Lambda_+ = 1/2$). Pronounced peaks and troughs at intermediate times identify fractional revival states [4] with special n -fold symmetries.

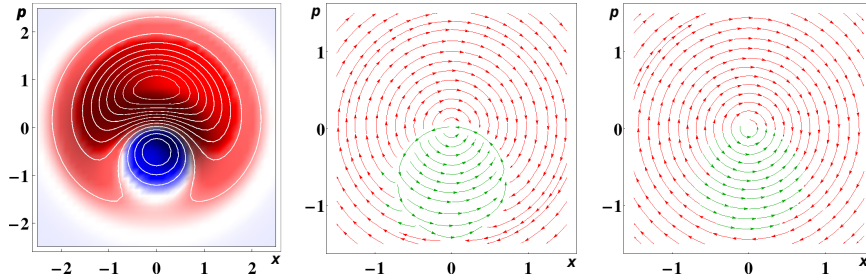


Figure 5.7: Wigner distribution, incorrect and correct Wigner current pattern for state $(|0\rangle + |1\rangle)/\sqrt{2}$. With $\Lambda = \lambda$ the dynamics of this superposition state is isomorphic to that of the harmonic oscillator, except for an extra phase due to the Kerr oscillator's different energy spectrum. The incorrect expression $\mathbf{J}^{(\sigma=1)}$ for the current (middle panel) does not respect this isomorphism, it breaks the system's circular symmetry and is therefore discarded. The correct expression $\mathbf{J}^{(\sigma=0)}$ for the current is depicted in the right panel. The region represented by green coloring is that where $W < 0$, this leads to current inversion [83]. For the Kerr system the only point of stagnation [83] of the current is the coordinate-origin. When the current stagnates elsewhere in phase space, it forms *lines of stagnation* [43].

Conclusion

In this thesis, many aspects of the Wigner current and quantum phase space dynamics are explored.

We show the integral form of the Wigner's representation of quantum mechanics is a valuable alternative to Moyal's formulation. It is in general numerically more stable, can make mathematical manipulations more transparent, and displays symmetries between position and momentum more clearly than Moyal's form.

For anharmonic quantum systems, converting the evolution equation into a Lagrangian form leads to singularities in the phase space velocity field, rendering the trajectory-based methods ill-defined. In quantum systems, the divergence term $\nabla \cdot \mathbf{w}$ is not equal to zero like in classical systems, but is instead non-zero, and can even feature singular values. This is needed for the generation of negativities in Wigner functions.

By creating a superoscillating Wigner function, it is shown that it is possible to create arbitrarily small structures below the sub-Planck scale.

A new quantum phase space measure is designed, based on the Wigner current, which calculates the suppression of the classical shear in quantum systems. It can be used to follow the dynamics of the system, and is able to dynamically pick up fractional revival states without knowing the initial state of the studied system.

It is shown that the concepts studied here, such as dynamic shear suppression, can be applied to Kerr oscillators.

Since the Wigner current has classical Liouvillian phase space current as its classical counterpart, the two can be compared to provide new understanding on the nature of quantum dynamics and its relationship with classical dynamics. This is well illustrated by the idea of viscosity applied to quantum systems, or how Wigner current invalidates the concept of trajectories in quantum phase space.

Wigner current sheds new lights on previously hidden aspects of quantum dynamics. I expect this present work constitutes the beginning of a much wider future research field that will be explored further.

References

- [1] Private communications with fellow scientists, and reviewer's reports.
- [2] Y. Aharonov, J. Anandan, S. Popescu, and L. Vaidman. Superpositions of time evolutions of a quantum system and a quantum time-translation machine. *Phys. Rev. Lett.*, 64(25):2965–2968, jun 1990. ISSN 00319007. doi:10.1103/PhysRevLett.64.2965.
- [3] Y. Aharonov, F. Colombo, I. Sabadini, D. C. Struppa, and J. Tollaksen. Some mathematical properties of superoscillations. *J. Phys. A Math. Theor.*, 44(36):365304, 2011. ISSN 17518113. doi:10.1088/1751-8113/44/36/365304.
- [4] I. S. Averbukh and N. F. Perelman. Fractional revivals: Universality in the long-term evolution of quantum wave packets beyond the correspondence principle dynamics. *Phys. Lett. A*, 139(9):449–453, aug 1989. ISSN 03759601. doi:10.1016/0375-9601(89)90943-2.
- [5] G. A. Baker. Formulation of quantum mechanics based on the quasi-probability distribution induced on phase space. *Phys. Rev.*, 109(6):2198–2206, mar 1958. ISSN 0031899X. doi:10.1103/PhysRev.109.2198.
- [6] L. E. Ballentine, Y. Yang, and J. P. Zibin. Inadequacy of Ehrenfest's theorem to characterize the classical regime. *Phys. Rev. A*, 50(4):2854–2859, 1994. ISSN 10502947. doi:10.1103/PhysRevA.50.2854.
- [7] H. Bauke and N. R. Itzhak. Visualizing quantum mechanics in phase space. jan 2011. URL <http://arxiv.org/abs/1101.2683>.
- [8] M. V. Berry. Evolution of semiclassical quantum states in phase space. *J. Phys. A Gen. Phys.*, 12(5):625–642, 1979. ISSN 03054470. doi:10.1088/0305-4470/12/5/012.
- [9] M. V. Berry. *'Faster than Fourier'*. World Scientific, Singapore, 1994.
- [10] M. V. Berry. Regular and irregular motion. In *Am. Inst. Phys. Conf. Ser.*, volume 46, pages 16–120, sep 2008. doi:10.1063/1.31417.
- [11] M. V. Berry and S. Popescu. Evolution of quantum superoscillations and optical superresolution without evanescent waves. *J. Phys. A Math. Gen.*, 39(22):6965–6977, 2006. ISSN 03054470. doi:10.1088/0305-4470/39/22/011.

- [12] F. Brosens and W. Magnus. Newtonian trajectories: A powerful tool for solving quantum dynamics. *Solid State Commun.*, 150(43-44):2102–2105, nov 2010. ISSN 00381098. doi:10.1016/j.ssc.2010.09.019.
- [13] R. Cabrera, D. I. Bondar, K. Jacobs, and H. A. Rabitz. Efficient method to generate time evolution of the Wigner function for open quantum systems. *Phys. Rev. A - At. Mol. Opt. Phys.*, 92(4):42122, oct 2015. ISSN 10941622. doi:10.1103/PhysRevA.92.042122.
- [14] M. S. Calder and A. Kempf. Analysis of superoscillatory wave functions. *J. Math. Phys.*, 46(1):12101, 2005. ISSN 00222488. doi:10.1063/1.1825076.
- [15] P. Carruthers and F. Zachariasen. Quantum collision theory with phase-space distributions. *Rev. Mod. Phys.*, 55(1):245–285, jan 1983. ISSN 00346861. doi:10.1103/RevModPhys.55.245.
- [16] G. Casati and B. V. Chirikov. Comment on "decoherence, chaos, and the second law". *Phys. Rev. Lett.*, 75(2):350, jul 1995. ISSN 00319007. doi:10.1103/PhysRevLett.75.350.
- [17] W. B. Case. Wigner functions and Weyl transforms for pedestrians. *Am. J. Phys.*, 76(10):937–946, oct 2008. ISSN 0002-9505. doi:10.1119/1.2957889.
- [18] P. Cvitanović, R. Artuso, R. Mainieri, G. Tanner, and G. Vattay. "*Chaos: Classical and Quantum*". ChaosBook.org, 2012. URL <http://chaosbook.org>.
- [19] J. P. Dahl and M. Springborg. The Morse oscillator in position space, momentum space, and phase space. *J. Chem. Phys.*, 88(7):4535–4547, apr 2002. ISSN 0021-9606. doi:10.1063/1.453761.
- [20] J. Daligault. Non-Hamiltonian dynamics and trajectory methods in quantum phase spaces. *Phys. Rev. A - At. Mol. Opt. Phys.*, 68(1):4, jul 2003. ISSN 10941622. doi:10.1103/PhysRevA.68.010501.
- [21] N. C. Dias and J. N. Prata. Wigner functions with boundaries. *J. Math. Phys.*, 43(10):4602–4627, 2002. ISSN 00222488. doi:10.1063/1.1504885.
- [22] T. Dittrich, E. A. Gómez, and L. A. Pachón. Semiclassical propagation of Wigner functions. *J. Chem. Phys.*, 132(21):214102, 2010. ISSN 00219606. doi:10.1063/1.3425881.
- [23] A. Donoso and C. C. Martens. Quantum tunneling using entangled classical trajectories. *Phys. Rev. Lett.*, 87(22):223202–223202–4, nov 2001. ISSN 10797114. doi:10.1103/PhysRevLett.87.223202.
- [24] A. Donoso, Y. Zheng, and C. C. Martens. Simulation of quantum processes using entangled trajectory molecular dynamics. *J. Chem. Phys.*, 119(10):5010–5020, 2003. ISSN 00219606. doi:10.1063/1.1597496.

- [25] R. P. Feynman. *Negative probability*. Routledge, 1987. URL <http://cds.cern.ch/record/154856/files/pre-27827.pdf>.
- [26] R. P. Feynman, R. B. Leighton, M. Sands, and S. B. Treiman. *The Feynman Lectures on Physics*, volume 17. Addison-Wesley, Reading, Ma., 2009. ISBN 0-201-02115-3. doi:10.1063/1.3051743.
- [27] O. D. Friedman and M. P. Blencowe. The Wigner Flow for Open Quantum Systems. 2017. URL <http://arxiv.org/abs/1703.04844>.
- [28] I. Gomez and M. Castagnino. On the classical limit of quantum mechanics, fundamental graininess and chaos: Compatibility of chaos with the correspondence principle. *Chaos, Solitons and Fractals*, 68:98–113, nov 2014. ISSN 09600779. doi:10.1016/j.chaos.2014.07.008.
- [29] J. Gong and P. Brumer. Chaos and quantum-classical correspondence via phase-space distribution functions. *Phys. Rev. A - At. Mol. Opt. Phys.*, 68(6):12, 2003. ISSN 10941622. doi:10.1103/PhysRevA.68.062103.
- [30] P. Grangier. Make it quantum and continuous. *Science (80-.)*, 332(6027):313–314, 2011. ISSN 00368075. doi:10.1126/science.1204814.
- [31] H. J. Groenewold. On the principles of elementary quantum mechanics. *Physica*, 12(7):405–460, oct 1946. ISSN 00318914. doi:10.1016/S0031-8914(46)80059-4.
- [32] S. Habershon, D. E. Manolopoulos, T. E. Markland, and T. F. Miller. Ring-Polymer Molecular Dynamics: Quantum Effects in Chemical Dynamics from Classical Trajectories in an Extended Phase Space. *Annu. Rev. Phys. Chem.*, 64(1):387–413, apr 2013. ISSN 0066-426X. doi:10.1146/annurev-physchem-040412-110122.
- [33] J. Hancock, M. A. Walton, and B. Wynder. Quantum mechanics another way. *Eur. J. Phys.*, 25(4):525–534, jul 2004. ISSN 01430807. doi:10.1088/0143-0807/25/4/008.
- [34] W. Heisenberg. Über den anschaulichen Inhalt der quantentheoretischen Kinematik und Mechanik. *Zeitschrift für Phys.*, 43(3-4):172–198, sep 1927. ISSN 14346001. doi:10.1007/BF01397280.
- [35] E. J. Heller. Wigner phase space method: Analysis for semiclassical applications. *J. Chem. Phys.*, 65(4):1289–1298, 1976. ISSN 00219606. doi:10.1063/1.433238.
- [36] N. E. Henriksen, G. D. Billing, and F. Y. Hansen. Phase space representation of quantum mechanics: Approximate dynamics of the morse oscillator. *Chem. Phys. Lett.*, 149(4):397–403, aug 1988. ISSN 00092614. doi:10.1016/0009-2614(88)85114-5.

- [37] B. J. Hiley. Phase space descriptions of quantum phenomena. In *Proc. Int. Conf. Quantum Theory Reconsideration ...*, volume 2, pages 1–22, 2004. URL <http://www.birkbeck.ac.uk/tpru/BasilHiley/ShadowPhaseVajxo03.pdf>.
- [38] M. Hillery, R. F. O’Connell, M. O. Scully, and E. P. Wigner. Distribution functions in physics: Fundamentals. *Phys. Rep.*, 106(3):121–167, 1984. ISSN 03701573. doi:10.1016/0370-1573(84)90160-1.
- [39] A. C. Hirshfeld and P. Henselder. Deformation quantization in the teaching of quantum mechanics. *Am. J. Phys.*, 70(5):537–547, may 2002. ISSN 0002-9505. doi:10.1119/1.1450573.
- [40] L. Huaqing, J. A. Poulsen, and G. Nyman. Tunneling dynamics using classical-like trajectories with an effective quantum force. *J. Phys. Chem. Lett.*, 4(17):3013–3018, 2013. ISSN 19487185. doi:10.1021/jz4012564.
- [41] R. L. Hudson. When is the wigner quasi-probability density non-negative? *Reports Math. Phys.*, 6(2):249–252, 1974. ISSN 00344877. doi:10.1016/0034-4877(74)90007-X.
- [42] J. R. Johansson, P. D. Nation, and F. Nori. QuTiP 2: A Python framework for the dynamics of open quantum systems. *Comput. Phys. Commun.*, 184(4):1234–1240, apr 2013. ISSN 00104655. doi:10.1016/j.cpc.2012.11.019.
- [43] D. Kakofengitis and O. Steuernagel. Wigner’s quantum phase-space current in weakly-anharmonic weakly-excited two-state systems. *Eur. Phys. J. Plus*, 132(9):381, 2017. ISSN 21905444. doi:10.1140/epjp/i2017-11634-2.
- [44] D. Kakofengitis, M. Oliva, and O. Steuernagel. Wigner’s representation of quantum mechanics in integral form and its applications. *Phys. Rev. A*, 95(2):22127, feb 2017. ISSN 24699934. doi:10.1103/PhysRevA.95.022127.
- [45] A. Kelly, R. Van Zon, J. Schofield, and R. Kapral. Mapping quantum-classical Liouville equation: Projectors and trajectories. *J. Chem. Phys.*, 136(8):84101, feb 2012. ISSN 00219606. doi:10.1063/1.3685420.
- [46] S. Kocsis, B. Braverman, S. Ravets, M. J. Stevens, R. P. Mirin, L. K. Shalm, and A. M. Steinberg. Observing the average trajectories of single photons in a two-slit interferometer. *2011 Int. Quantum Electron. Conf., IQEC 2011 Conf. Lasers Electro-Optics, CLEO Pacific Rim 2011 Inc. Australas. Conf. Opt. Lasers Spectrosc. Aust. Conf.*, 332(6034):105–107, 2011. doi:10.1109/IQEC-CLEO.2011.6193919.
- [47] S. I. Koda. Initial-value semiclassical propagators for the Wigner phase space representation: Formulation based on the interpretation of the Moyal equation as a Schrödinger equation. *J. Chem. Phys.*, 143(24):244110, dec 2015. ISSN 00219606. doi:10.1063/1.4938235.

- [48] R. Kosloff. Time-dependent quantum-mechanical methods for molecular dynamics. *J. Phys. Chem.*, 92(8):2087–2100, 1988. ISSN 00223654. doi:10.1021/j100319a003.
- [49] M. I. Krivoruchenko, B. V. Martemyanov, and C. Fuchs. Comment on "Dynamics of nuclear fluid. VIII. Time-dependent Hartree-Fock approximation from a classical point of view". *Phys. Rev. C*, 2(6):5–6, nov 2007. ISSN 0556-2813. doi:10.1103/PhysRevC.76.059801. URL <http://arxiv.org/abs/0709.2569> doi:<http://dx.doi.org/10.1103/PhysRevC.76.059801>.
- [50] C. Kurtsiefer, T. Pfau, and J. Mlynek. Measurement of the wigner function of an ensemble of helium atoms. *Nature*, 386(6621):150–153, mar 1997. ISSN 00280836. doi:10.1038/386150a0.
- [51] R. Landauer and T. Martin. Barrier interaction time in tunneling. *Rev. Mod. Phys.*, 66(1):217–228, jan 1994. ISSN 00346861. doi:10.1103/RevModPhys.66.217.
- [52] H. W. Lee. Quantum potential in the Wigner phase space. *Phys. Lett. A*, 146(6):287–292, jun 1990. ISSN 03759601. doi:10.1016/0375-9601(90)90956-O.
- [53] H. W. Lee. Theory and application of the quantum phase-space distribution functions. *Phys. Rep.*, 259(3):147–211, aug 1995. ISSN 03701573. doi:10.1016/0370-1573(95)00007-4.
- [54] H. W. Lee and T. F. George. Wigner phase space description above and below the classical threshold for the H+H₂ reaction. *J. Chem. Phys.*, 84(11):6247–6249, jun 1986. ISSN 0021-9606. doi:10.1063/1.450768. URL <http://aip.scitation.org/doi/10.1063/1.450768>.
- [55] H. W. Lee and M. O. Scully. Wigner phase-space description of a Morse oscillator. *J. Chem. Phys.*, 77(9):4604–4610, 1982. ISSN 00219606. doi:10.1063/1.444412.
- [56] H. W. Lee and M. O. Scully. The Wigner phase-space description of collision processes. *Found. Phys.*, 13(1):61–72, jan 1983. ISSN 00159018. doi:10.1007/BF01889411.
- [57] D. Leibfried, T. Pfau, and C. Monroe. Shadows and mirrors: Reconstructing quantum states of atom motion. *Phys. Today*, 51(4):22–28, 1998. ISSN 00319228. doi:10.1063/1.882256.
- [58] C. L. Lopreore and R. E. Wyatt. Quantum wave packet dynamics with trajectories. *Phys. Rev. Lett.*, 82(26):5190–5193, jun 1999. ISSN 10797114. doi:10.1103/PhysRevLett.82.5190.
- [59] V. I. Man'Ko, G. Marmo, and F. Zaccaria. Moyal and tomographic probability representations for f-oscillator quantum states. *Phys. Scr.*, 81(4):45004, apr 2010. ISSN 00318949. doi:10.1088/0031-8949/81/04/045004.

- [60] W. H. Miller. Perspective: Quantum or classical coherence. *J. Chem. Phys.*, 136(21), 2012. ISSN 00219606. doi:10.1063/1.4727849.
- [61] K. B. Møller, J. P. Dahl, and N. E. Henriksen. Wigner method dynamics in the interaction picture. *J. Phys. Chem.*, 98(13):3272–3279, 1994. ISSN 00223654. doi:10.1021/j100064a005.
- [62] J. E. Moyal. Quantum mechanics as a statistical theory. *Math. Proc. Cambridge Philos. Soc.*, 45(1):99–124, 1949. ISSN 14698064. doi:10.1017/S0305004100000487.
- [63] J. G. Muga, R. Sala, and S. Brouard. Wigner function for the square barrier. *Solid State Commun.*, 94(10):877–882, 1995. ISSN 00381098. doi:10.1016/0038-1098(95)00098-4.
- [64] D. D. Nolte. The tangled tale of phase space. *Phys. Today*, 63(4):33–38, 2010. ISSN 00319228. doi:10.1063/1.3397041.
- [65] M. Oliva and O. Steuernagel. Structures far below the sub-Planck scale in quantum phase space through superoscillations. *Phys. Rev. A*, 95(5):52112, may 2017. ISSN 24699934. doi:10.1103/PhysRevA.95.052112.
- [66] M. Oliva and O. Steuernagel. Quantum Kerr oscillators’ evolution in phase space: Wigner current, symmetries, shear suppression and special states. *Phys. Rev. A*, (in print), 2019. URL <http://arxiv.org/abs/1811.02952>.
- [67] M. Oliva and O. Steuernagel. Dynamic Shear Suppression in Quantum Phase Space. *Phys. Rev. Lett.*, 122(2):20401, jan 2019. ISSN 10797114. doi:10.1103/PhysRevLett.122.020401.
- [68] M. Oliva, D. Kakofengitis, and O. Steuernagel. Anharmonic quantum mechanical systems do not feature phase space trajectories. *Phys. A Stat. Mech. its Appl.*, 502:201–210, 2018. ISSN 03784371. doi:10.1016/j.physa.2017.10.047.
- [69] T. A. Osborn and K. P. Marzlin. Moyal phase-space analysis of nonlinear optical Kerr media. *J. Phys. A Math. Theor.*, 42(41):5302, oct 2009. ISSN 17518113. doi:10.1088/1751-8113/42/41/415302.
- [70] H. Paik, S. E. Nigg, G. Kirchmair, S. M. Girvin, B. Vlastakis, Z. Leghtas, E. Ginossar, M. Mirrahimi, L. Frunzio, and R. J. Schoelkopf. Observation of quantum state collapse and revival due to the single-photon Kerr effect. *Nature*, 495(7440):205–209, mar 2013. ISSN 0028-0836. doi:10.1038/nature11902.
- [71] C. Rasinariu. Shape invariance in phase space. *Fortschritte der Phys.*, 61(1):4–19, 2013. ISSN 00158208. doi:10.1002/prop.201200102.
- [72] M. Razavy. Wigner trajectories in quantum tunneling. *Phys. Lett. Sect. A Gen. At. Solid State Phys.*, 212(3):119–122, feb 1996. ISSN 03759601. doi:10.1016/0375-9601(96)00030-8.

- [73] M. Razavy. *Quantum Theory of Tunneling*. World Scientific, 2nd edition, 2014. doi:10.1142/8901. URL <https://www.worldscientific.com/doi/abs/10.1142/8901>.
- [74] R. W. Robinett. Quantum wave packet revivals. *Phys. Rep.*, 392(1-2):1–119, 2004. ISSN 03701573. doi:10.1016/j.physrep.2003.11.002.
- [75] E. T. F. Rogers, J. Lindberg, T. Roy, S. Savo, J. E. Chad, M. R. Dennis, and N. I. Zheludev. A super-oscillatory lens optical microscope for subwavelength imaging. *Nat. Mater.*, 11(5):432–435, 2012. ISSN 14764660. doi:10.1038/nmat3280.
- [76] A. Royer. Ehrenfest’s theorem reinterpreted and extended with Wigner’s function. *Found. Phys.*, 22(5):727–736, may 1992. ISSN 00159018. doi:10.1007/BF01889675.
- [77] R. Sala, S. Brouard, and J. G. Muga. Wigner trajectories and Liouville’s theorem. *J. Chem. Phys.*, 99(4):2708–2714, 1993. ISSN 00219606. doi:10.1063/1.465232.
- [78] W. P. Schleich. *Quantum Optics in Phase Space*. Wiley-VCH, apr 2005. ISBN 9783527602971. doi:10.1002/3527602976.
- [79] D. Sels, F. Brosens, and W. Magnus. Classical trajectories: A powerful tool for solving tunneling problems. *Phys. A Stat. Mech. its Appl.*, 391(1-2):78–81, jan 2012. ISSN 03784371. doi:10.1016/j.physa.2011.08.030.
- [80] D. Sels, F. Brosens, and W. Magnus. Wigner distribution functions for complex dynamical systems: A path integral approach. *Phys. A Stat. Mech. its Appl.*, 392(2):326–335, jan 2013. ISSN 03784371. doi:10.1016/j.physa.2012.09.007.
- [81] R. T. Skodje, H. W. Rohrs, and J. Vanbuskirk. Flux analysis, the correspondence principle, and the structure of quantum phase space. *Phys. Rev. A*, 40(6):2894–2916, sep 1989. ISSN 10502947. doi:10.1103/PhysRevA.40.2894.
- [82] O. Steuernagel. Equivalence between free quantum particles and those in harmonic potentials and its application to instantaneous changes. *Eur. Phys. J. Plus*, 129(6):114, jun 2014. ISSN 21905444. doi:10.1140/epjp/i2014-14114-3.
- [83] O. Steuernagel, D. Kakofengitis, and G. Ritter. Wigner flow reveals topological order in quantum phase space dynamics. *Phys. Rev. Lett.*, 110(3):30401, jan 2013. ISSN 00319007. doi:10.1103/PhysRevLett.110.030401.
- [84] M. Stobińska, G. J. Milburn, and K. Wódkiewicz. Wigner function evolution of quantum states in the presence of self-Kerr interaction. *Phys. Rev. A - At. Mol. Opt. Phys.*, 78(1):13810, jul 2008. ISSN 10502947. doi:10.1103/PhysRevA.78.013810.
- [85] T. Takabayasi. The Formulation of Quantum Mechanics in terms of Ensemble in Phase Space. *Prog. Theor. Phys.*, 11(4):341–373, apr 2006. ISSN 0033-068X. doi:10.1143/ptp.11.341.

- [86] K. Takahashi. Wigner and Husimi Functions in Quantum Mechanics. *J. Phys. Soc. Japan*, 55(3):762–779, mar 1986. ISSN 13474073. doi:10.1143/JPSJ.55.762.
- [87] T. Tilma, M. J. Everitt, J. H. Samson, W. J. Munro, and K. Nemoto. Wigner functions for arbitrary quantum systems. *Phys. Rev. Lett.*, 117(18):180401, oct 2016. ISSN 10797114. doi:10.1103/PhysRevLett.117.180401.
- [88] S. Tomsovic and E. J. Heller. Semiclassical dynamics of chaotic motion: Unexpected long-time accuracy. *Phys. Rev. Lett.*, 67(6):664–667, aug 1991. ISSN 00319007. doi:10.1103/PhysRevLett.67.664.
- [89] C. J. Trahan and R. E. Wyatt. Evolution of classical and quantum phase-space distributions: A new trajectory approach for phase space hydrodynamics. *J. Chem. Phys.*, 119(14):7017–7029, oct 2003. ISSN 00219606. doi:10.1063/1.1607315.
- [90] M. Veronez and M. A. M. De Aguiar. Phase space flow in the Husimi representation. *J. Phys. A Math. Theor.*, 46(48):485304, 2013. ISSN 17518113. doi:10.1088/1751-8113/46/48/485304.
- [91] E. P. Wigner. On the quantum correction for thermodynamic equilibrium. *Phys. Rev.*, 40(5):749–759, jun 1932. ISSN 0031899X. doi:10.1103/PhysRev.40.749.
- [92] C. Y. Wong. Dynamics of nuclear fluid. VIII. Time-dependent Hartree-Fock approximation from a classical point of view. *Phys. Rev. C*, 25(3):1460–1475, mar 1982. ISSN 05562813. doi:10.1103/PhysRevC.25.1460.
- [93] C. Y. Wong. Explicit solution of the time evolution of the wigner function. *J. Opt. B Quantum Semiclassical Opt.*, 5(3):S420–S428, 2003. ISSN 14644266. doi:10.1088/1464-4266/5/3/381.
- [94] Z. Xue-Feng and Z. Yu-Jun. Evolution of Quantum Phase Space Distribution: a Trajectory-Density Approach. *Chinese Phys. Lett.*, 26(2):023404, 2009. ISSN 0256-307X. doi:10.1088/0256-307x/26/2/023404.
- [95] C. Zachos, D. Fairlie, and T. Curtright. *Quantum Mechanics in Phase Space*. World Scientific, 2005. doi:10.1142/5287. URL <https://www.worldscientific.com/doi/abs/10.1142/5287>.
- [96] M. S. Zubairy. *Quantum Optics*. Springer, 1997.
- [97] W. H. Zurek. Sub-Planck structure in phase space and its relevance for quantum decoherence. *Nature*, 412(6848):712–717, aug 2001. ISSN 00280836. doi:10.1038/35089017.
- [98] W. H. Zurek and J. P. Paz. Decoherence, chaos, and the second law. *Phys. Rev. Lett.*, 72(16):2508–2511, apr 1994. ISSN 00319007. doi:10.1103/PhysRevLett.72.2508.

- [99] W. H. Zurek and J. P. Paz. Zurek and Paz Reply:. *Phys. Rev. Lett.*, 75(2):351, jul 1995. ISSN 00319007. doi:10.1103/PhysRevLett.75.351.